12-2020

Assessing the Performance of Reconditioned Railroad Tapered-Roller Bearings Used in Freight Rail Service

Veronica Valeria Hernandez
The University of Texas Rio Grande Valley

ASSESSING THE PERFORMANCE OF RECONDITIONED RAILROAD TAPERED-ROLLER BEARINGS USED IN FREIGHT RAIL SERVICE

A Thesis

by

VERONICA VALERIA HERNANDEZ

Submitted to the Graduate College of
The University of Texas Rio Grande Valley
In partial fulfillment of the requirements for the degree of

MASTER OF SCIENCE IN ENGINEERING

December 2020

Major Subject: Mechanical Engineering

ASSESSING THE PERFORMANCE OF RECONDITIONED RAILROAD TAPERED-ROLLER BEARINGS USED IN FREIGHT RAIL SERVICE

A Thesis
by
VERONICA VALERIA HERNANDEZ

COMMITTEE MEMBERS

Dr. Constantine Tarawneh
Chair of Committee

Dr. Arturo Fuentes
Committee Member

Dr. Robert Jones
Committee Member

December 2020

ABSTRACT

Hernandez, Veronica V., Assessing the Performance of Reconditioned Railroad Tapered-Roller Bearings Used in Freight Rail Service. Master of Science (MS), December 2020, 106 pp., 13 tables, 70 figures, 22 references.

The rail industry currently utilizes two wayside detection systems to monitor the health of freight railcar bearings in service: The Trackside Acoustic Detection System (TADS™) and the wayside Hot-Box Detector (HBD). Bearings that are removed from service are sent to specialized facilities where they undergo a reconditioning process before the bearings can be returned to rail service. The reconditioning process has been used for decades although there has been no previous study on the effectiveness of the reconditioning process on defective bearings that were removed from service. This persuaded the researchers from the University Transportation Center for Railway Safety (UTRCS) and the Transportation Technology Center Inc. (TTCI) to design an experimental study to assess the efficacy of the reconditioning process. The work in this thesis summarizes the results of the temperature and vibration signatures of twenty bearings. To assess the effectiveness of the reconditioning process, twelve of the twenty bearings were tested pre- and post-reconditioning process. The remaining eight bearings were tested post-reconditioning for a complete service life testing consisting of approximately 400,000 km (~250,000 mi) at the UTCRS testing facility.

DEDICATION

This thesis is dedicated to my family caring parents. To my mother, Noemi, who has encouraged and guided me to follow my dreams. To my father, David, for always pushing me to do my best. To my brother, Alex, for always believing in me. Thank you for all your love and support. I could not have done this without you.

ACKNOWLEDGEMENTS

I would like to express the deepest appreciation to my research advisor and mentor, Dr. Constantine Tarawneh. You are one of the most hardworking and determined professors I have had the pleasure to be taught by. Your passion and commitment to the University Transportation Center for Railway Safety is truly inspirational. You have supported and taught me throughout my years with being at the center and invested so much time into helping me reach my life goals. Thank you for giving me the opportunity to be a part of your well-known research team and guiding me to become a better engineer.

I would also like to thank Dr. Arturo Fuentes and Dr. Robert Jones for your continuous support. You are both great professors and I am thankful for having the opportunity to take your classes and learn about engineering from you. Your knowledge and expertise in engineering is something I hope to demonstrate to others.

To everyone from the UTCRS research team, thank you so much making my time at the center, an enjoyable one. I have had the pleasure to work with such a great team and learn from you. I will always remember all the time we have spent together, and I wish you all the best in your career endeavors.

Finally, I would like to acknowledge the Transportation Technology Center, Inc. (TTCI) for making this study possible and funding the work. Thank you to the TTCI engineers, Steven Belport and Dustin Clasby, who provided valuable guidance throughout this study.

DISCLAIMER

The contents of this thesis reflect the views of the authors, who are responsible for the facts and the accuracy of the information presented herein. This document is disseminated under the sponsorship of the Transportation Technology Center, Inc (TTCI), in the interest of information exchange. TTCI assumes no liability for the contents or use thereof.

TABLE OF CONTENTS

Page

LIST OF TABLES

Page

LIST OF FIGURES

Page

CHAPTER I

BACKGROUND AND INTRODUCTION

1.1 Introduction

1.1.1 Tapered-Roller Barings

Rail freight transportation has been one of the largest utilized methods of transporting cargo in the United States. The modern trains can haul 100 railcars or more with each freight railcar weighing between 30 to 130 tons. Each railcar is equipped with two bogies that are located at each end of the railcar. The bogies consist of the suspension components that include the springs, dampers, wheels, axles, and tapered-roller bearings to support the weight of the railcar. A single bogie contains two wheel-axle assemblies, corresponding to a total of eight tapered-roller bearings per freight railcar. The tapered-roller bearing is comprised of three essential components including the inner ring (cone), outer ring (cup), and the rollers. Each cone holds 23 rollers which are secured via a cage, thus producing one cone assembly. A single tapered-roller bearing consists of one cup that houses two cone assemblies, separated with a spacer ring. To prevent any foreign materials or debris from contaminating the lubricant in the bearing, each bearing is secured with two seals. An exploded view of the modern freight tapered-roller bearing and its components is shown in Figure 1.

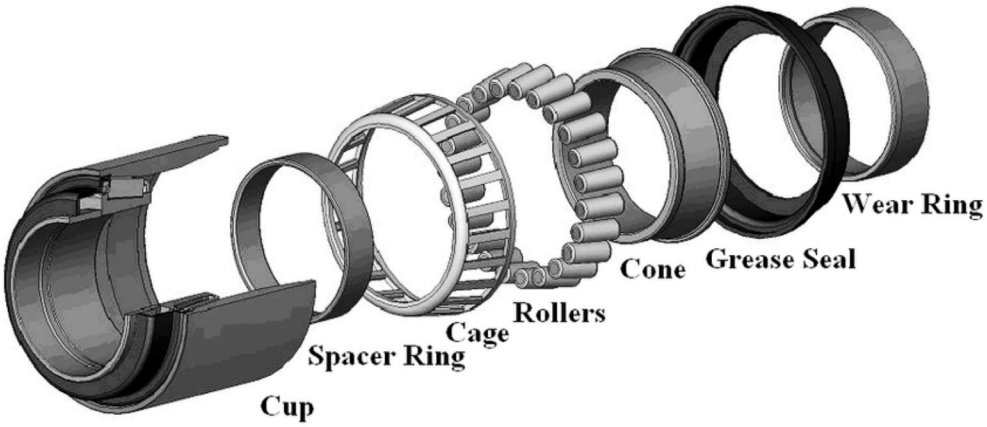

Figure 1. Typical railroad tapered-roller bearing components

The load of a freight railcar is applied onto the bearing outer ring (cup), causing the cup to stay stationary when in transit. As the freight train is in motion, the cup stays static while the inner rings (cones) are able to rotate freely in the cup. This causes the cone to cycle in and out of the loaded and unloaded zones, as depicted in Figure 2. Due to the cone cycling through the loaded zone, the cone experiences lower stresses and wear when compared to a bearing cup. The rollers receive the least amount of wear and stress because they revolve and rotate around the cone. Thus, the cup is the most susceptible to spalling because it sustains the most stress and wear.

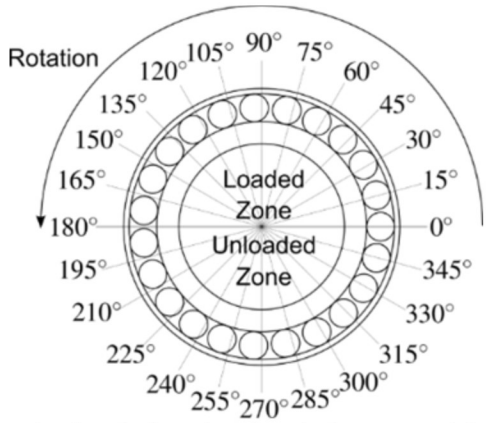

Figure 2: Schematic showing the loaded and unloaded zones with the rotation of the inner ring

1.2 Wayside Bearing Condition Monitoring Systems

Freight bearings are removed from service for many reasons with the most common being wheelset replacement when the wheel(s) develop defects. The rail industry currently utilizes two types of wayside bearing condition monitoring systems that monitor the bearing's health including the wayside Hot-Box Detector (HBD) and the Trackside Acoustic Detection System (TADS™). As the bearings pass by these wayside monitoring systems, data is collected and analyzed. If a certain bearing is identified as being defective, the train conductor is notified to stop the train so that the complete wheel-axle assembly containing the defective bearing is replaced. Train stoppages for wheelset replacement result in significant financial losses to the rail industry and railcar owners. About 580,000 wheelset replacements occur annually, which costs the rail industry around $825 million in losses [1].

1.2.1 Hot-Box Detectors (HBDs)

Hot-box detectors (HBDs), displayed in Figure 3, use non-contact infrared sensors to measure the temperature emitted from the bearings, axles, brakes, and wheels when they roll past the detector. In North America, there are over 6,000 HBDs in use, making HBDs the most utilized bearing condition monitoring systems [2]. Each HBD is placed every 40-rail km (25 mi) to 64-rail km (40 mi) on average depending on the rail-track traffic. If any bearing is operating at a temperature of 94.4°C (170°F) above the ambient temperature or at a temperature that is 52.8°C (95°F) above the operating temperature of the mate bearing that shares the same axle, the HBD will alert the train operator. Some railroads have adapted the use of HBDs to look for bearings operating at temperatures hotter than the average temperature of all bearings on the same side of the train. These bearings are identified as "warm trending" bearings and are flagged without triggering an HBD alarm [3]. They are removed from service via wheelset replacement

and are set for later disassembly and visual inspection. If upon inspection a bearing is determined to have no discernable defects, it is categorized as a “non-verified” bearing. A study conducted by Amsted Rail engineers concluded that 40% of bearings removed from service for “warm trending” from 2001 to 2007 turned out to be “non-verified”.

Several laboratory and field studies conducted have determined that the HBD temperature readings are inconsistent [4, 5, 6]. The recorded temperatures can be substantially different from the actual operating temperatures of the bearings. This can be due to a few factors including environmental conditions that can affect the IR sensor measurements, the class of the tapered-roller bearing and its position on the axle relative to the position of the wayside detector, among other possible factors. The inconsistency of the HBD readings caused 141 severely defective bearings not to be detected by these condition-monitoring systems in the United States and Canada from 2010 to 2019; 134 of which resulted in costly catastrophic derailments [7]. Additionally, the removal of non-verified bearings has resulted in many costly train stoppages and delays.

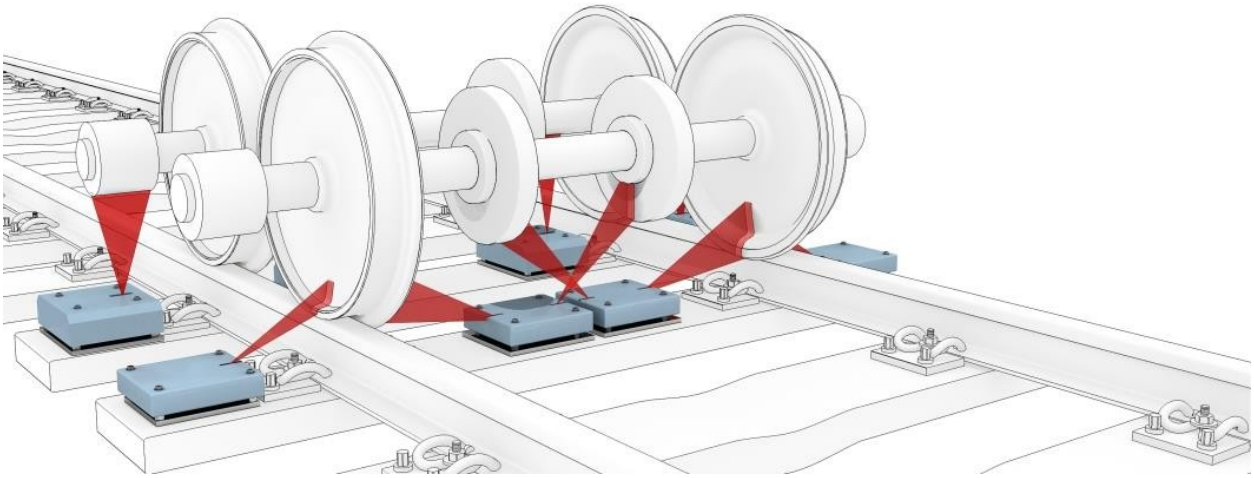

Figure 3: Example of a wayside Hot-Box Detector (HBD) [8]

1.2.2 The Trackside Acoustic Detection System (TADS™)

The Trackside Acoustic Detection System (TADS™), pictured in Figure 4, alerts the conductor of high-risk bearings. While TADS™ are reliable in detecting end-of-life bearings, they are not capable of detecting bearings with small defects that are in the early stages of initiation and propagation [9]. Many defective bearings may never be detected by TADS™ because: (1) a high-risk defect is one that spans almost 90% of a bearing's raceway (i.e., a growler), and (2) there are less than 30 systems in service throughout North America, which means that many bearings may spend their entire service life without passing through a TADS™ station.

Figure 4: Photograph of Trackside Acoustic Detection System site [10]

1.3 Bearing Defects

There are three main categories for classifying bearing defects, which include distributed, geometric, and localized. A distributed defect example is a water-etch on an inner ring (cone) raceway, shown in Figure 5 (right). A water-etch defect is caused when water enters the bearing

due to a defective seal. When moisture enters a bearing, the grease begins to degrade, resulting in metal-to-metal friction which will cause the raceways to wear at a faster rate. Geometric defects occur when there are inconsistencies in the manufacturing process that causes one or more of the bearing components to be out of tolerance. A bearing that has a geometric inconsistency can show no sign of surface flaw while still running at a higher operating temperature. Localized defects, shown in Figure 5 (left), are defects including cracks, pits, and spalls on one of the rolling components of the bearing.

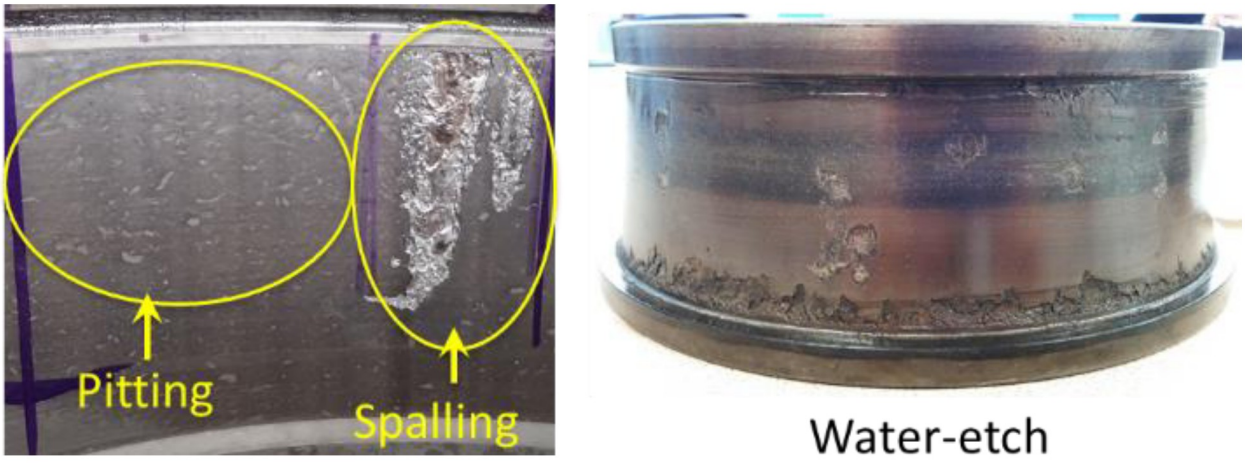

Figure 5: An example of localized defects (left) and distributed defect (right)

The localized defects like cracks, pits, and spalls are generated from subsurface inclusions. These subsurface inclusions develop into a localized defect when there is constant rolling contact fatigue (RCF). The subsurface inclusions are usually close to the raceway surface (around 400 μm below the surface), creating micro-cracks that propagate to the raceway of the bearing component [11]. The micro-cracks cause metal fragments to break off, introducing metal shards in the grease which can create pits on the surface. A spall is created on the raceway in the region where the metal fragments broke off.

1.4 Need for Reconditioned Bearings

Bearing reconditioning is a very common practice in the railroad industry with around 90% of bearings in revenue service having underwent a reconditioning process. The practice of reconditioning and remanufacturing of tapered-roller bearings became widely used in North America in the early 1980s [12]. Railroad bearings are removed from service for several reasons but most commonly due to wheelset replacement when wheels develop defects. Most railroad bearings are removed from service before reaching their full service life [13].

1.4.1 Reconditioning benefits

The reconditioning process has some valuable advantages that help benefit the railroad industry. One of the benefits is reduction of cost, with a repaired bearing having a savings of up to 70 percent off the total cost of a new bearing [14]. A reconditioned bearing is considered to have a better product quality because of repairs made on any worn parts that can cause unnecessary vibrations. If a bearing causes damage, this can affect the freight train during transport with downtime, maintenance and delivery schedules. A bearing's performance will reduce overtime due to any contamination or corrosion in the bearing. The life of a bearing can be extended by performing a bearing repair, shown in Figure 6, extending the life of the bearing closer to the theoretical bearing life. While a bearing is being inspected for the reconditioning process, any problem with the bearing can be found, mitigated, and prevented to avoid problem recurrence. Overall, the reconditioning process requires less lead time, less material, and less energy to repair a bearing than the time it takes to manufacture a new one.

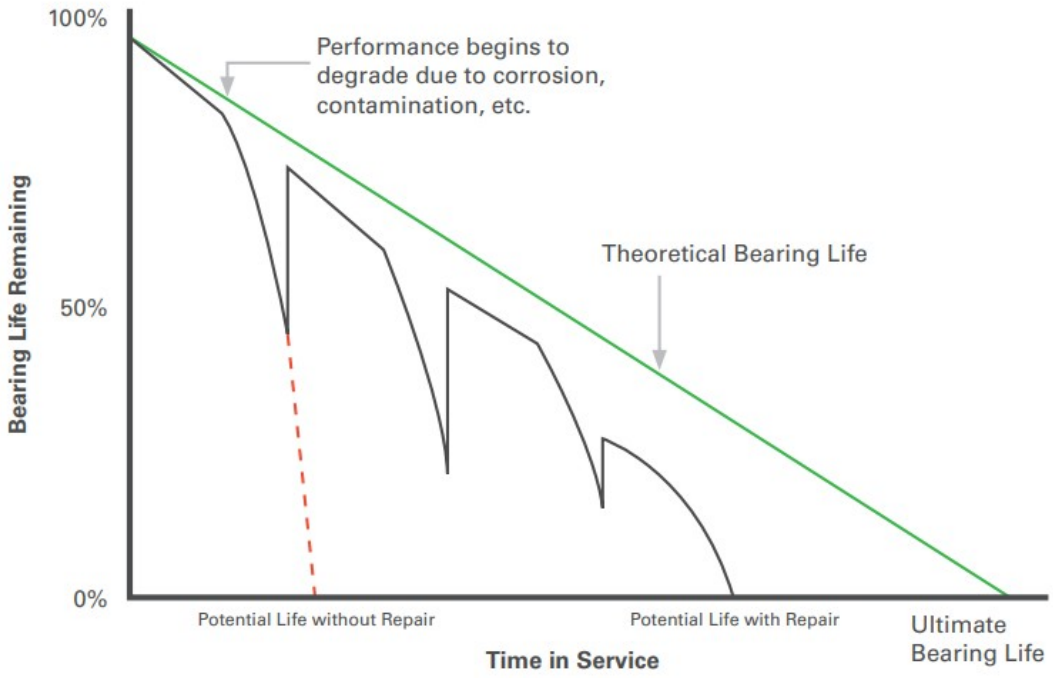

Figure 6: Potential life of a bearing with and without repair [15]

Indications of bearings that require attention for service or repair include bearings exceeding normal operating temperatures, excessive vibration, and sudden lubricant drop. A bearing that is continuously running at higher than normal operating temperatures is an indicator that a problem may be present within the bearing. Bearings that have too much clearance can show excessive vibrations. When the bearing has increased vibration levels, one or more of its raceways may have developed spalls. To ensure that the bearing does not cause any damage or impact the product quality due to excessive vibration, a scheduled inspection and repair is warranted. If the bearing is experiencing a drop in lubricant, an abnormality may have occurred with the bearing such as a broken seal which would require attention.

1.4.2 Why Made Codes [16]

Bearings are commonly removed from service due to wheel set replacement which have a "Why Made Code" to categorize the removal. Wheel removals are grouped into 4 general

categories including Administrative, Wear Related, Environmental, and Wheel Failures. Several bearings in this study were selected for having “Why Made Code 11” which is classified in the Administrative Category. From 513,129 wheels removed in 2003, 56.21% of them were categorized as administrative removals. Of the 288,437 wheels removed from the admirative category, 236,102 were removed for “Why Made Code 11” which denotes that the bearings were removed from service for reasons not associated with the bearings.

CHAPTER II

RECONDITIONING PROCESSES AND DEFECT DETECTION ALGORITHM

2.1 Reconditioning Processes

The reconditioning requirements for railroad freight bearings are specified by the Association of American Railroads (AAR) Manual of Standards and Recommended Practices, Section H – Part II [13]. The reconditioning process requires a disassembly, cleaning, repair, and inspection of the bearing components. Reconditioning and remanufacturing processes can only be performed by AAR approved organizations. After bearings undergo the reconditioning process and are approved to be sent into rail service, the bearings are greased and reassembled.

2.1.1 Schaeffler Technologies [17]

There are four reconditioning levels, stated by Schaeffler Technologies, to determine which reconditioning steps are needed, shown in Figure 7. Level I is called “Requalifying” which includes, disassembling, cleaning, inspecting and assessing, measuring, and preparing and assessment for an assessment report for the bearing and its components. Level II, Level III, and Level IV are called, “Refurbishment”, “Remanufacturing”, and “Remanufacturing Plus”, respectively. All bearings undergoing a reconditioning process must go through the first level of reconditioning steps.

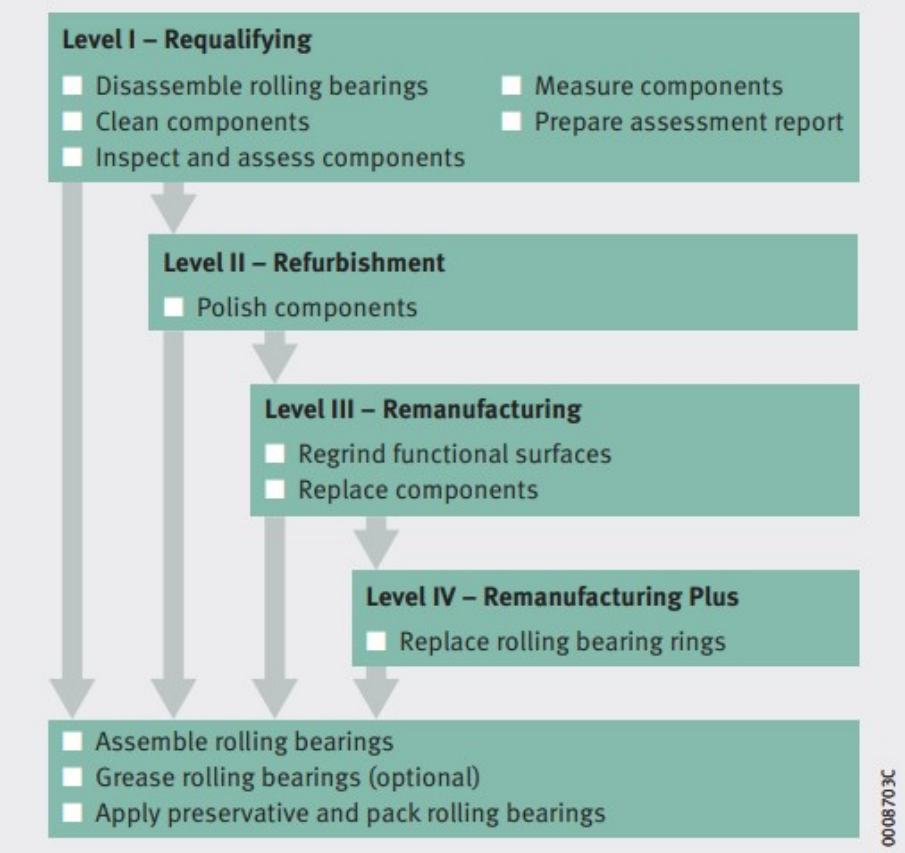

Figure 7: Reconditioning levels for rolling bearings [17]

2.1.1.1 Level I – Requalifying

Level I of the reconditioning process for rolling bearings includes a complete disassembly, cleaning, inspection, and measuring of the bearing components. The reconditioning facility will receive the bearing, dismantle the bearing, and place the bearing components in the wash system to remove all lubricants. After the components have been cleaned, a rust-prevention agent is applied, and the components are then ready for inspection [13]. Each of the components is inspected for any visual or dimensional characteristics using measuring and inspection equipment. The assessment report provides detailed information on any damage found on the components, what methods were used in the examination, and the results of the measurements from the inspection. If there is no visible damage during the inspection and assessment, the

bearing is greased and assembled. Bearings that have damage go through a higher level of reconditioning that would be documented in the report. Finally, a proposal is prepared if the bearing was found to contain damage. The proposal informs the customer on the plan, amount of time, and price for the reconditioning process.

2.1.1.2 Level II – Refurbishment

The refurbishment reconditioning process is performed on bearings that have minimal damage on the raceways. The bearings' rings, rolling elements, and cages are polished while the components that do not serve as an important function to the bearing, are cleaned. During the polishing step of reconditioning, any stubborn marks, fretting, or corrosion on the main components of the bearing (outer ring, inner ring, rollers) is removed. After the polishing is performed, the components are cleaned.

2.1.1.3 Level III – Remanufacturing

Bearings that have a significant amount of damage on any raceways are reground and new rolling elements are used. The surfaces of the components are required to have the same dimensions as a new rolling bearing to ensure the performance capacity would not be compromised. The regrinding machines and tools used are the same that are used to manufacture new rolling bearings. During the regrinding process, the production engineer will ensure that the hardening depth is considered when machining the surfaces. When the raceways need to be reground, new rolling elements must be used to account for the surface material that was removed from the raceways. The new rolling elements would be manufactured with a larger size to compensate for the loss of material.

2.1.1.4 Level IV – Remanufacturing Plus

If any of the bearing components do not meet the specifications due to extreme damage that cannot be repaired or resurfaced, the components are scrapped. The remanufacturing plus process involves scrapping unrepairable bearing components and rebuilding the bearing using only the components that are within the manufacturer's specifications along with newly manufactured components to replace the damaged ones. Usually, the cost of this level of reconditioning is comparable to the cost of manufacturing a new rolling bearing.

2.1.2 AAR Manual of Standards and Recommended Practices [18]

Railway roller bearing reconditioning includes the disassembly, cleaning, inspection, repair (if needed), and reassembly of the bearing. If the bearing was in service, then removed from the axle, the bearing must be reconditioned before reapplication. The AAR Manual indicates that if there are small cracks on raceway surfaces, the crack should be grinded out to prevent spalling. Bearings are prohibited from entering service when one or more of the following issues are present: rollers have spalls or cracks, any unrepaired spalls on the inner or outer rings, repaired spalls that are greater than a specified length/width or depth, more than two repaired spalls in a 2 inch circumferential area, a separation of less than 3/16 inch long between any two repaired spalls, or more than six repaired spalls on a raceway.

2.1.2.1 Disassembly cleaning inspection

The backing ring and seal wear rings must be removed from the bearing while removing excess grease. The roller assemblies and spacer ring are also removed, and the seals are then scrapped. Residual grease is removed from the components before cleaning the components from all remaining grease. Bearings then undergo a visual inspection ensuring that components with defects that are unrepairable are rejected.

2.1.2.2 Reconditioning requirements

The recommended device to repair the spalls is a portable hand grinder with fine abrasive grinding wheels or shank rotary tools. The grinding wheels must be around 5/16 inch or less in diameter and the shank rotary tools must be 1/8 inch or 1/4 inch in diameter. To begin the spall repair, loose material must be ground away. Edges of grinded areas should be smoothed with 180-grit or finer abrasive cloth or grinding wheel. However, the bottom of the spall does not need to be polished smooth. For outer rings to be reground, the acceptable types of wear are some brinelling, water etch, corrosion, scoring, indentations, pitting, repairable spalling, smearing, and peeling. If the outer ring has cracks, the component must be scrapped. Outer rings (cups) can only be reground once and cannot be returned to service if they were previously reground. The measurements must be in tolerance to those described in the manual or the component will be scrapped. An inspection stand and feeler gauge can be used to determine if the inner ring (cone) assembly has spalls by utilizing the light on the inspection stand while rotating the cone. If a spall(s) is present on the cone that has a metal cage, the cage must be removed to repair any spalls, allowing the cone to be reused. The bearing will then require a new cage to be used and the bearing must be assembled by its original manufacturer or an authorized representative.

2.1.2.3 Marking of bearings

After any spalls are repaired, the bearing component must be scribed indicating that the bearing was reconditioned. The outer ring (cup) must be marked near the spall on the spacer ring location, and the inner ring (cone) must be marked on the large diameter end face by the approved shop that performed the repair. The markings must include the month and year along with the reconditioning company's initials and shop code letters. When a bearing's inner and/or

outer ring has reground raceways, the symbol “R” is scribed and circled by the manufacturer that grinded the raceway.

After inspection and reconditioning, the bearings can then be reassembled, ensuring the components are free from any dirt or grit. The AAR manual recommends that the outer rings and inner rings that have been reground are used in separate assemblies.

2.2 Bearing Defect Detection Algorithm

A field-tested bearing defect detection algorithm was developed in 2015 by Gonzalez [19] that can detect tapered-roller bearing defects. The algorithm determines which component of the bearing has the defect and can estimate the size of the defect. For field implementation and to save in battery power consumption, the algorithm is triggered when the bearing’s operating temperature is above 93°C (200°F) or if the operating speeds are above 65 km/h (40 mph). However, for the purposes of the laboratory testing performed for this study, the algorithm was triggered continuously since it was powered via a designated power supply. After the accelerometer is triggered, the algorithm will run through an analysis consisting of three levels. The algorithm, will check for vibration levels that indicate the presence of a spall, classify the defect, and approximate the defect size, as demonstrated in the flowchart of Figure 8. A description of each level of analysis is provided hereafter.

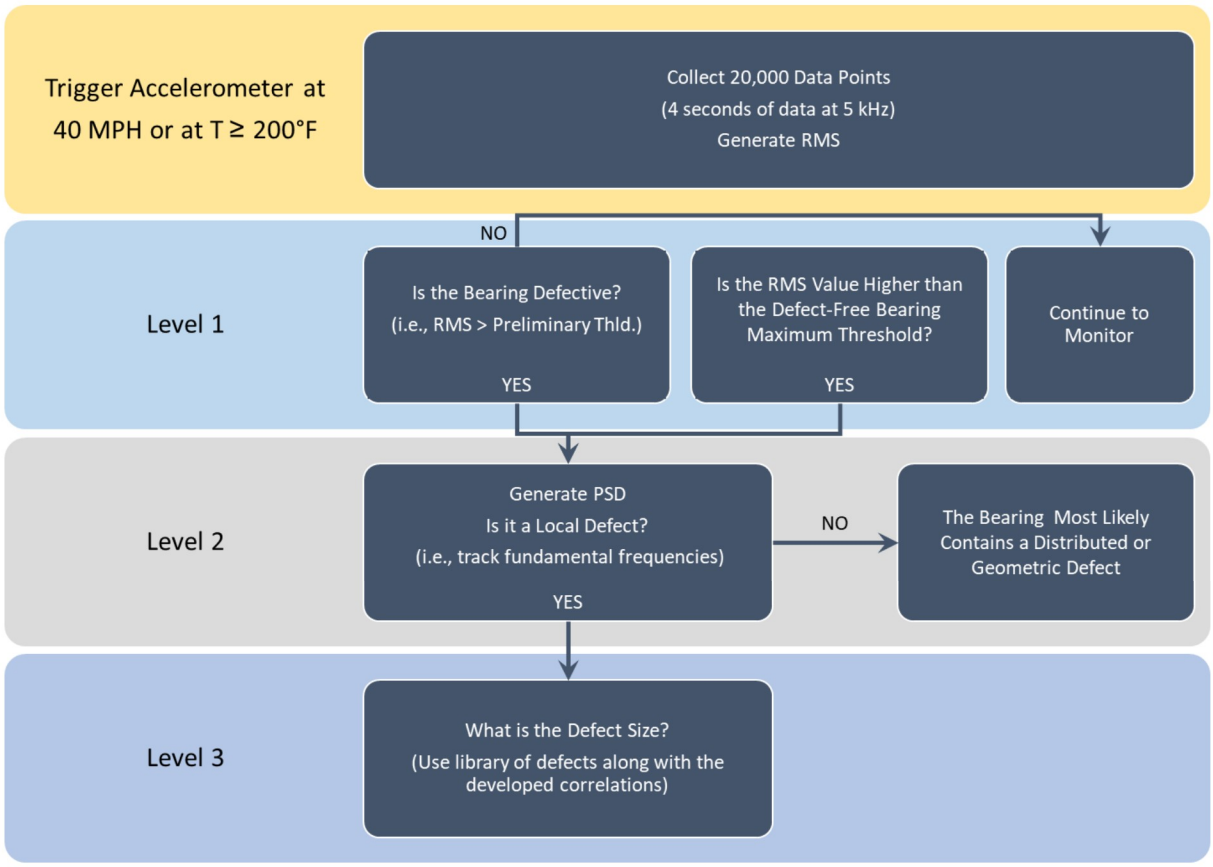

Figure 8: Defect Detection Algorithm Flowchart [19]

2.2.1 Level 1: Is the Bearing Defective?

Level 1 analysis identifies if the bearing is defective or healthy (defect-free). A preliminary threshold (T_p) and a maximum threshold (T_{max}) were generated utilizing the vibration signature data collected from laboratory testing performed over the past decade. The calculated root-mean-square (RMS) values were compared to these thresholds to determine the condition of the bearing.

Note that the preliminary and maximum thresholds were obtained through a statistical analysis that was performed on numerous RMS versus simulated train speed data sets collected for many healthy and defective bearings. For the purposes of this study, only the linear regression models for T_p and T_{max} will be provided here in Eq. (1) and Eq. (2), respectively. The

reader can refer to the thesis by Gonzalez [19] for detailed information on the analysis performed to obtain these thresholds.

$$\begin{aligned} T_P &= 7.331 \times 10^{-2} \times V\ [km/h] - 9.059 \times 10^{-2} \\ T_P &= 4.556 \times 10^{-2} \times V\ [mph] - 9.059 \times 10^{-2} \\ T_P &= 4.879 \times 10^{-3} \times V\ [rpm] - 9.059 \times 10^{-2} \end{aligned} \quad (1)$$

$$\begin{aligned} T_{max} &= 1.788 \times 10^{-1} \times V\ [km/h] - 1.008 \\ T_{max} &= 1.111 \times 10^{-1} \times V\ [mph] - 1.008 \\ T_{max} &= 1.119 \times 10^{-2} \times V\ [rpm] - 1.008 \end{aligned} \quad (2)$$

Typically, the vibration levels within a bearing measured in RMS are compared to the RMS values given by the T_p and T_{max} correlations for the specific operating speed. If the vibration RMS value for the bearing is below the T_p, the bearing is considered to be a defect-free (healthy) bearing. When the RMS value is above the T_p, the bearing is categorized as possibly defective. However, when the vibration RMS value for a bearing exceeds that of the T_{max}, the bearing is flagged as defective. In the cases where the vibration RMS values of bearings exceed the T_p or T_{max}, the algorithm will proceed to Level 2 analysis where the defect type is determined.

2.2.2 Level 2: What is the Defect Type?

The tapered-roller bearing defect type present is categorized in the Level 2 analysis. Level 2 utilizes frequency-domain analysis to create power spectral density (PSD) plots. The PSD, described in Eq. (3), is found by taking the square of the magnitudes in the frequency domain. There are six frequencies tracked, shown in Eq. (4) – Eq. (9), which include the cone

(ω_{cn}), cage (ω_{cg}), roller (ω_r), outer ring (cup) defect (ω_{out}), inner ring (cone) defect (ω_{in}), and roller defect (ω_{rd}) frequencies [20].

$$PSD = |X(f)|^2 \tag{3}$$

$$\omega_{cn} = \omega_o \tag{4}$$

$$\omega_{cg} = \left(\frac{R_{cn}}{R_{cn} + R_{cp}}\right)\omega_{cn} \tag{5}$$

$$\omega_r = \left(\frac{R_{cn}}{D_r}\right)\omega_{cn} \tag{6}$$

$$\omega_{out} = 23\omega_{cg} \tag{7}$$

$$\omega_{in} = 23\left(\omega_{cn} - \omega_{cg}\right) \tag{8}$$

$$\omega_{rd} = \left(\frac{R_{cp}}{R_r}\right)\omega_{cg} \tag{9}$$

The six frequencies are based on the rotational speed of the tapered-roller bearing components. D_r and R_r refer to the diameter and radius of the roller, respectively, and R_{cn} and R_{cp} refer to the radii of the inner ring (cone) and outer ring (cup), respectively. The last three equations, Eq (7) – Eq (9) give the defect frequencies for a defective outer ring (cup), inner ring (cone), and roller, respectively. When there is a localized defect, there will be a peak in power for the defect frequency in the PSD plot. Figure 9 shows examples of PSD plots for a healthy (defect-free) bearing versus bearings with a cup, cone, or roller defect. The vertical red lines in Figure 9 indicate the defect frequencies and their harmonics up to 1000 Hz.

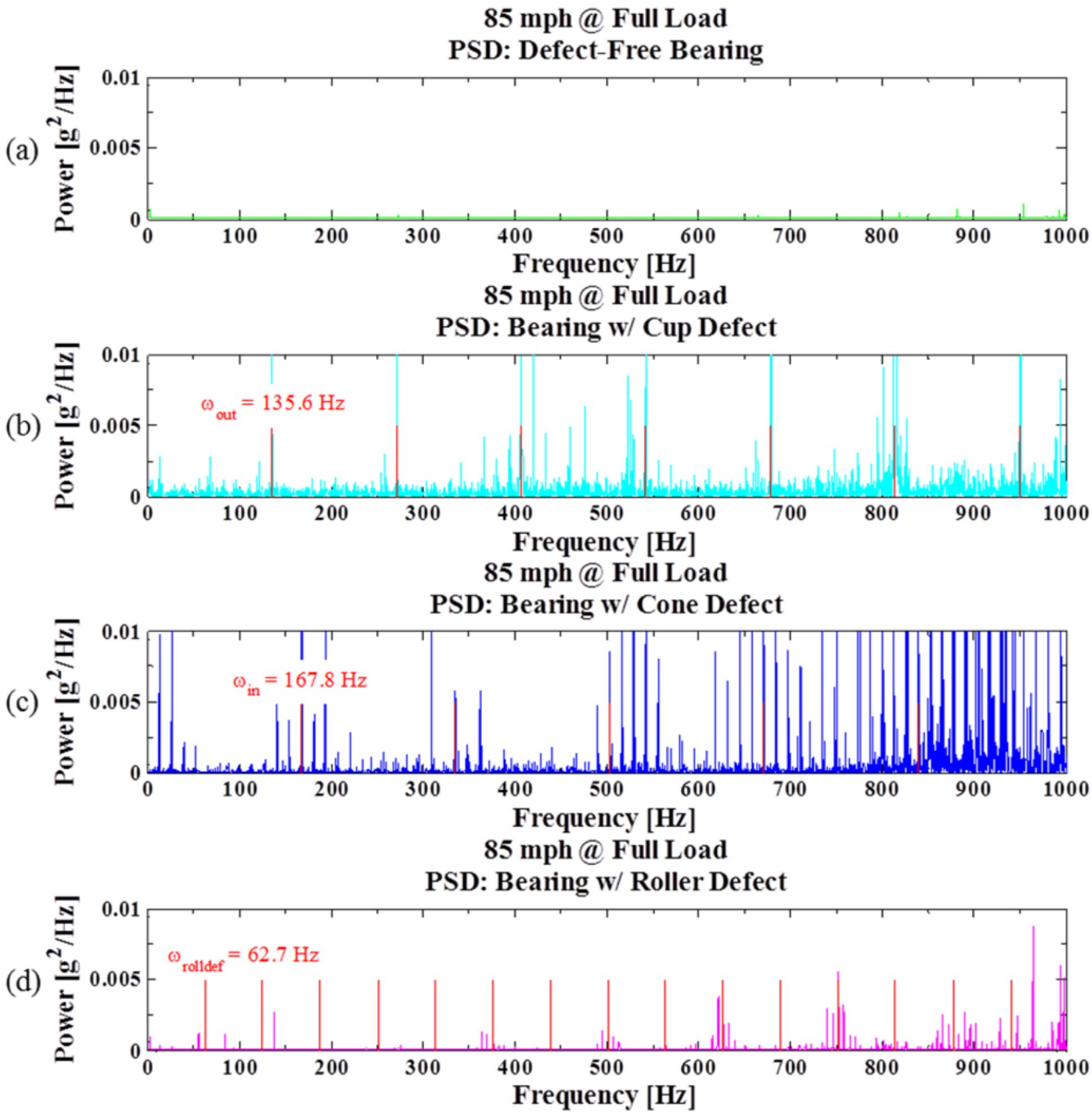

Figure 9: Power Spectral Density (PSD) plot of (a) a healthy bearing, (b) a bearing with an outer ring (cup) defect, (c) a bearing with an inner ring (cone) defect, and (d) bearing with a roller defect.

The defect frequencies are then used to determine the normalized defect energy (NDE) to evaluate the type of defect [21]. The NDE is found by taking the summation of the areas under

the defect frequency and its harmonics in the PSD plot. To account for small shifts in the fundamental frequencies caused by dimensional tolerances or rotational slipping, a hunting range (h_r) that is a function of the PSD resolution (*rs*) and varies with the rotational speed (ω_o) of the bearing was implemented as follows:

Low Speed: $\omega_o < 355\ rpm, h_r = \pm rs \times 6$

Medium Speed: $355\ rpm \leq \omega_o < 610\ rpm, h_r = \pm rs \times 10$

High Speed: $610\ rpm \leq \omega_o, h_r = \pm rs \times 15$

The resolution (*rs*) is obtained by dividing the sampling frequency by the number of data points in the PSD plot. The normalized defect energy is calculated using Eq. (10) – Eq. (12) for each defect type. To capture the total area under the harmonics of the defect frequencies, an integration range ($i_r = rs \times 3$) was utilized. The variable *n* in Eq. (10) – Eq. (12) refers to the total number of harmonics for a specific defect frequency in the chosen frequency range.

$$NDE_{cup} = \frac{\sum_{i=1}^{n} \int_{i\omega_{out}-i_r}^{i\omega_{out}+i_r} |X(f)|^2 df}{n} \tag{10}$$

$$NDE_{cone} = \frac{\sum_{i=1}^{n} \int_{i\omega_{in}-i_r}^{i\omega_{in}+i_r} |X(f)|^2 df}{n} \tag{11}$$

$$NDE_{roller} = \frac{\sum_{i=1}^{n} \int_{i\omega_{rolldef}-i_r}^{i\omega_{rolldef}+i_r} |X(f)|^2 df}{n} \tag{12}$$

Equation (13) is used to categorize the defect type (localized, distributed, or geometric) present in the defective bearing by dividing the maximum value of the three normalized defect energies by their summation. If the ratio is above 50%, then the bearing has a localized defect on the component with the highest normalized defect energy. When the ratio is below 50%, the bearing could have a geometric defect, a distributed defect on multiple bearing components, or the bearing is a falsely flagged healthy bearing, which is not common.

$$\frac{\max\left(NDE_{cup,cone,roller}\right)}{NDE_{cup} + NDE_{cone} + NDE_{roller}} \times 100 \geq 50\% \tag{13}$$

2.2.3 Level 3: What is the Defect Size?

Level 3 analysis determines the approximate defect size after the bearing is determined to have a localized defect in Level 2 analysis. The estimated defect size is obtained from correlations of vibration RMS values for defective bearings with inner ring (cone) and outer ring (cup) defects versus defect area initially developed by Gonzalez [19] and later optimized by Lima [22]. These optimized correlations found in the thesis by Lima [22] are presented in Figure 10 and Figure 11 for cone and cup defects, respectively. Note that no correlation was developed for roller defects as this type of defect is not common in rail service and is usually the result of other bearing components failing first.

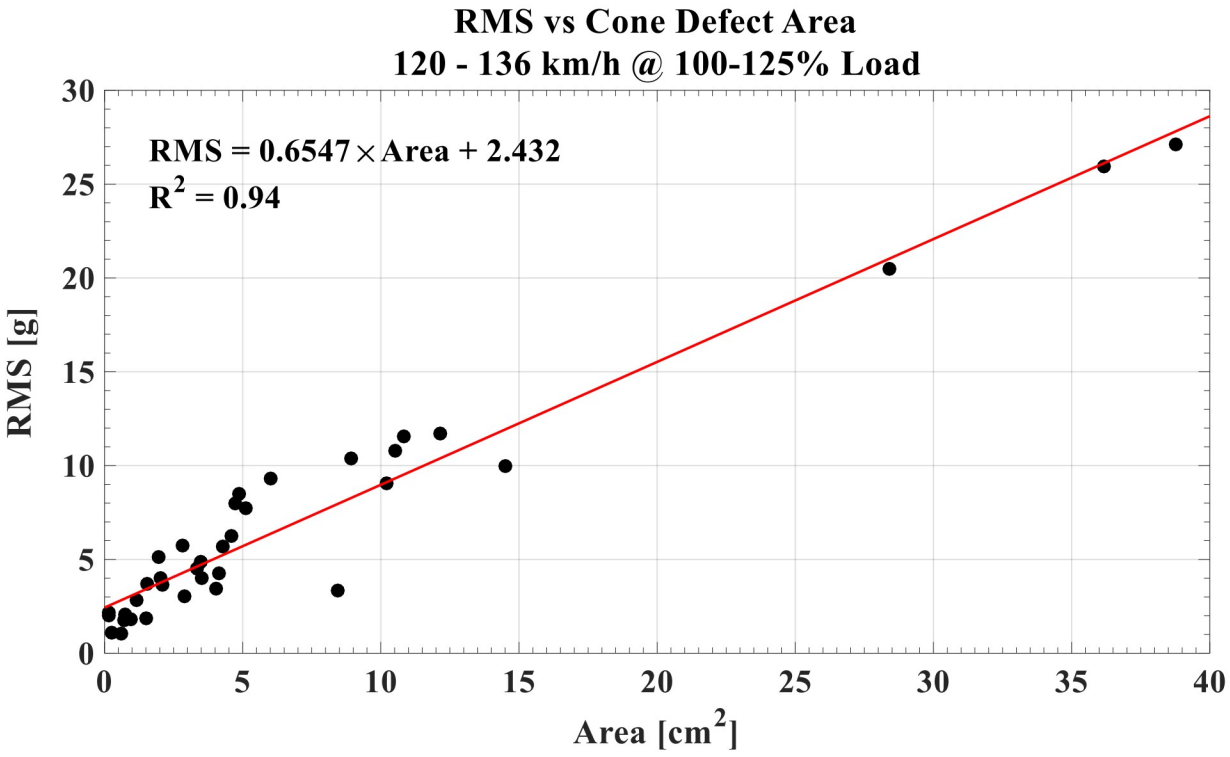

Figure 10: Improved Cone defect size correlation at 137 km/h (85 mph) and full load [22]

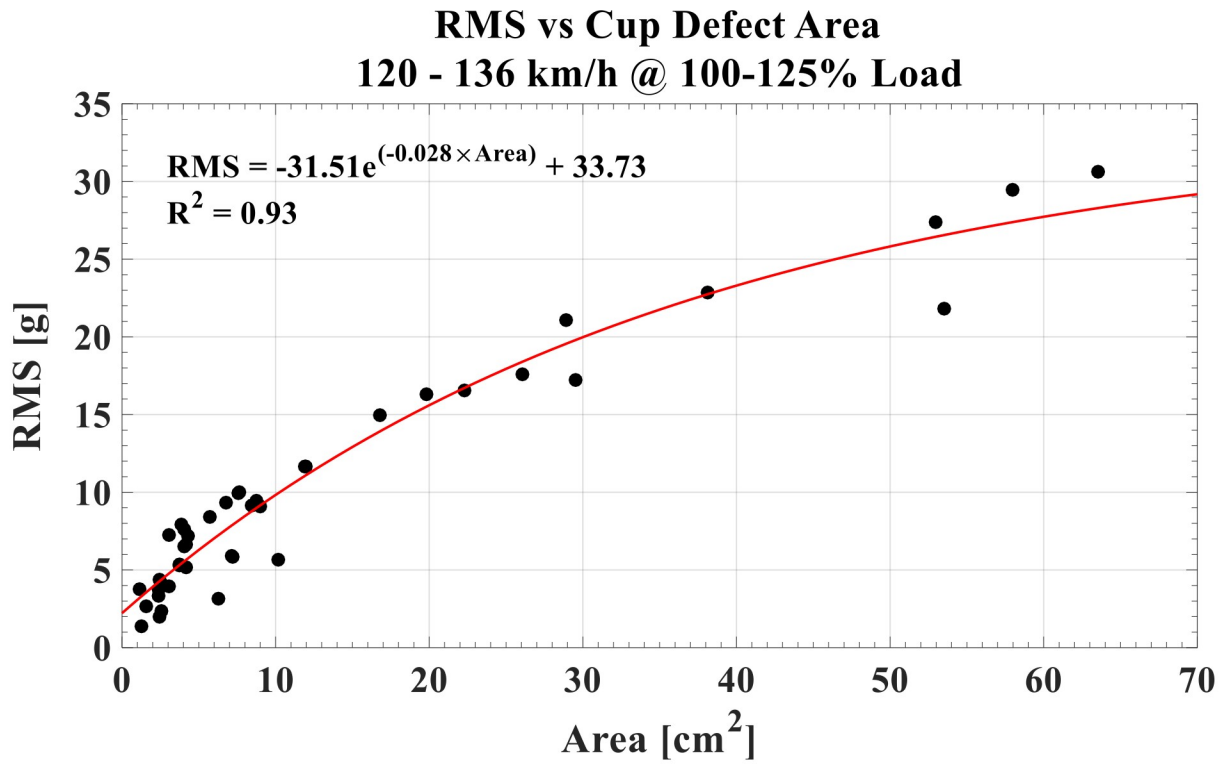

Figure 11: Improved Cone defect size correlation at 137 km/h (85 mph) and full load [22]

CHAPTER III

EXPERIMENTAL SETUP AND PROCEDURES

The efficacy of reconditioned railroad tapered-roller bearings and the effect of the reconditioning process can be assessed through thermal and vibration analysis. To that end, two batches of reconditioned railroad tapered-roller bearings were tested over the past two years.

The first batch of bearings examined involved twelve class F bearings that were chosen by engineers from the Transportation Technology Center, Inc. (TTCI) in consultation with a bearing reconditioning facility. These twelve bearings were first shipped to the University Transportation Center for Railway Safety (UTCRS) at the University of Texas Rio Grande Valley (UTRGV) to be tested before undergoing the reconditioning process. Once this initial testing was performed, the twelve bearings were shipped back to the reconditioning facility to go through their reconditioning process. After they were reconditioned, the twelve bearings were shipped to UTRGV to be tested again. The effect of the reconditioning process on the thermal and vibrational behavior of the twelve bearings was assessed by comparing their performance before and after reconditioning.

The second batch of testing involved eight class K bearings that were selected by engineers from TTCI in consultation with a bearing reconditioning facility. These eight bearings went through the reconditioning process and were then shipped to UTRGV to undergo extended service life testing. The service life testing consisted of running the eight bearings for a simulated

400,000 km (~250,000 mi) of service or until the bearing(s) developed a defect (e.g., a spall on the cup raceway). The thermal and vibrational performance of the bearings was closely tracked during this extended service life testing and was used to assess the efficacy of the reconditioning process.

It is important to note at this point that one of the main differences between the two batches of bearings tested relates to the cause of removal from rail service. The cause of removal from service for the first batch of twelve bearings was unknown, whereas the second batch of eight bearings were removed from service for reasons not related to the bearings (i.e., Why Made Code WM-11). For both batches of bearings tested, only the bearing outer ring (cup) was reconditioned. The rest of the components used to build the bearings were new or defect-free components shipped to UTRGV by TTCI. Each of the railroad tapered-roller bearings tested for this study were assembled at UTRGV following the Association of American Railroads (AAR) standards and protocols.

The twenty bearings were tested using two identical dynamic four-bearing test rigs at UTRGV, one of which is housed in an environmental chamber that allows the ambient conditions to be controlled in the range from -40°C to 60°C (-40°F to 140°F). The two testers can accommodate four different classes of railroad bearings listed in Table 1. Each tester is equipped with a hydraulic cylinder that allows each test bearing to experience up to 150% of the load of a standard fully-loaded railcar as defined by the Association of American Railroads (AAR) and given in Table 1. For the experiments performed for this study, two main loading conditions were utilized, namely, 153 kN (34.4 kips) per bearing which simulates a fully-loaded railcar (100% load), and 26 kN (5.85 kips) which represents an empty railcar (17% load). Note that the load capacities for both class F and K bearings are similar, as shown in Table 1.

Table 1. Bearing classes and dimensions along with AAR load capacities

Bearing Class	Size [in.]	Load [kN]	Load [lbf]
Class E	6 × 11	117	26,300
Class F	6½ × 12	153	34,400
Class G	7 × 12	169	38,000
Class K	6½ × 9	153	34,400

Each tester is powered by a 22 kW (30 hp) variable speed motor controlled by a variable frequency drive (VFD) to allow the bearings to be tested at various speeds, as listed in Table 2. Both testers utilize two to three industrial fans that produce an air stream velocity of 6 m/s (13.4 mph) to simulate the airflow a bearing experiences in field service.

Table 2. Typical simulated track speeds used to perform the experiments in this study.

Axle Speed [rpm]	Track Speed [km/h]	Track Speed [mph]
498	85	53
560	106	60
799	137	85

3.1 Bearing Assembly

The experiments in this study will include Class F and K bearings as these two classes are the most widely used bearing classes in freight rail transportation in North America. Both classes of bearings are fabricated from AISI 8620 steel and contain hardened tapered rollers. The total width of the outer ring (cup) is the difference between the two bearing classes. Class F bearings have a larger cup with than class K bearing by 2.34 cm (0.92 in). Therefore, class F bearings

need a spacer ring that is larger in width. Class F spacer rings are approximately 3.68 to 3.94 cm (1.45 to 1.55 in) whereas class K spacer rings are between 1.46 to 1.48 cm (0.575 to 0.583 in). Furthermore, more grease is required to be applied in the spacer ring location when assembling class F bearings as opposed to class K bearings. Thus, class F bearings weigh slightly more than class K bearings.

3.1.1 Lubrication

Each tapered roller bearing is lubricated and assembled following the Association of American Railroad (AAR) standards. The quantities of grease applied to each bearing region is specified in Table 3.Due to class F and K bearings utilize identical cone assemblies, each cone assembly requires the same amount of grease. The amount of grease listed under cone assembly is split evenly between the two cone assemblies for each bearing (i.e., each individual cone assembly requires 192.25 mL or 6.5 oz). Previously mentioned, class F haver larger spacer ring regions than class K bearings. An additional 226.2 mL (9 oz) of grease must be applied to the spacer ring region of the class F bearings, while no grease is applied to the spacer region of the corresponding class K bearings.

Table 3. Lubrication (grease) quantities for Class K and Class F bearings

Bearing Class	Total Grease [mL] / [oz]	Spacer Region Grease [mL] / [oz]	Cone Assembly Grease [mL] / [oz]
K	384.5 / 13	N/A	384.5 / 13
F	650.6 / 22	266.2 / 9	384.5 / 13

Once the appropriate amounts of grease are applied to the bearing locations specified in Table 3, the bearing is secured with a seal on each end of the bearing to prevent grease from leaking out of the bearing assembly and avoids contaminants from entering the bearing. After the

bearing is assembled, the bearing is then weighed to ensure that it has been properly lubricated. The weight of the bearings varies depending on the material of the cage used in the cone assembly. For cone assemblies that utilize polyamide (polymer based) cages, class F bearings weigh on average about 30 kg (66 lb) while class F bearings weigh on average about 35 kg (78 lb). The weight of bearings that have cone assemblies built with steel cages will weigh more than those made with polymer cages.

3.1.2 Measurements

Each inner ring (cone) assembly used in this study underwent measurement verification for roller spacing, cage lift, and cage shake. The roller spacing measurements require precision feeler gauges that are inserted between the rollers and the cage to measure the spacing between them. The AAR specifies that roller assemblies having a spacing larger than 1.524 mm (0.060 in) between the rollers and cage should not be returned to service [18]. For the cage lift and cage shake, a chuck device was placed on a table and was used to firmly grip the cone assembly, shown in Figure 12. A dial gauge was used to measure the movement of the cage with respect to the cone to obtain the lateral displacement for cage shake. Similarly, the dial gauge was used to measure the vertical displacement of the cage which provided the cage lift measurements.

The abovementioned measurements were taken to minimize the possibility of roller misalignment due to abnormal spacing. Additionally, bearing lateral measurements were taken before the bearing was sealed. The minimum and maximum lateral measurements for each test bearing were recorded to ensure the correct size spacer ring was selected. This lateral measurement was performed using a dial gauge with the desired measurement ranging between 0.0584 cm and 0.711 cm (0.023 in to 0.028 in). The spacer ring serves a significant role in preventing the bearing from rolling slightly skewed.

Figure 12. Inner ring (cone) assembly measurements: cage lift (left) and cage shake (right)

The inside diameter of the cones and the outside diameter of the test axle were also carefully evaluated before the bearings were pressed onto the test axle. The inside diameter of each cone was measured using a 3-point internal micrometer, shown in Figure 13 (left), to ensure the cone diameter was within the AAR tolerance of 15.7150 to 15.7188 cm (6.1870 to 6.1885 in) [18]. Each axle shaft was measured using a 15.24 to 17.78 cm (6 to 7 in) outside micrometer, shown in Figure 13 (right). A total of eight measurements were recorded around each of the four cone assembly locations to verify that the axle was within the AAR tolerance of 15.7239 cm to 15.7264 cm (6.1905 in to 6.1915 in). The recorded measurements for the cones and axles utilized in this study are given in Appendix A.

Figure 13. Three-point internal micrometer (left) and outside micrometer (right)

3.2 Chamber Four-Bearing Tester and Four-Bearing Tester

The Chamber four-bearing tester (C4BT) and four-bearing tester (4BT), shown in Figure 14, can accommodate four Class K, F, E or G tapered-roller bearings. These railroad bearings were assembled following AAR (Association of American Railroads) standards and pressed onto a custom test-axle by utilizing a 300-ton hydraulic press. The bearings on these testers were labeled, starting at the pulley, as B1, B2, B3, B4, respectively, as shown in Figure 15. The C4BT/4BT applies a load using a hydraulic cylinder to the two middle bearings or test bearings (B2 and B3) which are referred to as “top-loaded” bearings. The two outer bearings (B1 and B4) counteract the applied load from the middle bearings, denoted as “bottom-loaded” bearings. In field conditions, the freight train bearings are “top-loaded”, similar to the two middle bearings (test bearings) on the UTCRS C4BT/4BT. The data for this study will be taken from the two middle bearings to simulate field service conditions. The C4BT was contained within a

temperature-controlled environmental chamber that can generate an ambient temperature as low as -40°C (-40°F) and as high as 60°C (140°F).

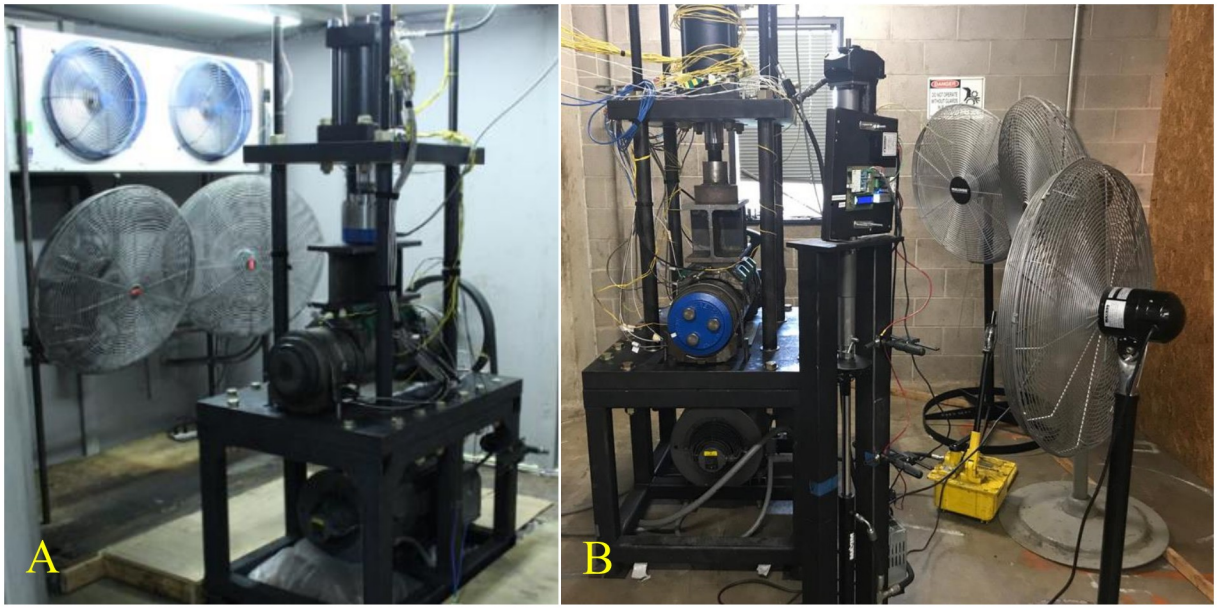

Figure 14. A) Chamber Four-Bearing Tester (C4BT). B) Four-Bearing Tester (O4BT).

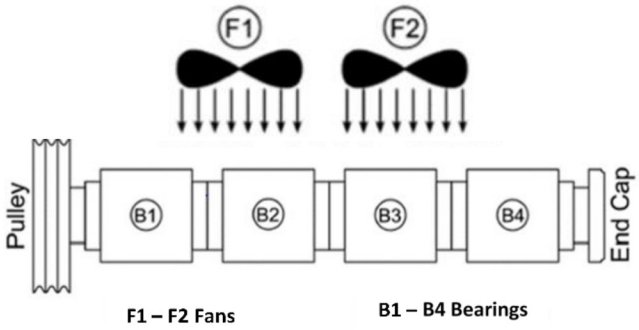

Figure 15. Top view of C4BT/4BT with bearing locations labeled.

3.3 Tester Instrumentation

Each of the middle two bearings was equipped with an AdapterPlus™ bearing adapter and an AdapterPlus™ suspension pad. The AdapterPlus™ bearing adapters were machined to accommodate two K-type bayonet thermocouples, two 70g accelerometers, and one 500g PCB accelerometer. Each K-type bayonet thermocouple was aligned with the middle of each cup

raceway. Additionally, each bearing was also equipped with a K-type thermocouple that is placed between the two bayonet thermocouples and held in place with a hose clamp. The 500g PCB accelerometer was placed in the radial (R) location, and the two 70g accelerometers were placed in the Smart Adapter (SA) and Mote (M) location, shown in Figure 16. Two additional thermocouples were placed on the fan and non-fan side of the test rigs to record the surrounding ambient temperature.

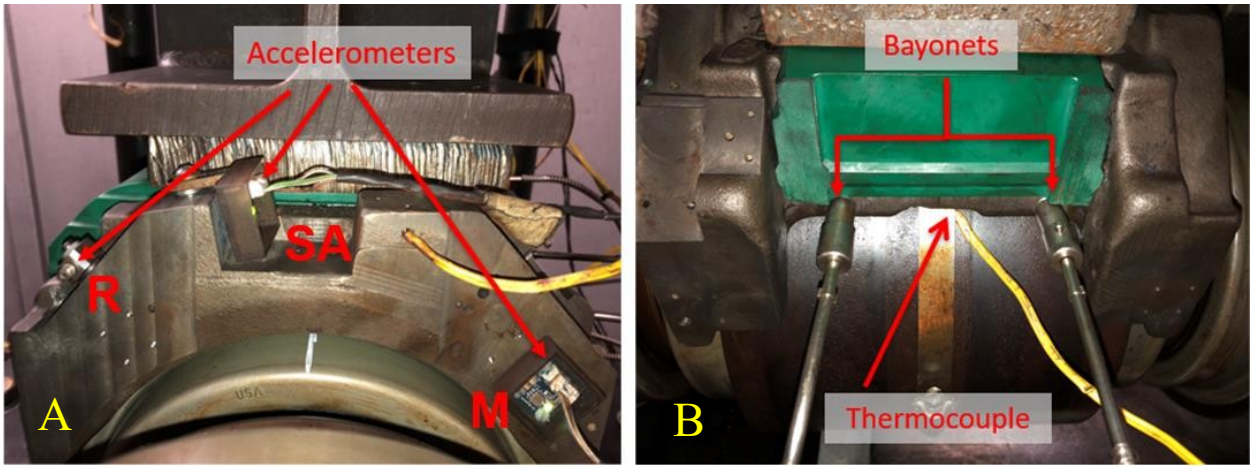

Figure 16. Modified C4BT/4BT adapters showing: A) Vibration Sensors B) Temperature Sensors

3.4 Data Acquisition

The data was collected from the two test rigs by the instrumentation equipped on the test bearings. Temperature data was acquired using K-type thermocouples and K-type bayonet thermocouples; vibration data was acquired using 500g PCB accelerometers and 70g accelerometers (created by the UTCRS research team). The data from the instrumentation was recorded using the National Instruments (NI) NIcDAQ-9174 data acquisition system (DAQ) which was programmed using LabVIEW™ software. The data from the K-type thermocouples was collected every twenty seconds at a sampling rate of 128 Hz for half a second using a NI 9213 card. The accelerometer data was collected every ten minutes at a sampling rate of 5,120

Hz for sixteen seconds using a NI 9234, a NI 9239, and a NI USB-6008 card. The angular speed and motor power data was collected every twenty seconds at a sampling rate of 100 Hz for half a second using a NI-9205 card.

The data from the thermocouples, accelerometers, and motor power was then analyzed using a mathematical computing program, MATLAB™, to generate the bearings temperature, vibration, and motor power profiles. The temperature profile was created by averaging the two K-type bayonet thermocouples and the K-type thermocouple for each bearing, providing a complete temperature average for its total width. The accelerometer that resides in the Mote (M) location was used as a resource backup for the Smart Adapter (SA) accelerometer. Hence, the accelerometer in the SA location was used to show the vibration profiles.

CHAPTER IV

RESULTS AND DISCUSSION

The testing performed in this study consisted of two batches of bearings, with twelve bearings in the first batch (batch 1) and eight bearings in the second batch (batch 2). The bearings were removed from service and sent to a reconditioning facility to undergo a reconditioning process. For the first batch, the engineers from the Transportation Technology Center Inc. (TTCI) visited the reconditioning facility and selected twelve bearings for this study before they were reconditioned. The bearings were selected randomly from a group with similar defects (raceway spalls) with a removal reason that was unknown. For the second batch, the bearings were selected in the same manner, however, the bearing removal reason was known. Removed bearings must have a removal code called a "Why Made Code". The second batch of bearings were all tagged with "Why Made Code 11" which denotes a removal code designated for bearings that were removed from service for reasons not associated with the bearings themselves. The bearings under this removal code are commonly removed from the field due to wheel replacements. After a bearing is removed from an axle, the bearing must be sent to an authorized reconditioning facility to undergo a complete disassembly and inspection.

It was noticed that the reconditioning process was different for each batch of bearings. This observation was made based on the positioning of the stress-relief holes that were done during reconditioning. For batch 1, most of the outer rings (cups) had their stress-relief holes

located near the edge of the spacer ring region with some cups also having stress-relief holes in the middle of the raceway, as pictured in Figure 17. These stress-relief holes were mostly circular in shape and noticeably larger than those from batch 2. The cup stress-relief holes from batch 2 were smaller in size and mostly located close to the middle of the raceway. These stress-relief holes were both circular-shaped and oval-shaped, as depicted in Figure 18.

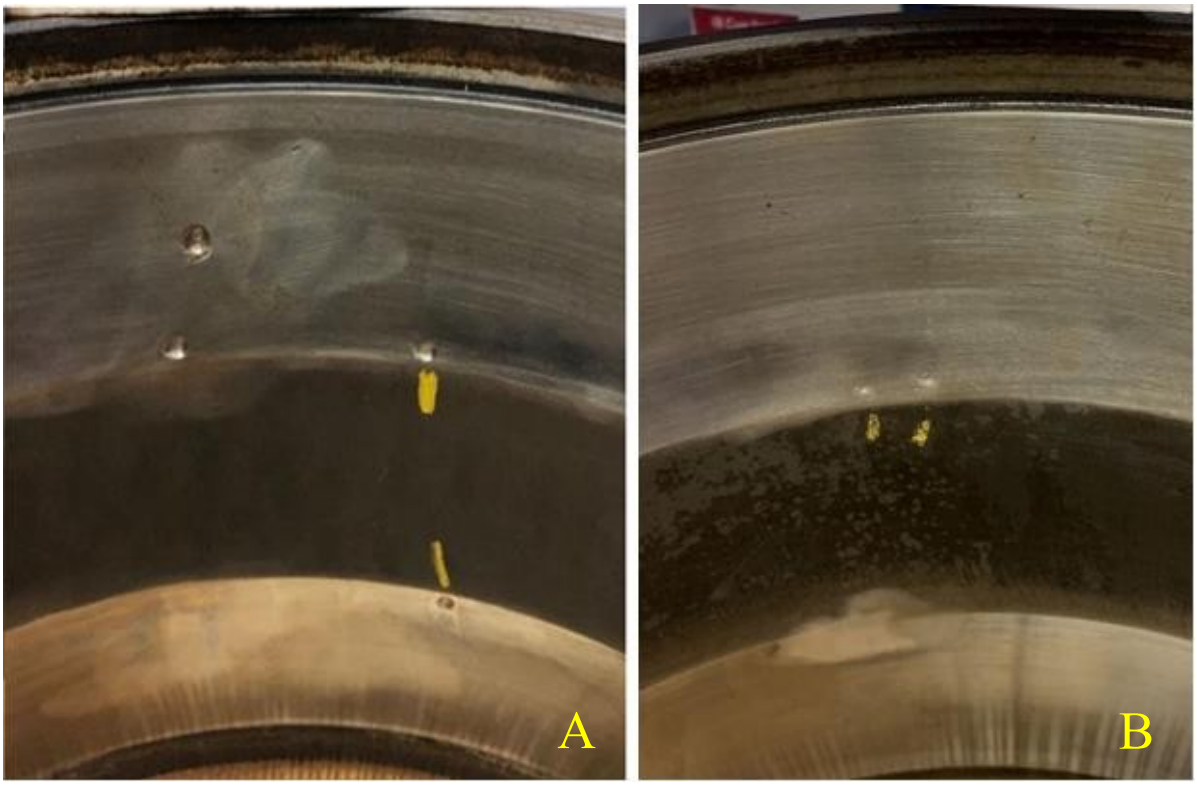

Figure 17. Stress-relief holes for batch 1: A) Stress-relief holes in the middle of the raceway and near the edge of the spacer ring region, B) Two circular closely grouped stress-relief holes near the edge of the spacer ring region

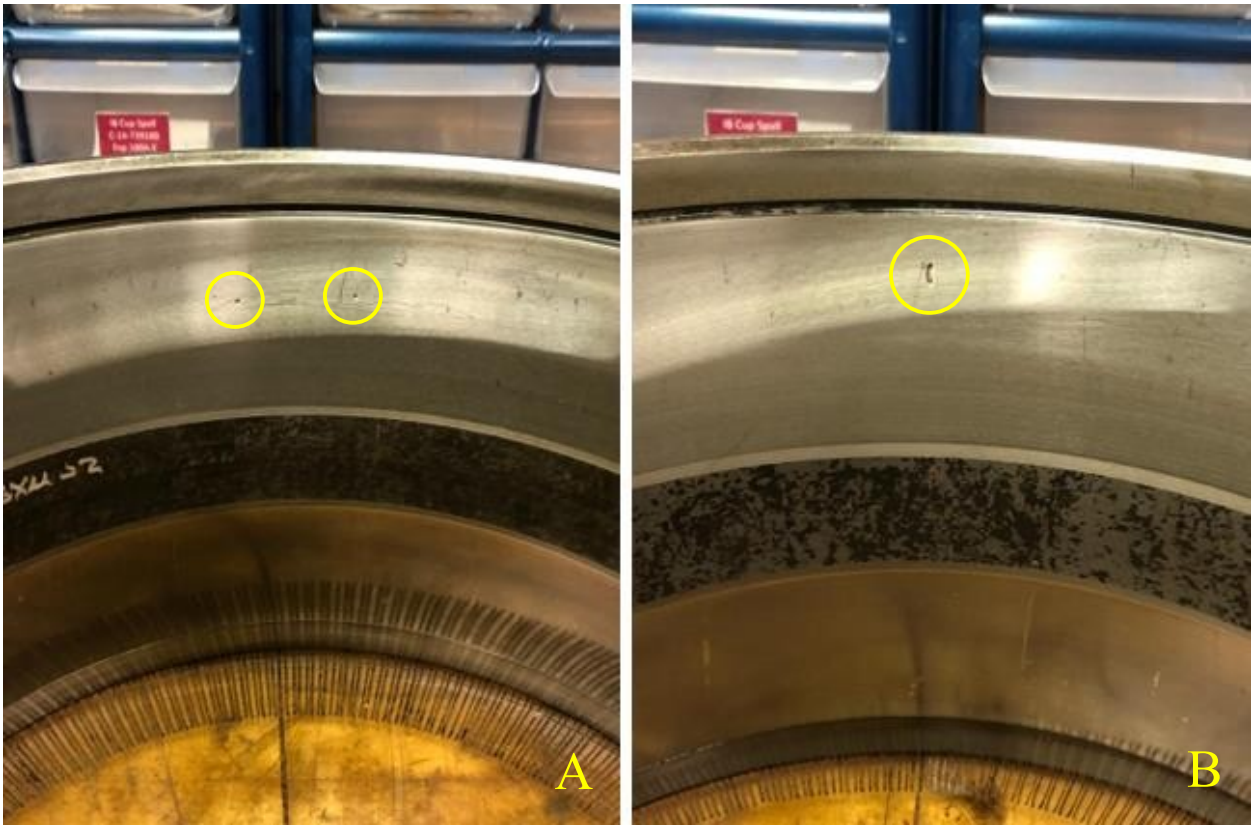

Figure 18. Types of stress-relief holes for batch 2: A) Two closely grouped circular stress-relief holes near the middle of the cup raceway, B) A singular oval-shaped stress-relief hole near the middle of the cup raceway

4.1 Batch 1 Bearings

Twelve bearings were sent to the University of Texas Rio Grande Valley (UTRGV) to be tested at the UTCRS facility after being selected from the reconditioning facility. The pre-reconditioning phase of the testing consisted of running the bearings on the chamber four-bearing tester for about 16,093 km (10,000 mi) and recording reference vibration and temperature histories for each test bearing. These reference vibration and temperature profiles were compared to those acquired post-reconditioning to assess the efficacy of the reconditioning process. After the twelve bearings operated for about 16,093 km (10,000 mi) at the UTCRS facility, they were thoroughly inspected, and they were sent to a designated reconditioning facility, chosen by TTCI

engineers, to undergo the reconditioning process.

Once the bearings were reconditioned, they were sent back to UTRGV to begin the next stage of testing. Before the second phase of the testing commenced, the twelve bearings were thoroughly inspected and the outside surface of the bearing cup (outer ring) was marked with indices, marking the locations of reconditioning stress-relief holes based on their severity with the most severe labeled “Index I”, second most severe labeled “Index II”, and so forth. The post-reconditioning phase of the testing consisted of running the bearings about 16,093 km (10,000 mi) with the bearing cup (outer ring) positioned at the same exact orientation as when it was tested before reconditioning. The latter allows for a direct comparison of the vibration and temperature profiles before and after the reconditioning process.

After that, the test is momentarily stopped so that the bearing cup is rotated to align the region labeled as “Index I” at the top center where the maximum load is applied. Figure 19 shows the bearing cup location labeled as “Index I”. The test is then allowed to run at full load and 137 km/h (85 mph) until a defect develops or the bearings have run for about 96,560 km (60,000 mi), at which point, the test is stopped, and a full teardown and disassembly followed by a thorough inspection of the test bearings is performed. The technical inspection consists of opening the bearings and identifying any defects that may have developed on the outer ring (cup) of the bearing and carefully documenting the condition of the bearing cup raceways. If the test bearings did not develop any defects, they were reassembled using the same grease that was used at the start of the second phase of testing and mounted on the test axle following the same configuration that was used at the beginning of the second phase of testing. Again, the test bearings were aligned so that the cup region corresponding to “Index I” was top center where the maximum load is applied. The test bearings are run until they develop defects or reach 193,120

km (120,000 mi) of operation. A complete teardown and inspection were performed if either milestone was reached.

Figure 19: Picture on the left side shows test bearing 2 (B2) before the reconditioning process. The picture on the right shows test bearing 2 (B2) after it was reconditioned with the "Index I" region shown.

4.1.1 Experiment 211B

Experiment 211B featured two test bearings (B1 and B2) that were previously flagged and removed from service. As mentioned previously, the removal reason for the bearings in batch 1 was unknown and could not be tracked. TTCI engineers selected these bearings and arranged for them to be sent to UTRGV to be run on the UTCRS chamber four-bearing tester (C4BT). As described earlier, the first phase of testing consisted of running the test bearings for 96 hours or until the bearings reached steady state operating conditions. The first two test bearings ran for a total of 14,867 km (9,238 mi) while the vibration and temperature reference profiles were collected, as presented in Figure 20. Following the test, a thorough technical inspection of the two test bearings was performed and did not find any defects on the bearing cup raceways. The test bearings were initially run at a speed of 64 km/h (40 mph) and 17% load capacity

(simulating an empty railcar) to allow the grease to break-in, after which, the test conditions were changed to 137 km/h (85 mph) and 100% load (simulating a full railcar).

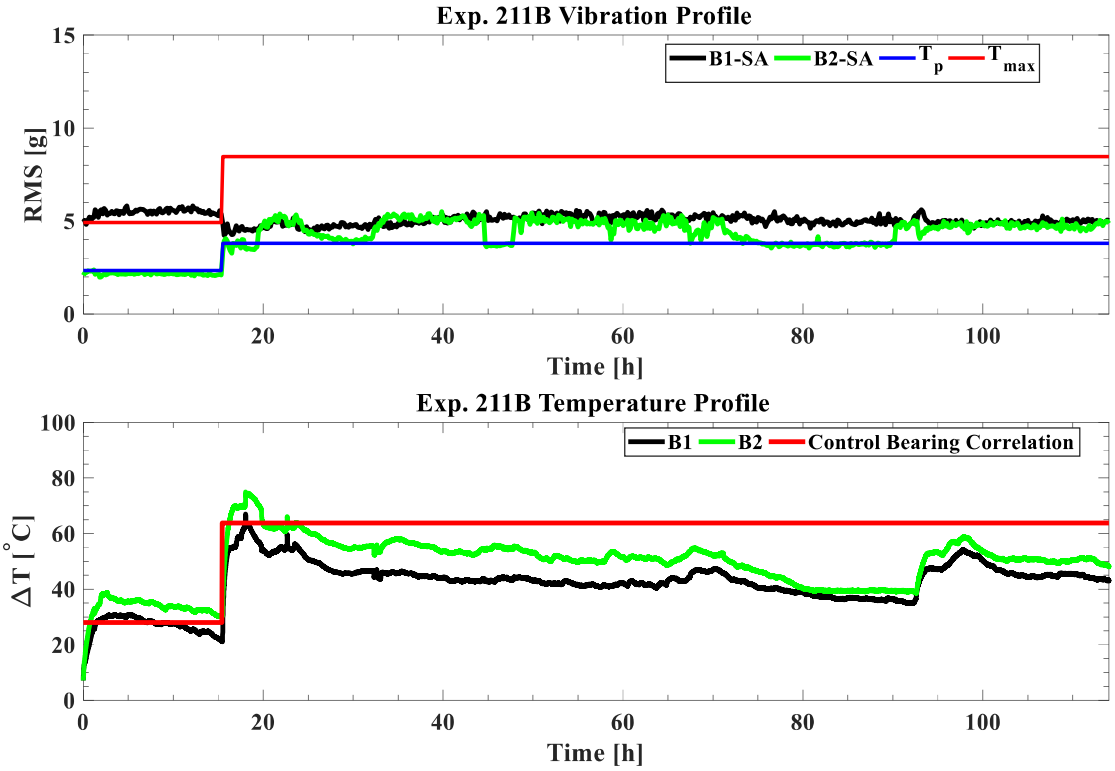

Figure 20: Vibration and temperature profiles for Experiment 211B

Analyzing Figure 20, two observations can be made regarding the temperature profiles of both test bearings. First, both bearings are operating below the average normal operation temperature correlation for control (defect-free) bearings denoted by the red solid line, except for the initial break-in period of the grease and the period immediately following sudden changes in operating conditions. Second, B2 ran slightly hotter (≤ 10°C or 18°F) than B1 throughout the entire experiment meaning that B2 experienced more frictional heating than B1.

Examining the vibration signatures of test Bearings 1 and 2, a couple of observations can be made. First, the accelerometer mounted on the Smart Adapter (SA) location of bearing 1 (i.e., B1-SA) was above the solid red line, denoted as 'T_{max}', only during the initial break-in period

when the bearings were running at 17% load (empty railcar) and 64 km/h (40 mph). Once the operating conditions were set to 100% load and 137 km/h (85 mph), B1-SA ran with vibration levels that were below the maximum threshold (T_{max}) but above the preliminary threshold (T_p) represented by the solid blue line. Second, test bearing B1 ran with stable vibration levels throughout the duration of testing under full load and speed while test bearing B2 exhibited several fluctuations in the vibration RMS value in the range of ±1.25g during that same period, as seen by the data presented by B2-SA. Upon careful inspection of this test bearing after the completion of the experiment, there were no discernable defects that can account for that erratic vibration behavior, so it was assumed that the cause was either geometric in nature or a result of the bearing component tolerances.

4.1.2 Experiment 211C

Upon the conclusion of the first phase of testing, the test bearings were sent to a designated facility to be reconditioned. Once they were reconditioned, they were sent back to UTRGV to commence the second phase of testing, which consisted of a service life performance testing where the bearings were run until they either developed a defect or reached a milestone distance.

In Experiment 211C, test bearings 1 and 2 that were previously run in Experiment 211B and were later reconditioned as exhibited by the stress-relief holes on the bearing cup raceways (refer to picture on the right in Figure 19), were run on the chamber four-bearing tester (C4BT). Initially, the reconditioned bearings 1 and 2 were set up utilizing the same exact configuration and bearing cup orientation on the test axle as that used for Experiment 211B. The latter was done to allow for a direct comparison of the vibration and temperature profiles pre- and post-reconditioning, as presented in Figure 21 and Figure 22. The test bearings ran a total of 21,905

km (13,611 mi) before the test was momentarily stopped to rotate the bearing cups of the two test bearings to the location marked as “Index I”, which corresponds to the region that contained the most stress-relief holes generated by the reconditioning process.

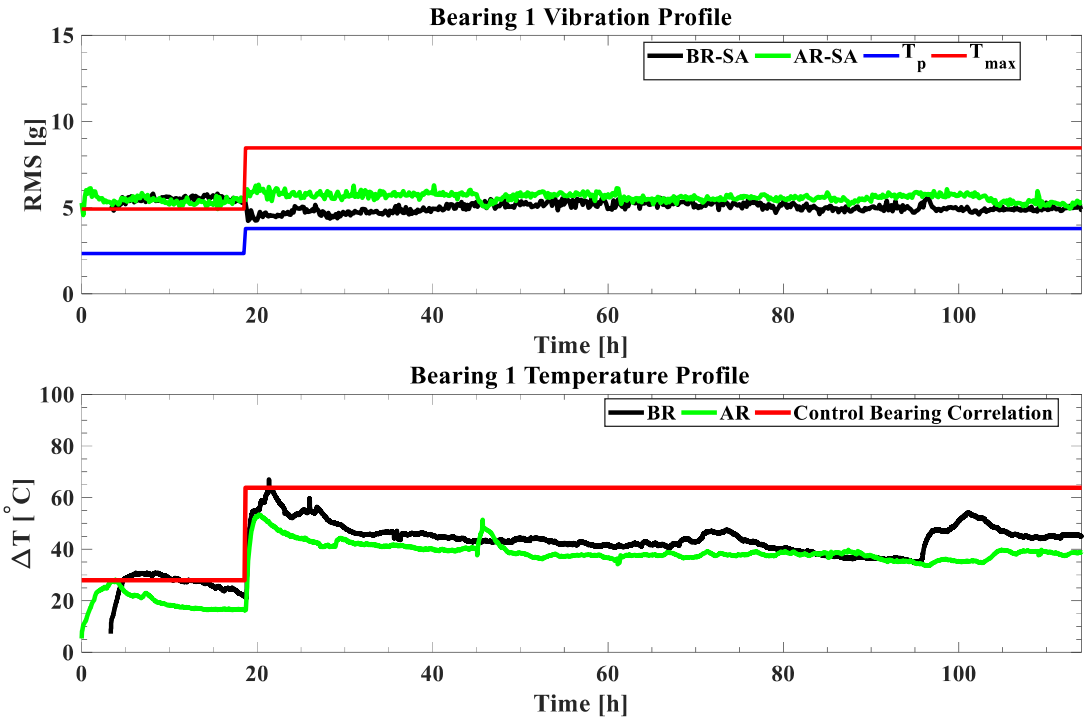

Figure 21: Vibration and temperature profiles for test bearing 1 (B1) before (BR) and after (AR) the reconditioning process

The vibration and temperature profiles for test bearing 1 (B1) are displayed in Figure 21, where BR stands for ‘Before Reconditioning’ and AR stands for ‘After Reconditioning’. Analyzing the temperature profiles, it can be observed that the operating temperature of test bearing 1 after reconditioning was noticeably below the average operating temperature for defect-free bearings (solid red line). Moreover, the operating temperature of test bearing 1 was steadier and slightly lower after the reconditioning process as compared to before reconditioning.

Examining the vibration profile for test bearing 1, the following observations can be made. First, the vibration levels picked up by the accelerometer located in the smart adapter (SA)

position before (BR) and after (AR) reconditioning were above the solid red line, denoted as 'T_{max}', during the initial break-in period when the bearings were running at 17% load (empty railcar) and 64 km/h (40 mph). In addition, comparing the vibration data from the smart adapter (SA) locations before and after reconditioning, it can be observed that the vibration levels after the reconditioning process were similar (within 1g) to those before this bearing was reconditioned. The latter implies that the reconditioning process did not have any substantial effect on the vibration characteristics of test bearing 1 (B1). In summary, the reconditioning process seems to have stabilized and slightly improved the operating temperature of test bearing 1 but did not have a substantial effect on the vibration levels within the bearing.

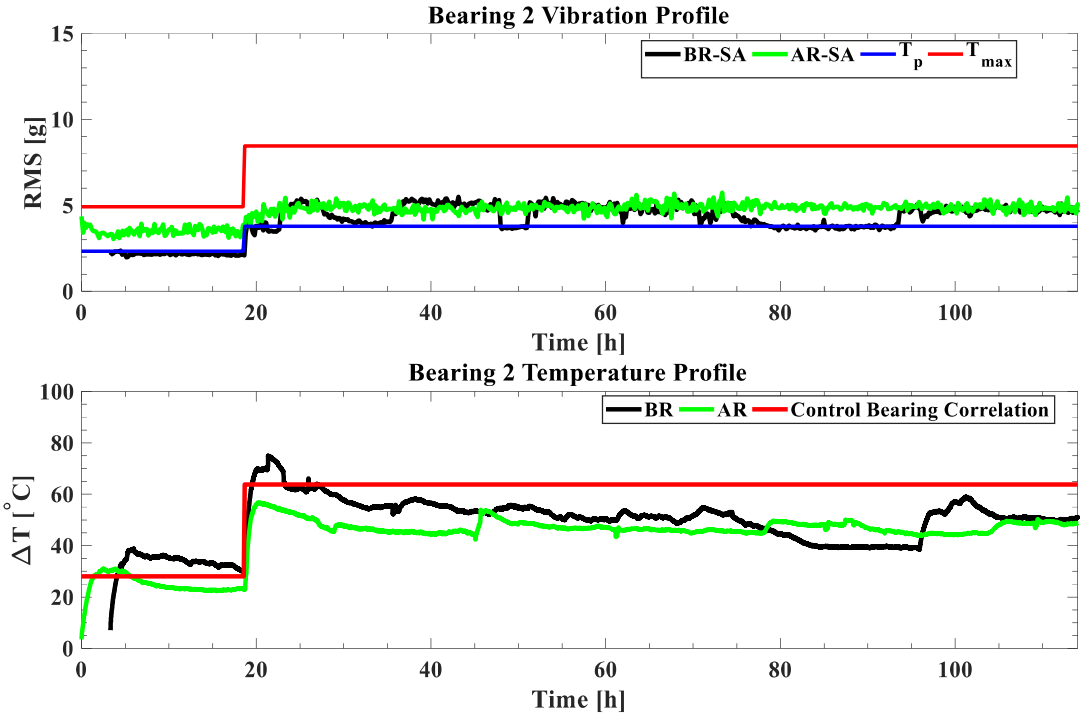

Figure 22: Vibration and temperature profiles for test bearing 2 (B2) before (BR) and after (AR) the reconditioning process

The vibration and temperature profiles for test bearing 2 (B2) are given in Figure 22. Analyzing the temperature profiles for test bearing 2 before (BR) and after (AR) reconditioning,

it can be observed that the reconditioning process helped stabilize and noticeably lower the operating temperature of this test bearing, as was the case for test bearing 1. Comparing the vibration profiles for test bearing 2 before and after reconditioning, the vibration levels after reconditioning are much more stable than before reconditioning where the vibration levels exhibited some distinct fluctuations. Hence, the reconditioning process seems to have improved the overall temperature and vibration performance of test bearing 2 more so than it did for test bearing 1.

Following the indexing of the test bearings, they were run continuously with very minimal interruption until they reached 98,434 km (61,164 mi) of operation after reconditioning, at which point, a complete teardown and disassembly were performed followed by a thorough visual inspection. The vibration and temperature profiles of the two test bearings are provided in Figure 23. The inspection revealed no major changes to the conditions of the test bearings and their cup raceways. Hence, the test bearings were rebuilt using the same components and original grease that was used at the beginning of Experiment 211C and were mounted utilizing the same configuration as before the teardown, with the bearing cups oriented so that the region marked as “Index I” was placed top center where the maximum load was applied.

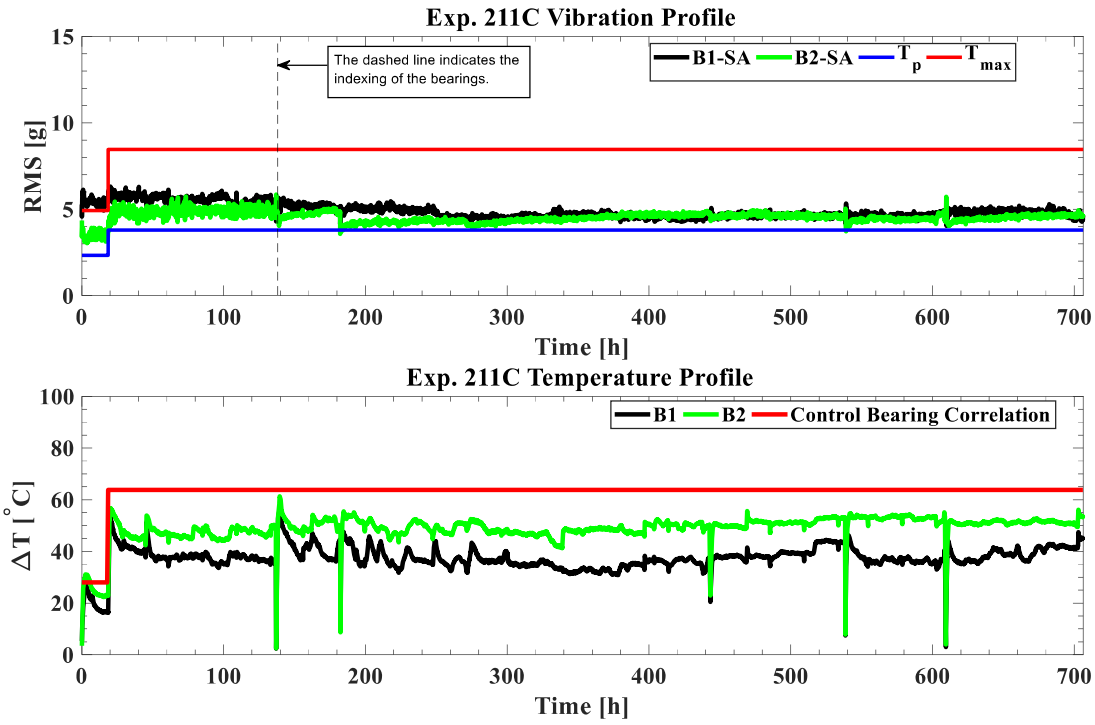

Figure 23: Vibration and temperature profiles for Experiment 211C before the complete teardown and inspection. The cups of the two test bearings were oriented with “Index I” in the top center location after 21,905 km (13,611 mi) of operation

After the test bearings ran an additional 45,866 km (28,500 mi), the bearing condition monitoring algorithm indicated that a defect had initiated on one of the cup raceways of test bearing 2 (B2). The defect initiation was indicated by the sudden increase in the vibration levels of B2 around 350 hours into the experiment, as can be observed in Figure 24. Note that the sudden increase in the vibration levels of test bearing 1 (B1), that lags by a few hours, is a direct consequence of crosstalk between the two test bearings, where B1 picks up the loud vibrations from B2. Interestingly, the operating temperatures of both B1 and B2 remain well below the average operating temperature of defect-free (healthy) bearings at the same load and speed, with B2 running, on average, about 12°C (22°F) hotter than B1.

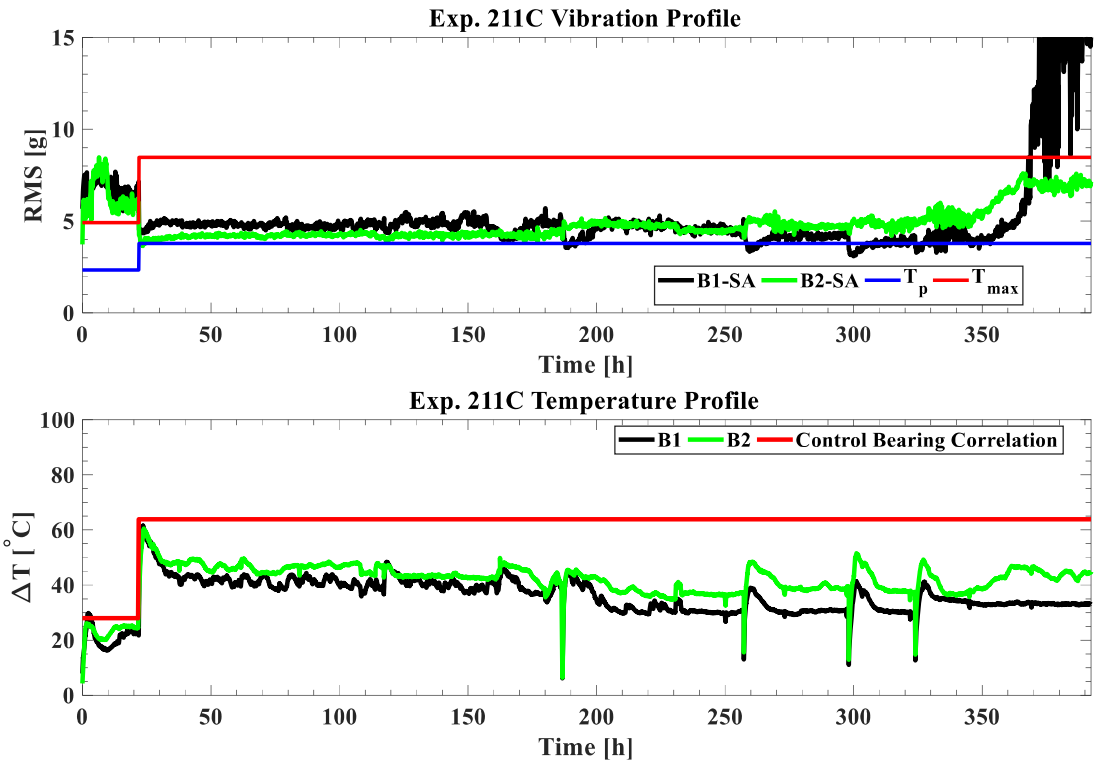

Figure 24: Vibration and temperature profiles for Experiment 211C after the completion of the first teardown and inspection

Table 4 shows the Level 1 analysis for B1 and B2 at the end of the experiment for the last 6 days of testing. Examining the RMS values, it can be seen that the B1 accelerometer in the SA location was reading an RMS value of 9.8g and 14.8g for the last two columns, surpassing the T_{max} which indicates the presence of a defect. The B2-SA RMS readings were around 7.0g, surpassing the T_p and indicating the possibility of a defect present within the bearing. Hence, the defect detection algorithm proceeds to Level 2 analysis.

Table 4: Experiment 229C test Bearing 1 and 2 Level 1 analysis RMS values at the end of the experiment

Experiment 211C						
Day	1	2	3	4	5	6
Load [%]	100	100	100	100	100	100
Speed [RPM] / [km/h]	796 / 137	796 / 137	796 / 137	796 / 137	796 / 137	796 / 137
B1-SA [g]	3.8	3.9	3.9	4.2	**9.8**	**14.8**
B2-SA [g]	4.8	4.8	5.2	5.4	6.9	7.0
T_p [g]	3.8	3.8	3.8	3.8	3.8	3.8
T_{max} [g]	8.5	8.5	8.5	8.5	8.5	8.5

Table 5 displays the results of the Level 2 analysis for B2 at the end of the experiment for the last 6 days of testing. The table identifies the type of local defect detected and the defect percent certainty. The results of Table 5 clearly indicate the presence of an outer ring (cup) defect with a percent certainty of up to 99%.

Table 5: Test bearing 2 (B2) Level 2 analysis at the end of Experiment 211C

Test Bearing 2 (B2)							
	Day	1	2	3	4	5	6
	Speed [RPM] / [km/h]	796 / 137	796 / 137	796 / 137	796 / 137	796 / 137	796 / 137
SA	Max/Sum [%]	**79**	**96**	**99**	**99**	**99**	**98**
	Highest NDE	**Cup**	**Cup**	**Cup**	**Cup**	**Cup**	**Cup**

Since the bearing condition monitoring algorithm indicated that a defect had developed, the experiment was stopped after the test bearings had run 52,721 km (32,759 mi) from the last teardown and inspection. Consequently, a second teardown and thorough visual inspection

ensued. The visual inspection confirmed the findings of the bearing condition monitoring algorithm that a defect had initiated on one of the bearing cup raceways. A picture of the defect that developed is provided in Figure 25.

Figure 25: A picture of the defect that developed on test bearing 2 (B2) after 151,154 km (93,923 mi) of total operation since the bearing was reconditioned

Looking at Figure 25, it can be observed that the defect that developed on B2 initiated from the two stress-relief holes that were made during the reconditioning process and propagated across the width of the cup raceway. The size of the spall (defect) that developed on the cup raceway is about 1.50 cm^2 (0.23 in^2). At this point, the test bearings have run a total of 151,154 km (93,923 mi) of operation since they were reconditioned. A visual inspection of B1 revealed no defects on the cup raceways but the stress-relief holes were starting to grow slightly. That confirms that the elevated vibration levels picked up by the B1-SA accelerometer were an artifact of the crosstalk with the adjacent defective bearing (B2).

4.1.3 Experiment 212B

Similar testing was performed on bearings 3 and 4 (B3 and B4) in Experiment 212B as that carried out in Experiment 211C. The test bearings were run using the same operating conditions for speed and load. The bearing condition monitoring algorithm indicated that a defect had developed on test bearing 3 (B3) around 45 hours into the experiment, as can be seen in Figure 26. Test bearing 3 experienced a steady increase in its vibration levels while the operating temperatures for both B3 and B4 remained below the average operating temperature of defect-free (healthy) bearings at the same speed and load. The experiment was stopped after the test bearings had run 14,001 km (8,700 mi) of operation and a complete teardown and visual inspection were performed.

Test bearing 3 (B3) had two visible stress-relief holes, one in the middle of the cup raceway, and a second at the edge of the spacer ring region right below the first one, as pictured in Figure 27. These stress-relief holes were placed directly under the full load path. These bearings were tested using the same configuration and operating conditions as those used before the reconditioning process. The visual inspection revealed no defects on the cup raceways of test bearing 4 (B4), but the stress-relief holes were starting to flatten and grow slightly in size.

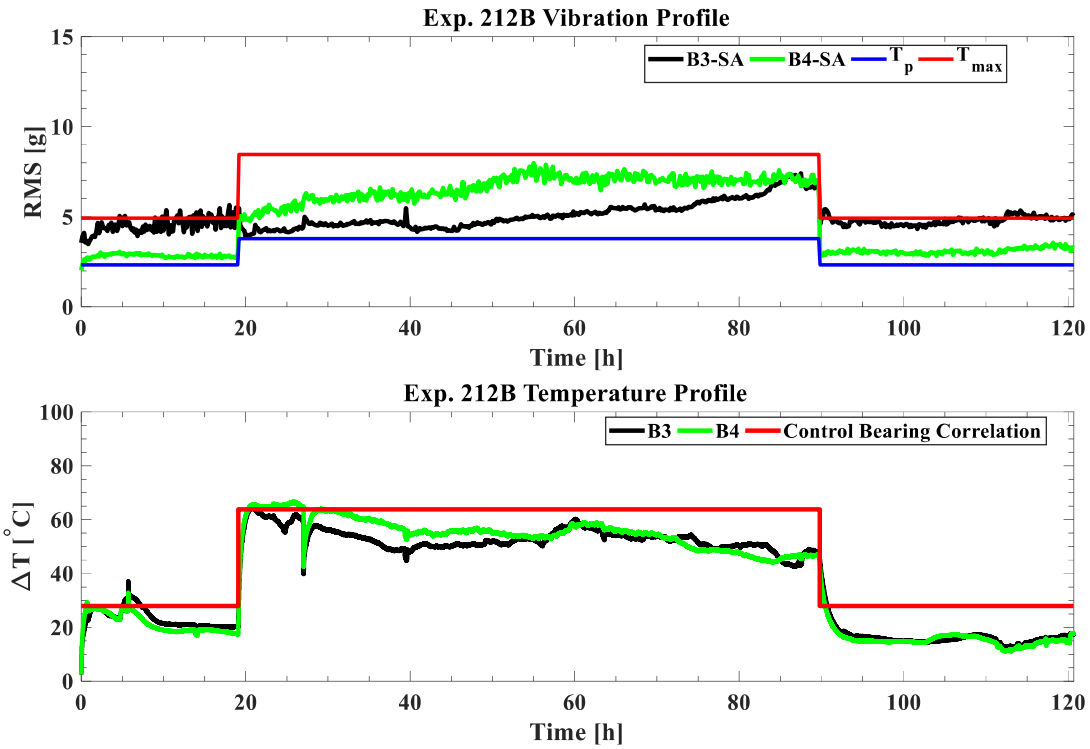

Figure 26: Vibration and temperature profiles for Experiment 212B where bearings 3 and 4 were tested

Figure 27: A picture of the defect that developed on test bearing 3 (B3) after 14,001 km (8,700 mi) of total operation since the bearing was reconditioned

Table 6 shows the Level 1 analysis results for B3 before and after reconditioning for the duration of the first 10,527 km (6,541 mi). It can be seen that the vibration RMS values for B3 exhibited a steady increase in magnitude once the load was set to full (100% load), as demonstrated by the after reconditioning (AR) smart adapter (SA) location accelerometer readings. The AR-SA was reading an average value of 6.5g on day 6. Because the RMS values were above the T_p, this signified that B3 may possibly be defective, and the algorithm proceeds to Level 2 analysis.

Table 6: Level 1 analysis results for test bearing 3 (B3) before and after reconditioning

Test Bearing 3 (B3)						
Day	1	2	3	4	5	6
Load [%]	17	17	100	100	100	100
Speed [RPM] / [km/h]	498 / 85	498 / 85	796 / 137	796 / 137	796 / 137	796 / 137
BR-SA [g]	3.4	3.6	5.3	5.4	5.5	5.5
AR-SA [g]	4.3	4.7	4.3	4.7	5.4	6.5
T_p [g]	2.3	2.3	3.8	3.8	3.8	3.8
T_{max} [g]	4.9	4.9	8.5	8.5	8.5	8.5

Table 7 displays the Level 2 analysis results for B3 after the reconditioning process. The table indicates that B3 has an outer ring (cup) defect with a percent certainty of up to 99%. This, of course, was validated by the teardown and visual inspection performed on B3 and pictured in Figure 27.

Table 7: Level 2 analysis for test bearing 3 (B3) after reconditioning

Test Bearing 3 (B3)							
		1	2	3	4	5	6
	Speed (RPM)	498 / 85	498 / 85	796 / 137	796 / 137	796 / 137	796 / 137
SA	Max/Sum [%]	**83**	**78**	**98**	**97**	**99**	**99**
	Highest Magnitude	**Cup**	**Cup**	**Cup**	**Cup**	**Cup**	**Cup**

4.1.4 Summary of Batch 1 Testing

Similar testing as that described for test bearings 1, 2, 3, and 4 (B1, B2, B3, and B4) was carried out for the remaining eight bearing in batch 1. Table 8 summarizes the testing results for batch 1 where the effects of reconditioning on the vibration and temperature histories of the twelve test bearings were examined. In Table 8, the effectiveness of the bearing reconditioning process can be assessed by contrasting the performance of the twelve test bearings before and after reconditioning. The values listed in Table 8 for the vibration RMS and the temperature difference above ambient are average values obtained from the steady state operation data collected before and after reconditioning excluding the initial break-in periods. Note that for the operating condition of 100% load (full railcar) and 137 km/h (85 mph), the average normal operating temperature above ambient for control (defect-free) bearings is about 64°C (115.2°F) with a maximum RMS value not exceeding 8.5g.

Table 8: Assessing the effects of reconditioning on the vibration and temperature profiles of the twelve test bearings examined in Batch 1

Bearing Number	Testing Phase	RMS			ΔT above ambient		
		Avg. [g]	Max. [g]	Min. [g]	Avg. [°C]	Max. [°C]	Min. [°C]
B1	**BR**	5.0	5.6	4.4	43.9	59.7	34.8
	AR	5.5	6.3	4.3	38.5	51.4	33.6
B2	**BR**	4.5	5.5	3.5	50.9	66.1	38.4
	AR	4.9	5.9	4.3	47.2	54.1	42.4
B3	**BR**	5.4	6.0	5.0	50.6	58.7	44.0
	AR	5.3	7.4	4.2	51.3	60.2	42.6
B4	**BR**	7.5	8.5	6.7	56.3	63.9	46.4
	AR	6.8	7.9	5.7	53.7	63.9	44.2
B5	**BR**	5.2	6.2	4.4	52.3	63.0	41.0
	AR	3.2	4.3	2.6	54.3	64.9	45.2
B6	**BR**	5.5	7.0	3.9	50.9	63.2	41.7
	AR	2.9	3.1	2.5	36.1	46.3	31.2
B7	**BR**	4.0	4.6	3.4	48.1	56.1	39.2
	AR	3.3	4.0	2.9	55.7	64.1	36.5
B8	**BR**	5.5	6.3	4.2	48.2	56.7	38.7
	AR	4.6	5.0	4.0	45.7	59.0	30.7
B9	**BR**	4.6	5.8	3.9	42.9	49.2	37.3
	AR	2.9	3.6	2.4	48.3	59.4	40.8
B10	**BR**	3.2	5.3	2.6	49.6	57.3	44.6
	AR	5.0	5.8	4.2	48.4	58.3	41.2
B11	**BR**	7.8	8.5	6.2	59.6	65.6	52.2
	AR	6.9	7.6	6.0	61.3	68.6	53.0
B12	**BR**	7.4	9.4	6.5	43.7	60.2	37.6
	AR	5.7	7.2	5.1	53.2	67.9	42.9

Examining the data presented in Table 8, it can be observed that the reconditioning process helped lower the vibration levels within the bearing (as measured by the RMS values) for eight of the twelve test bearings. Specifically, bearings B4, B7, B8, and B11 exhibited a slight improvement in their vibration levels after reconditioning, whereas bearings B5, B6, B9, and B12 demonstrated noticeable improvements in their vibration levels as a result of the

reconditioning process. As for bearings B1, B2, B3, and B10, they exhibited no signs of improvement and in the case of B1, B2, and B10, the reconditioning process resulted in higher vibration levels.

In terms of the thermal performance, the reconditioning process helped lower the operating temperature for only five of the twelve test bearings. Specifically, bearings B1, B2, B4, and B8 exhibited a slight improvement in their operating temperatures, whereas bearing B6 demonstrated a significant improvement in its operating temperature as a result of reconditioning. Bearings B3, B5, B10, and B11 experienced no noticeable change in their operating temperatures after reconditioning, however, bearings B7, B9, and B12 exhibited a marked increase in their operating temperatures post-reconditioning.

Moreover, two of the test bearings (B2 and B3) developed spalls on the cup raceways in the region where the stress-relief holes were made during the reconditioning process. Test bearing 2 (B2) developed a spall after running a total of 151,154 km (93,923 mi) after reconditioning, whereas B3 developed a spall after only running a total of 14,001 km (8,700 mi) after the reconditioning process. Finally, note that, due to time constraints, only six of the twelve test bearings underwent extended service life testing beyond what was needed to directly compare the performance of the bearings before and after reconditioning.

4.2 Batch 2 Bearings

Batch 2 consisted of eight bearings handpicked by TTCI engineers from an authorized reconditioning facility. The removal reason for all eight bearings was tagged with an AAR Why Made Code 11, which indicates that these bearings were removed for reasons not associated with the bearings themselves. The bearings underwent the reconditioning process before they were shipped to the University of Texas Rio Grande Valley to be tested at the UTCRS. The

reconditioned bearings were carefully inspected when they arrived at the UTCRS to determine the locations of the most severe reconditioning stress-relief holes on the cup raceways. The most severe locations are decided by stress-relief holes that are larger in area (size) or the presence of two or more holes that are closely located on the cup raceway. To simulate a worst case scenario, the bearing cups were positioned such that the most severely reconditioned regions were under the direct path of the applied load.

The intent for the second batch of testing was for the reconditioned bearings to undergo a complete service life testing, which consists of running the bearings a total distance of about 400,000 km (~250,000 mi) or until a bearing defect develops. To ensure that the test axle and bearings did not develop any defects during the long periods of continuous operation, a complete teardown and a thorough visual inspection were carried out approximately every 100,000 km (~62,500 miles). During this technical inspection, the bearings are completely disassembled, and the condition of the bearing components, especially the cup raceways, is carefully documented. If the test bearings did not develop any defects, the bearings were rebuilt using the same grease, mounted on the test axle in the same location as before the teardown, and run until they developed a defect or reached the next milestone for teardown and inspection (i.e., 200,000 km or ~125,000 mi of operation). This testing cycle continues until either a defect develops or 400,000 km (~250,000 mi) of operation has been reached.

Note that if the defect detection algorithm indicated an abnormal behavior or the possibility of a defect developing within a bearing at any time during testing, the test was immediately stopped, and a complete teardown and visual inspection ensued.

The testing involved running the bearings initially at operating conditions of 85 km/h (53 mph) and 17% load (empty railcar) to allow the grease to break-in and to achieve steady state

operating conditions. This break-in period was usually around one full day of operation. After that, to expedite the testing, the operating conditions were set to 137 km/h (85 mph) and 100% load (full railcar load) for the remainder of the test period. As mentioned earlier, all experiments in batch 2 had the most severe stress-relief holes on the test bearing outer rings (cups) oriented on the top where the maximum load would be applied.

4.2.1 Experiment 225

In Experiment 225, test bearings 1 and 2 (B1 and B2) from batch 2, pictured in Figure 28, were run on the four-bearing tester (4BT). The test bearings ran for a total of 18,660 km (11,595 mi) of operation initially at operating conditions of 17% load and a speed of 85 km/h (53 mph). After the initial break-in period, the operating conditions were set to full-load (100% load) and a speed of 137 km/h (85 mph), and the bearings were run at these conditions until a defect developed or the bearings reached the first milestone for teardown and inspection (i.e., 100,000 km or ~62,500 mi or operation).

Figure 28: Batch 2 – Test bearing 1 (left) and test bearing 2 (right)

The vibration and temperature profiles of the two test bearings along with the corresponding motor power profile for this experiment are plotted in Figure 29. During this experiment, near the 100-hour mark, a noticeable increase in the operating temperatures of both test bearings mirrored by an increase in motor power can be seen. The bearings were run for an additional 40 hours of operation to see whether the bearing operating temperatures would decrease. However, the operating temperatures of both test bearings continued to rise. The vibration RMS values of the two accelerometers mounted on B1 and B2 remained stable and well below the T_{max}, which implied that no spalling had occurred on the two test bearings. During that same period, the motor power increased from 2.8 kW to 4.6 kW in the span of the last 40 hours. Motor power should exhibit a steady behavior when the bearings are operating normally. Thus, the rapid increase in motor power indicated that the test bearings were operating abnormally.

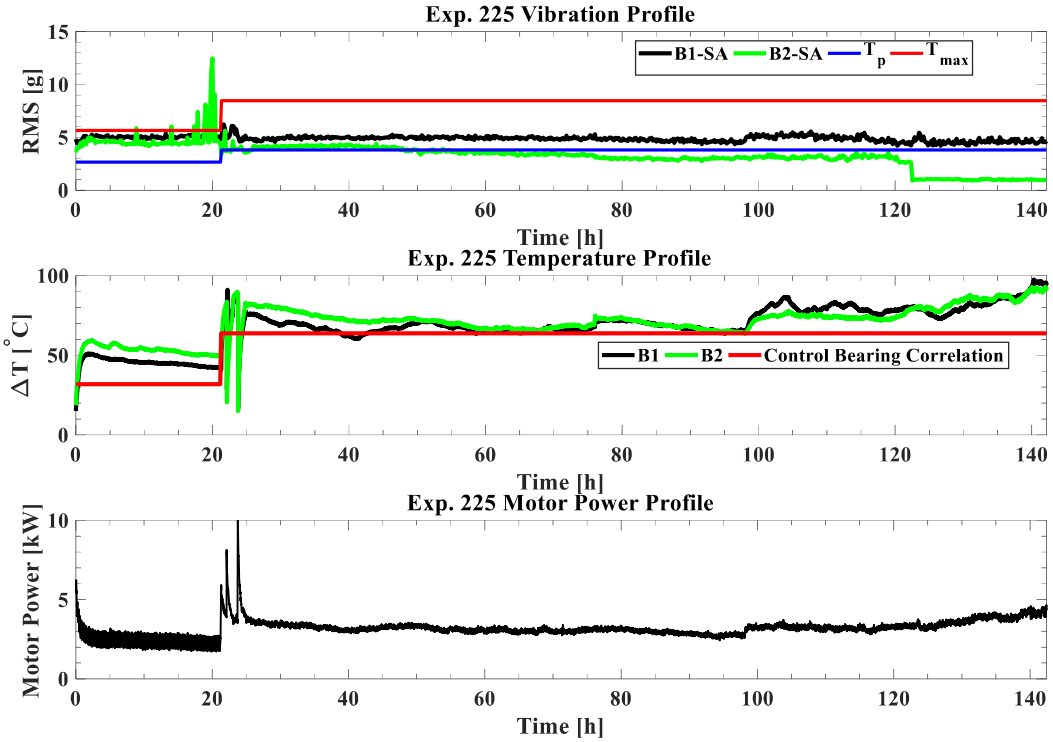

Figure 29: Vibration, temperature, and motor power profiles for Experiment 225

To avoid further damage to the test setup, the experiment was stopped. A full teardown, disassembly, and inspection were subsequently performed on the entire test axle assembly to look for reasons that might have contributed to the sudden increase in operating temperatures and motor power. Hence, the bearings were pressed off from the axle at which point it became evident that all inner rings (cones) from the four bearings on the test axle had spun and had damaged the axle, as can be seen in the picture of Figure 30.

Figure 30: Experiment 225 axle damage

Other than the obvious damage to the test axle, the inspection revealed no noticeable damage to the cups of the test bearings and their raceways, but the cones that spun needed to be

replaced. Therefore, all four bearings were rebuilt using new cone assemblies and fresh grease and were mounted on a new test axle to continue testing bearings B1 and B2 of batch 2.

Note that the exact reason for why the cone assemblies had spun on the test axle was not identified. The test axle and all cone assemblies were carefully measured and documented to ensure that they were within the specified manufacturer's tolerance and met all AAR guidelines. One hypothesis that can explain this incident is that the reconditioned cup raceways of test bearings 1 and 2 caused the cone assembly rollers to be caught misaligned, thus requiring additional power from the motor to maintain the same axle rotational speed. This additional exerted power resulted in the steady increase seen in the operating temperatures of both B1 and B2, and eventually led to the cone assemblies spinning on the axle causing the damage shown in Figure 30.

To prove whether the aforementioned hypothesis holds merit, re-running bearings B1 and B2 using new cone assemblies, fresh grease, and a brand-new axle and observing their thermal and dynamic performance can shed light into this incident.

4.2.2 Experiment 227E

In Experiment 227E, test bearings 1 and 2 (B1 and B2) from batch 2 were run on the four-bearing tester (4BT). These bearings were previously run in Experiment 225 and in all iterations of Experiment 227. Test bearings B1 and B2 ran for a total of 248,356 km (154,321 mi) of operation with initial operating conditions set at 17% load and a speed of 106 km/h (60 mph). After the initial break-in period, the operating conditions were set to full-load and 137 km/h (85 mph) with the intention of running the test bearings for another 100,000 km (62,500 mi). However, the mileage for this iteration was cut short to 79,201 km (49,213 mi) because critical damage was detected, and the motor was halted immediately by the emergency failsafe

measures of the tester put in place to safeguard against catastrophic failure. Upon inspection of the tester, the test axle was found to have sheared, as seen in the pictures of Figure 31. Interestingly, the test axle had sheared between the two test bearings (B1 and B2) and close to the middle of the axle length.

Figure 31: Experiment 227E axle damage

The vibration, temperature, and motor power profiles for Experiment 227E are presented in Figure 32. Examining the thermal performance of B1 and B2, it can be seen that both test bearings were operating at temperatures that are above the maximum threshold for control (defect-free) bearings for the first 110-hours of the test. Following that, the operating temperatures of B1 and B2 experienced several fluctuations with one of these occurring around the 280-hour mark where the operating temperatures above ambient increased from about 48°C (86°F) to 69°C (124°F) and were mirrored by an increase in motor power. Another significant increase in bearing operating temperatures occurred near the 450-hour mark which correlates with an increase in motor power from 1.5 to 2.5 kW. The axle sheared near the end of Figure 32 where an exponential surge in motor power occurred. This can be more clearly seen in Figure 33 which shows the last five hours of this test. At the moment the axle sheared,

the operating temperatures of both test bearings B1 and B2 climbed to 58°C (104°F) above ambient, and the motor power reached a maximum value of 10.4 kW. The exponential spike in motor power exceeded the maximum safety limit and triggered the emergency shutdown countermeasure to avoid catastrophic failure.

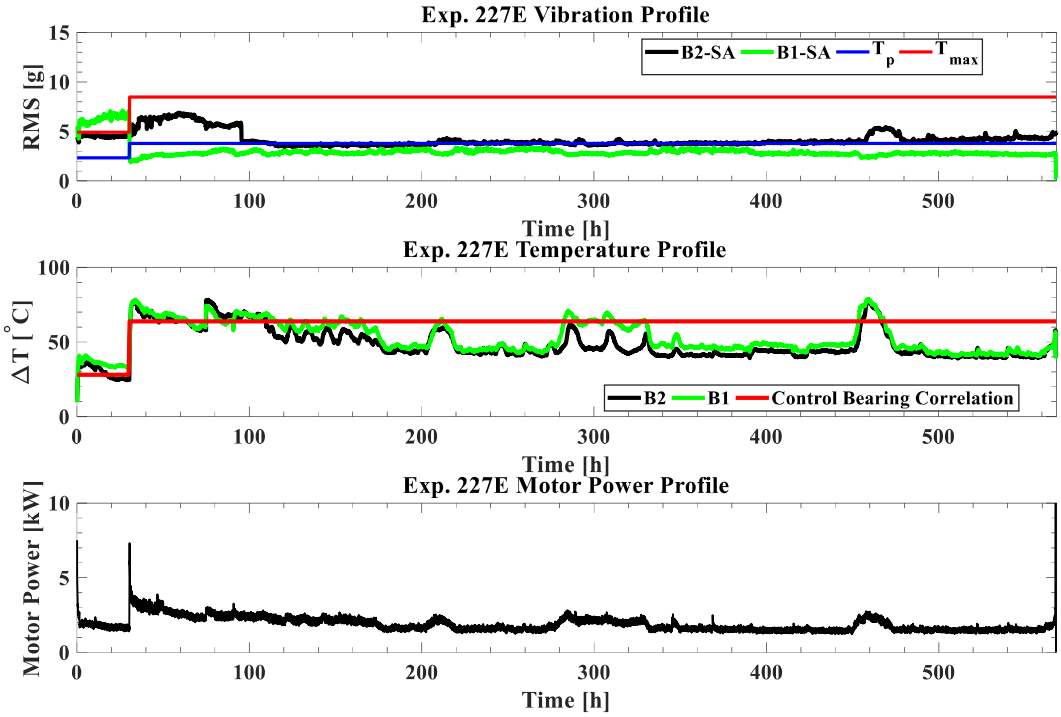

Figure 32: Vibration, temperature, and motor power profiles for Experiment 227E

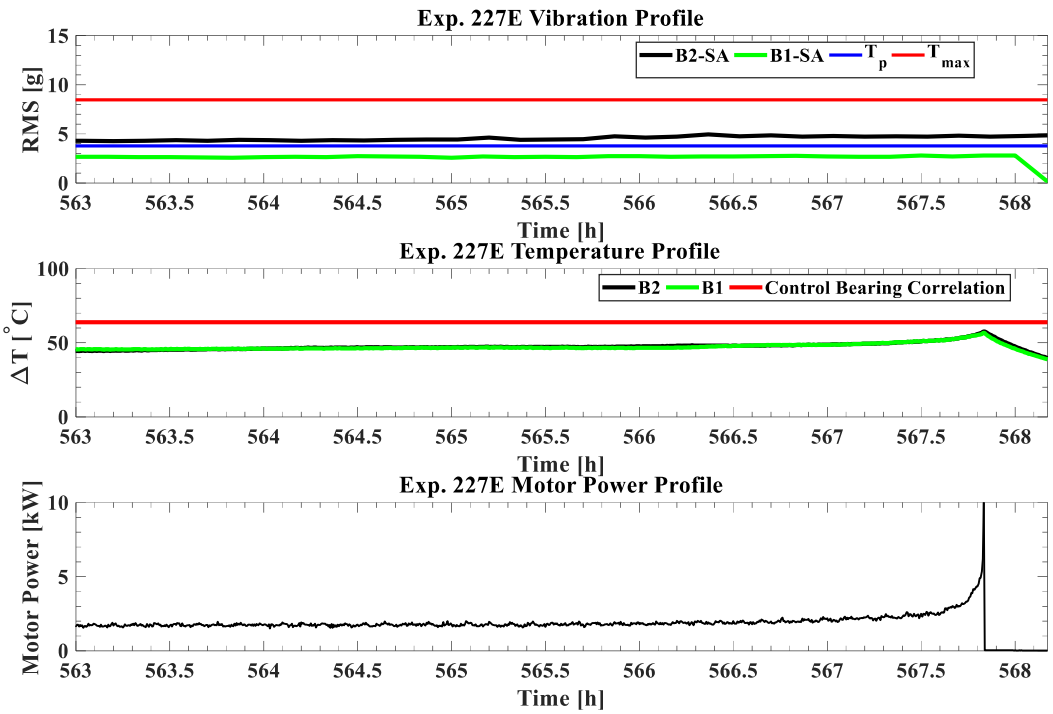

Figure 33: Vibration, temperature, and motor power profiles for Experiment 227E for the last 5 hours of operation

In consultation with TTCI engineers, it was decided to terminate the testing of bearings B1 and B2 since they exhibited abnormal operating temperature behavior and resulted in the damage of the first test axle and the shearing of the second test axle which was a brand-new axle used for the first time in testing B1 and B2.

4.2.3 Experiment 229A

Experiment 229A was conducted on the four-bearing tester (4BT) using test bearings 5 and 6 (B5 and B6) from batch 2, pictured in Figure 34. The reconditioning stress-relief holes were oriented so that they are directly beneath the point of maximum load application. Experiment 229A was performed successfully without interruption. This experiment ran for a total of 98,558 km (61,241 mi) of operation with the operating conditions set at 17% load (empty

railcar) and 85 km/h (53 mph) for the initial break-in period and were then changed to 100% load and 137 km/h (85 mph) for the remainder of this experiment.

Figure 34: Batch 2 – Test bearing 5 (left) and test bearing 6 (right)

The vibration, temperature, and motor power profiles for Experiment 229A are given in Figure 35. The vibration levels within test bearings 5 and 6 (B5 and B6) as indicated by the two accelerometers B5-SA and B6-SA mounted on B5 and B6, respectively, exceed the maximum threshold (T_{max}) during the initial break-in period where the operating conditions were set at 17% load and 85 km/h. However, once the operating conditions were changed to full-load and 137 km/h, the vibration signatures of both bearings settled and remained at or slightly above the preliminary threshold (T_p) for the rest of this test. The operating temperatures of both test bearings were noticeably above the control bearing correlation during the initial break in period and while acclimating to the change in operating conditions to full load and 137 km/h. The operating temperatures of both bearings eventually decreased to levels below the control bearing

correlation and normalized at average temperatures above ambient of 51.6°C (92.9°F) and 45.4°C (81.7°F) for bearings B5 and B6, respectively. Likewise, the motor power steadied at roughly 1.5 kW.

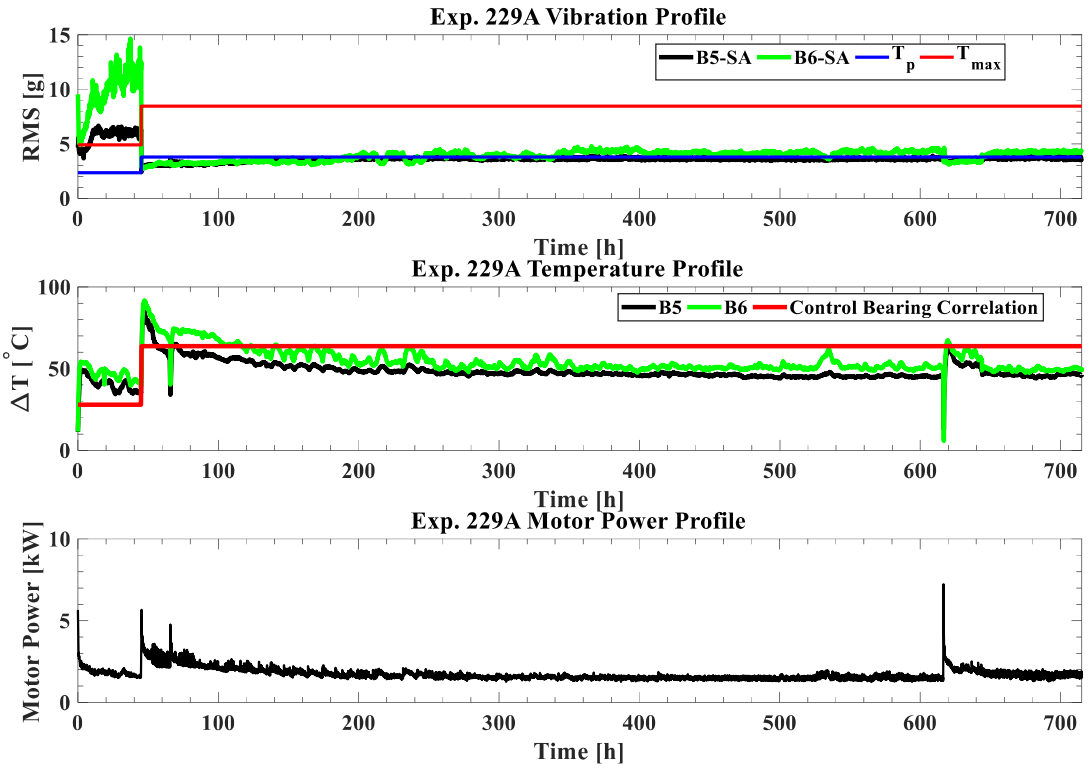

Figure 35: Vibration, temperature, and motor power profiles for Experiment 229B

Note that the short duration sudden spikes in motor power and drop-offs in operating temperatures are associated with the tester momentarily being stopped to perform minor adjustments to the tester instrumentation and then turned back on. As expected, the motor initially draws more power to overcome friction and get the axle with all four bearings rotating at the desired speed and load but then stabilizes when steady state conditions prevail.

4.2.4 Experiment 229B

Following a complete teardown and thorough inspection of the test axle and all four bearings performed at the conclusion of Experiment 229A, testing of B5 and B6 from batch 2

was resumed on the four-bearing tester (4BT). Note that the inspection revealed no damage to any of the bearing components or the test axle. All cone assemblies as well as the test axle were carefully measured to ensure that they remained within tolerance. The bearings were rebuilt using the same grease used in Experiment 229A, but the spacer rings were replaced to ensure that the bearing lateral remained within the AAR standards.

The intent of this experiment was to run B5 and B6 at operating conditions of full load and 137 km/h (85 mph) for an additional 100,000 km (62,500 mi) of operation and then perform another teardown and inspection. However, after running a simulated travel distance of 76,214 km (47,357 mi), this experiment was halted abruptly by the four-bearing tester emergency shutdown process which was triggered after the test axle sheared. The shear occurred in the center of test bearing 6 (B6) at the spacer ring region. The damage also included a ruptured grease seal, a broken cage, and ejected rollers, as shown in Figure 36 and Figure 37. Visual inspection of B6 revealed distinct damage on its cup raceway near the spacer ring region as well as visible heat tint patterns at the middle of the cup raceway that stretch almost the entire circumference of the raceway, as can be seen in Figure 38.

Figure 36: Experiment 229B four-bearing tester inspection

Figure 37: Experiment 229B axle damage

Figure 38: Damage on cup raceways of test bearing 6 (B6)

To understand what might have transpired in this test, the vibration, temperature, and motor power profiles of Experiment 229B were plotted in Figure 39. It is evident from this figure that the vibration, temperature, and motor power profiles were stable and remained constant throughout the experiment until the end when the vibration, temperature, and motor power values spiked abruptly leading to the axle shearing. For more clarity, Figure 40 presents the last five hours of this experiment which provide a better picture of the behavior of the vibration, temperature, and motor power profiles during the critical period when the axle sheared off.

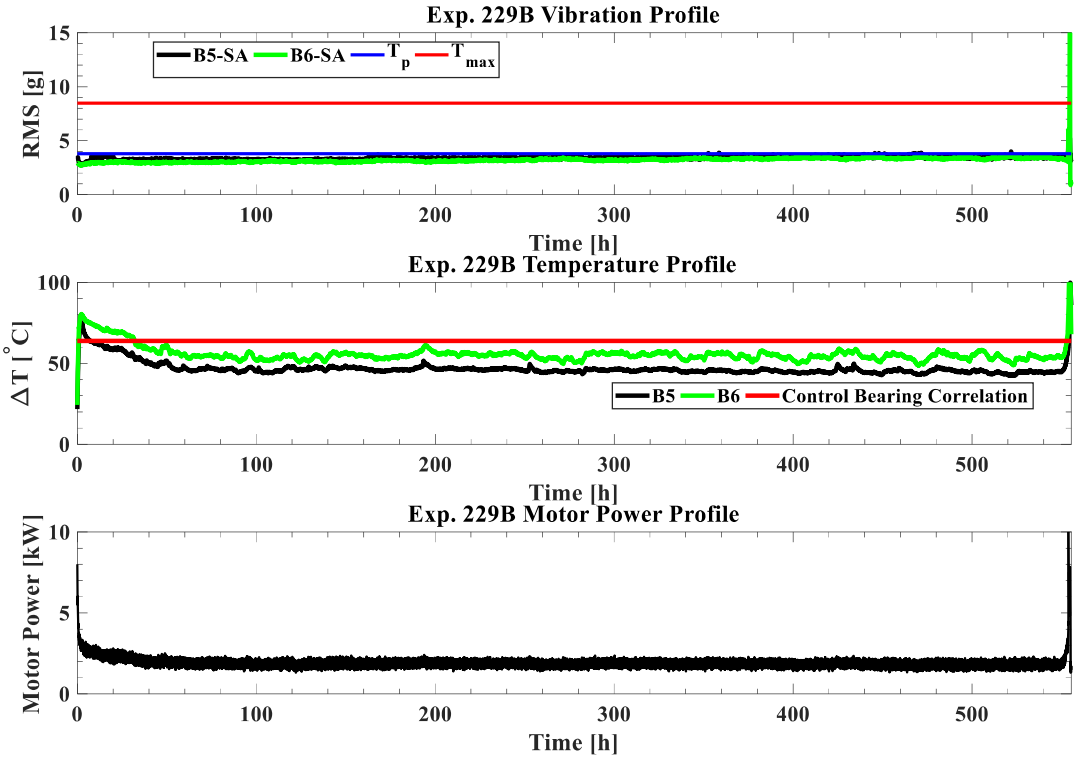

Figure 39: Vibration, temperature, and motor power profiles for Experiment 229B

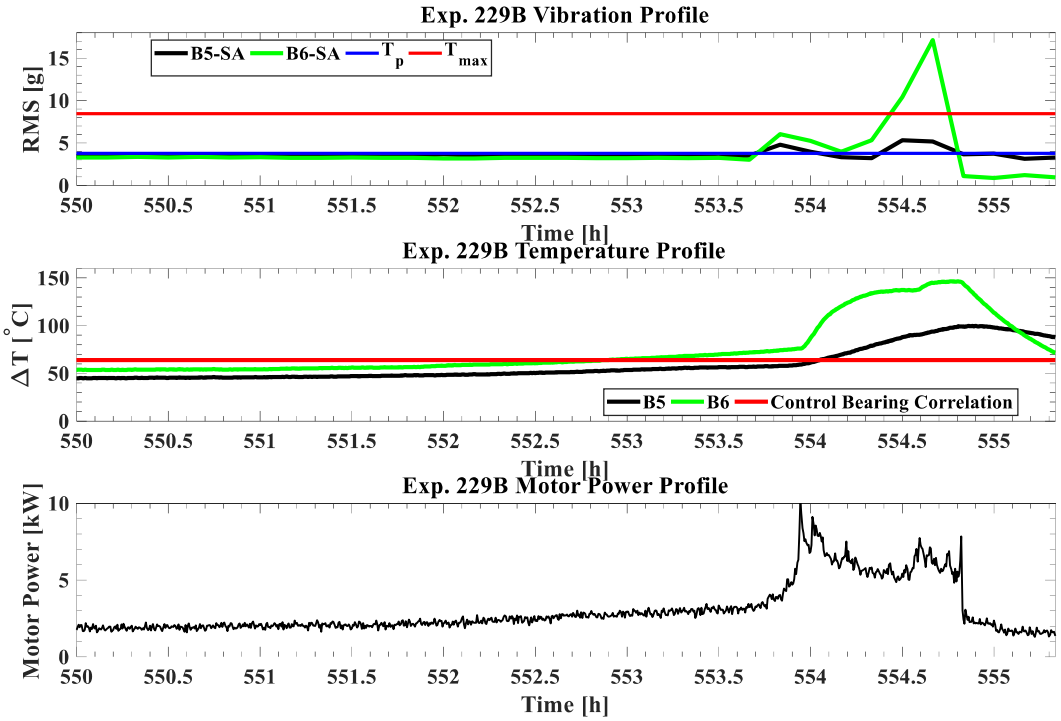

Figure 40: Vibration, temperature, and motor power profiles for Experiment 229B over the last five hours of operation

Examining Figure 40, a steady increase in motor power can be seen starting around the 551.5-hour mark and continuing until the 553.8-hour mark at which point the motor power began to exponentially spike reaching a little over 10 kW in less than 10 minutes. During that same period, the operating temperatures of B5 and B6 also exhibited a steady increase reaching temperatures above ambient that exceed the threshold for control defect-free bearings. It is believed that roller misalignment was responsible for the steady increase in both motor power and bearing operating temperatures. The roller misalignment continued to worsen over time exerting large forces on the cage and causing the motor power and bearing operating temperatures to continue to climb eventually leading to the fracture of the polyamide cage. Once the cage broke, the motor power dropped momentarily but the continued effect of roller misalignments resulted in an erratic behavior as the motor was trying to maintain the axle rotation speed. Over the span of the next 48 minutes starting with the 554-hour mark, the motor power fluctuated at levels well above those of normal operation causing the operating temperatures of B5 and B6 to continue to increase. In fact, B6 reached a maximum operating temperature of 153°C (275°F) above ambient around the 554.8-hour mark. Furthermore, over the same time frame, the vibration levels within B6 as read by the B6-SA accelerometer reached a maximum value of 17.3g, which is well above the T_{max}. The abnormal temperature and vibration levels of B6 are a direct consequence of the polyamide cage breaking, thus, affording the rollers enough space to oscillate and increasing their chances of misaligning.

The continuous stress exerted on the test axle as a result of the broken cage and loose rollers eventually led to shearing of the axle at the location of the cone assembly with the broken cage shortly after the 554.8-hour mark. Shearing of the axle resulted in a sudden drop in motor

power from 7.9 to 2.4 kW accompanied by an abrupt decrease in the vibration levels of both test bearings (B5 and B6) and a steady decrease in the operating temperature of both bearings.

In consultation with TTCI engineers, it was decided to terminate the testing of B6 given the damage to the bearing. Test bearing B6 had operated for a total simulated distance of 174,772 km (108,598 mi) since it was reconditioned.

4.2.5 Experiment 229C

Since the visual inspection of B5 did not reveal any discernable damage, it was decided to continue testing this bearing on the four-bearing tester (4BT). A control (defect-free) bearing was pressed on the test axle at the same position as that previously occupied by the removed test bearing 6 (B6). The intent was to run B5 uninterrupted for a simulated travel distance of about 100,000 km (62,500 mi) or until a defect developed, following the same protocols as in all previous tests.

Unfortunately, the test had to be stopped after running a total distance of about 89,777 km (55,785 mi). Briefly before the test was terminated, the operating temperature of B5 started to increase reaching levels that are noticeably above the threshold of defect-free healthy bearings, as can be seen in Figure 41 and more clearly in Figure 42 which shows the last 10 hours of this experiment. This abnormal temperature behavior of B5 prompted the termination of this test to avoid damage to the experimental setup.

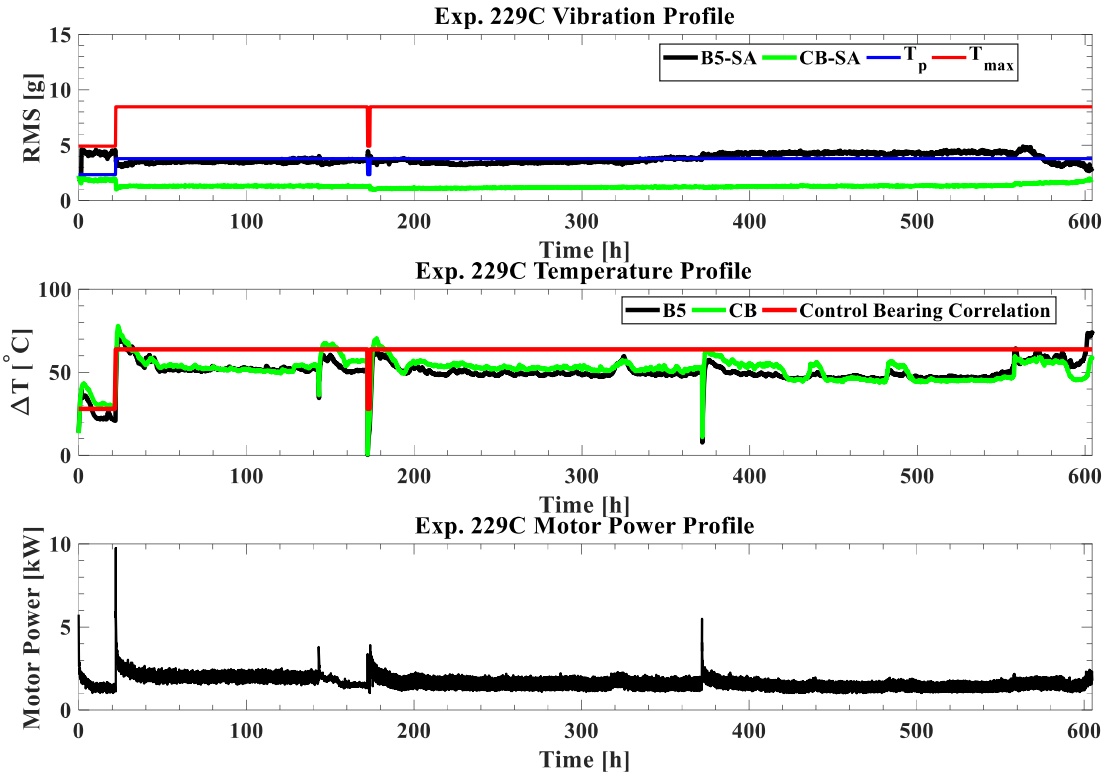

Figure 41: Vibration, temperature, and motor power profiles for Experiment 229C

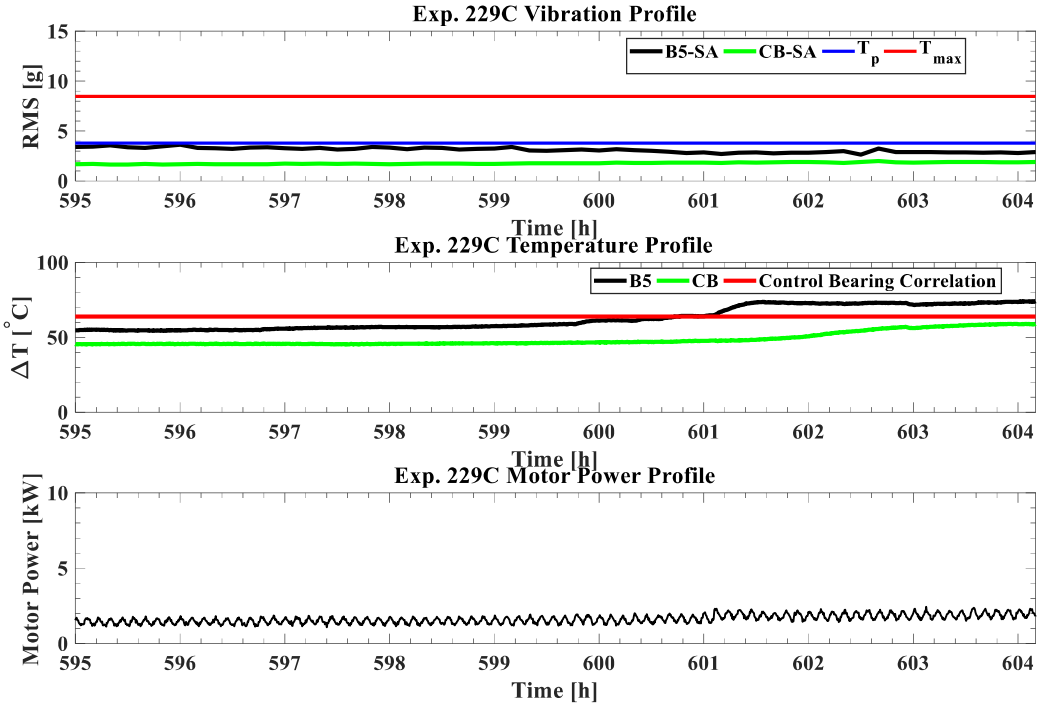

Figure 42: Vibration, temperature, and motor power profiles for Experiment 229C for the last 10 hours of operation

Examining Figure 41 and Figure 42, it is clear that the temperature, vibration, and motor power profiles remained stable and within normal operating conditions until shortly before the 600-hour mark. At that point, the motor power began to steadily increase accompanied by a more noticeable increase in the operating temperature of B5 which reached levels that are above the threshold for control (healthy) bearings. Examining the vibration levels of B5 and the adjacent control bearing, it can be observed that the vibration levels within B5 were at or above the T_p throughout the duration of the test, and only decreased towards the end of the experiment. In contrast, the vibration levels of the control bearing remained well below the T_p throughout this test, which is typical behavior for healthy defect-free bearings. The increase in motor power and in the operating temperature of B5 coupled with the abrupt decrease in the vibration levels within B5 indicated that one or both of the cone assemblies of B5 might have spun on the test axle. As a precaution, the test was stopped, and a complete teardown and inspection ensued.

The bearings were pressed off the test axle, which revealed damage to the axle where B5 was positioned, as shown in Figure 43. As predicted earlier, the inboard cone assembly of B5 had spun on the test axle causing the damage seen in Figure 44.

Visual inspection of B5 revealed abnormal wear patterns on both cup raceways, as depicted in Figure 44. The abnormal wear patterns suggest that B5 might have developed a geometric defect that caused the abnormal operation witnessed towards the end of the experiment. The abnormal operation of B5 exerted additional forces on the cone assembly causing it to spin on the test axle. Note that B5 was the only bearing to have spun on the test axle. The adjacent control bearing did not spin on the axle and the inspection found no discernable damage to any of the components of that bearing.

Figure 43: Experiment 229C axle damage

Figure 44: Abnormal wear on cup raceways of test bearing 5 (B5)

Based on the findings of this experiment, and in consultation with TTCI engineers, it was decided to terminate the testing of B5. This bearing had run a total simulated distance of about 264,549 km (164,383 mi) since it was reconditioned.

4.2.6 Experiment 230D

The final two test bearings in batch 2 (B7 and B8), pictured in Figure 45, were operated on the four-bearing tester (4BT). These two bearings were tested in all previous iterations (A-C) of Experiment 230 running a total simulated distance of 299,373 km (186,022 mi). In each iteration, the operating conditions were set to 17% load (empty railcar) and 85 km/h (53 mph) for the initial break-in period, and then switched to full load and 137 km/h (85 mph) for the remainder of the test. A complete teardown and visual inspection were carried out at the end of each iteration to document the condition of the two test bearings.

Figure 45: Batch 2 – Test bearing 7 (left) and test bearing 8 (right)

Experiment 230D was set to be the last iteration in testing B7 and B8, and the intent was to run these two bearings uninterrupted for about 100,000 km (62,500 mi) or until a defect

developed. However, after only 6,070 km (3,772 mi) of operation, the experiment had to be halted. Figure 46 provides the vibration, temperature, and motor power profiles for Experiment 230D.

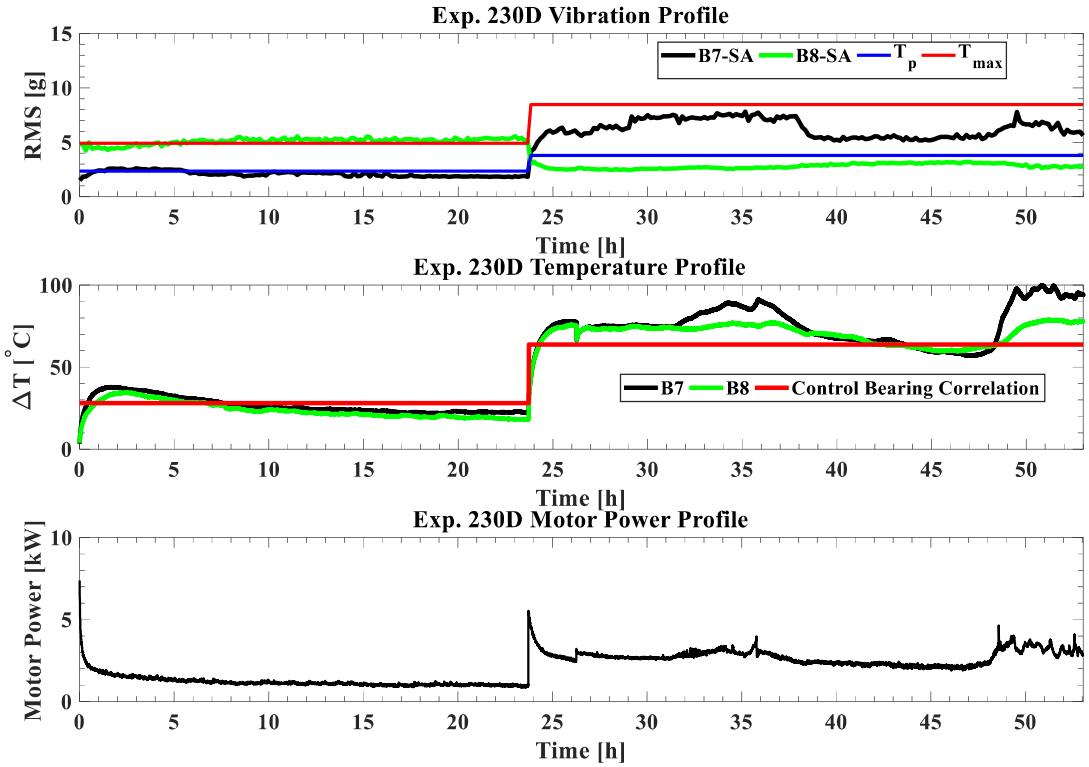

Figure 46: Vibration, temperature, and motor power profiles for Experiment 230D

Examining the vibration profiles of B7 and B8, it can be seen that the vibration RMS values of B8 were at or slightly above the T_{max} when the operating conditions were set to 17% load and 85 km/h and then dropped below the T_p once the operating conditions were changed to full load and 137 km/h. In contrast, B7 had vibration RMS values that were around the T_p during the break-in period and increased to levels well above the T_p reaching a maximum RMS of 7.8g after the operating conditions changed to full load and 137 km/h (85 mph).

The operating temperatures of B7 and B8 were noticeably above the threshold for control bearings for most of the test period when the operating conditions were at full load and 137

km/h. Test bearing 7 exhibited two major spikes in operating temperature around the 35 and 50-hour mark which were mirrored by increases in motor power around the same time frame. The maximum operating temperature above ambient for B7 reached 106°C (191°F) just after the 50-hour mark. Shortly before that, the motor power experienced an increase from 2.1 to 4.6 kW. Interestingly, the vibration levels within B7 exhibited a steady decrease around that same time frame. Again, the increase in motor power and in the operating temperature of B7 coupled with the decrease of the vibration RMS values indicated that B7 might have spun on the test axle.

Hence, a complete teardown and inspection were performed to examine the test axle and all bearing components. The bearings were pressed off the axle which revealed damage at several locations, especially those occupied by test bearings B7 and B8, as shown in Figure 47. Note that the test axle for this experiment has been used in several other tests, and although it was within the tolerance set by AAR standards outlined in Appendix A, the dimensions were on the lower end of the acceptable tolerance.

Figure 47: Experiment 230D axle damage

Since the visual inspection found no discernable damage present on any of the cup raceways of the two test bearings (B7 and B8), it was decided to continue testing B7 and B8. However, to assess their performance free from speculation regarding the effect of the other test components (i.e., test axle condition, control bearings, cone assemblies, and grease condition), a brand-new test axle was utilized for this test, and two new control (defect-free) bearings were used. Furthermore, new cone assemblies were used to build test bearings 7 and 8, and fresh new grease was applied in all four bearings of the test axle assembly. Hence, the only two

components of this test that were the same as in Experiment 230D were the two bearing cups of B7 and B8.

4.2.7 Experiment 230E

In Experiment 230E, test bearings 7 and 8 (B7 and B8) from batch 2 were run on the four-bearing tester (4BT). These bearings were previously run in all iterations of Experiment 230. As in previous iterations, the operating conditions were initially set at 17% load and a speed of 85 km/h (53 mph) for the initial break in period, and then changed to full load (100% load) and 137 km/h (85 mph) for the remainder of this experiment.

The vibration, temperature, and motor power profiles for Experiment 230E are presented in Figure 48. Examining the thermal performance of B7 and B8, it can be seen that both test bearings were operating at temperatures above the maximum threshold for control (defect-free) bearings for the first 210 hours of the test. Following that, the operating temperatures of B7 and B8 decreased below the maximum threshold for control bearings. The operating conditions were then set to 17% load and a speed of 85 km/h (53 mph) after the tester was stopped for a couple of days at the 360-hour mark. The operating conditions were then set to full load and 137 km/h (85 mph) for another 120 hours of operation. During this duration, the operating temperatures of B7 and B8 experienced several fluctuations with one of these occurring around the 395-hour mark where the operating temperatures above ambient increased from about 57°C (103°F) to 72°C (130°F). This increase in operating temperature was mirrored by an increase in motor power from 2.0 to 2.8 kW. After a total of 500 hours of operation, the operating conditions were systematically changed during the experiment to lower speeds so that the operating temperatures of B7 and B8 remain below the maximum threshold for control bearings. Throughout the

duration of this experiment, the vibration levels for B7 and B8 remained at or slightly below the T_p.

A complete teardown and inspection were performed to examine the test axle and bearing components. The bearings were pressed off the test axle revealing no damage to the test axle or the bearing components of B7 and B8. Test bearings B7 and B8 ran for a total simulated distance of 373,469 km (232,063 mi) since they were reconditioned.

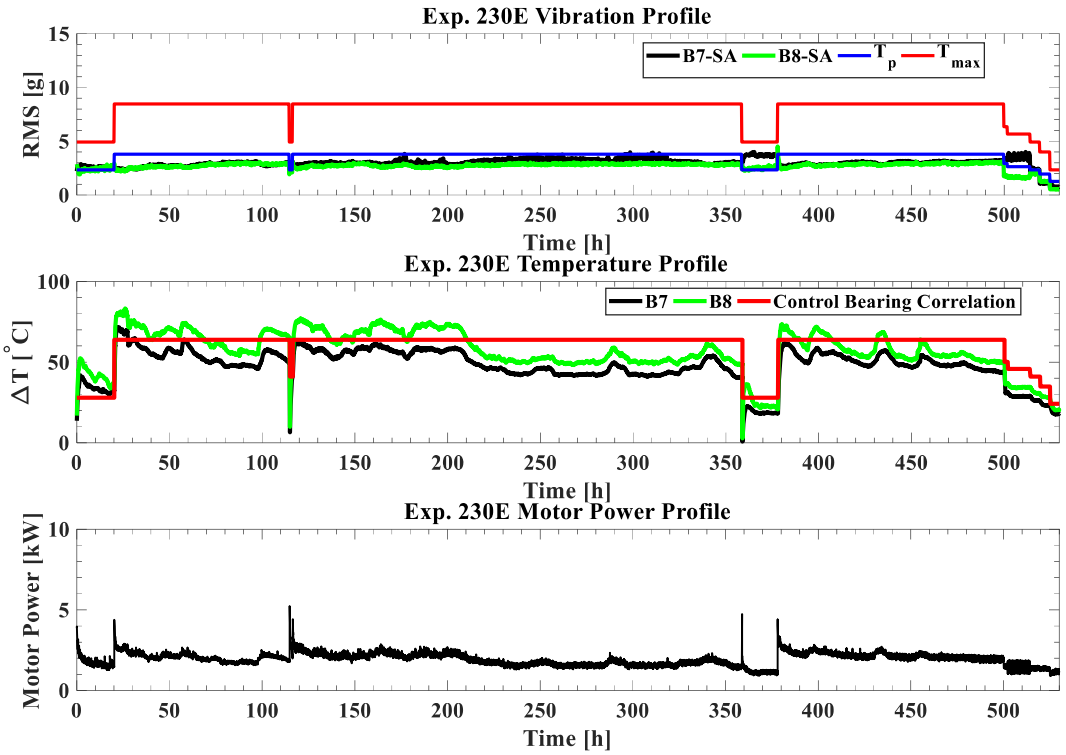

Figure 48: Vibration, temperature, and motor power profiles for Experiment 230E

4.2.8 Summary of Batch 2 Testing

The testing results for batch 2 bearings are summarized in Table 9 and Table 10. In Table 9, the mean, maximum, and minimum values of the vibration RMS and operating temperature above ambient are listed for each test bearing from batch 2. The vibration RMS and operating

temperature values were obtained from the steady state data while the bearings were operating at conditions of full load and 137 km/h (85 mph). For convenience, the values exceeding the maximum thresholds for normal operation were **bolded**. Table 10 gives the total simulated distance traveled (in kilometers and miles) for each of the eight test bearings of batch 2 since the bearings were reconditioned, as well as a brief description of the testing outcome for each bearing.

Table 9: Summary of the vibration RMS and operating temperatures of the eight test bearings examined in batch 2 testing

Bearing Number	Vibration RMS			ΔT above ambient		
	Avg. [g]	Max. [g]	Min. [g]	Avg. [°C]	Max. [°C]	Min. [°C]
B1	4.8	**12.0**	2.3	53.2	**95.0**	28.5
B2	5.3	**10.2**	0.9	48.4	**93.0**	26.3
B3	3.8	**9.2**	2.3	42.3	**70.5**	28.3
B4	3.4	6.3	2.5	42.2	**65.0**	27.5
B5	3.6	5.2	2.7	48.1	**97.9**	42.4
B6	3.6	**17.1**	2.9	54.4	**146.6**	47.5
B7	2.6	7.8	2.0	51.0	**99.8**	39.6
B8	2.7	4.1	2.0	50.9	**78.9**	38.8

Table 10: Summary of the total simulated distance traveled and testing outcome for each of the eight bearings from batch 2 testing

Bearing Number	Total Distance Traveled [km] / [mi]	Testing Outcome
B1	354,238 / 220,113	Testing of this bearing was terminated after completing its service life testing. This bearing resulted in spun cone assemblies and shearing of the test axle.
B2	354,238 / 220,113	Testing of this bearing was terminated after completing its service life testing. This bearing resulted in spun cone assemblies and shearing of the test axle.
B3	394,088 / 244,875	Testing of this bearing was terminated after completing its service life testing without any spall or defect initiation or incidents.
B4	394,088 / 244,875	Testing of this bearing was terminated after completing its service life testing without any spall or defect initiation or incidents.
B5	264,549 / 164,383	Testing of this bearing was halted after its abnormal operation resulted in the shearing of the test axle and its cone assembly spun on the axle.
B6	174,772 / 108,598	Testing of this bearing was halted after its abnormal operation resulted in the shearing of the test axle.
B7	373,469 / 232,063	Testing of this bearing was terminated after completing its service life testing. This bearing resulted in spun cone assemblies and shearing of the test axle.
B8	373,469 / 232,063	Testing of this bearing was terminated after completing its service life testing. This bearing resulted in spun cone assemblies and shearing of the test axle.

The testing results summarized in Table 9 show that the vibration RMS values for test bearings B1 and B2 were higher than those of the other test bearings. Test bearings B1, B2, B3, and B6 had maximum RMS values that surpassed the maximum threshold (T_{max}). The mean operating temperatures of B1 and B6 were higher than those of the other test bearings. Note that the threshold for normal operation for control (defect-free) bearings at operating conditions of full load and 137 km/h (85 mph) is about 64°C (115°F) above ambient. Bearings in rail service are flagged by Hot-Box Detectors (HBDs) when their operating temperatures are 94.4°C (170°F) above ambient conditions. If this occurs, the train conductor would be alerted, and the bearing would have to be immediately pulled from service. Examining the maximum operating temperatures, listed in Table 9, reveals that all eight bearings operated at levels beyond the threshold operating temperature for defect-free (healthy) bearings. More importantly, test bearings B1, B5, B6, and B7 each recorded maximum operating temperatures greater than 94.4°C (170°F) above ambient, which implies that these four bearings would have been flagged by HBDs and would have been immediately pulled from rail service.

None of the eight test bearings from batch 2 experienced any major spalling. However, the stress-relief holes of all eight test bearings slightly expanded as a result of the service life testing. Moreover, test bearing 1 (B1) generated a small pit on the outer ring (cup) raceway after traveling a simulated distance of 169,154 km (105,108 mi), as shown in Figure 49. The total area of the initial stress-relief hole and pit was 0.099 cm^2 (0.0153 in^2) which increased to 0.102 cm^2 (0.0158 in^2) after running an additional distance of 185,084 km (115,006 mi).

Finally, it is worth mentioning that out of the eight test bearings in batch 2, only test bearings 3 and 4 (B3 and B4) completed their service life testing in its entirety without any incidents, and generally operating within the thresholds for normal healthy bearing operation.

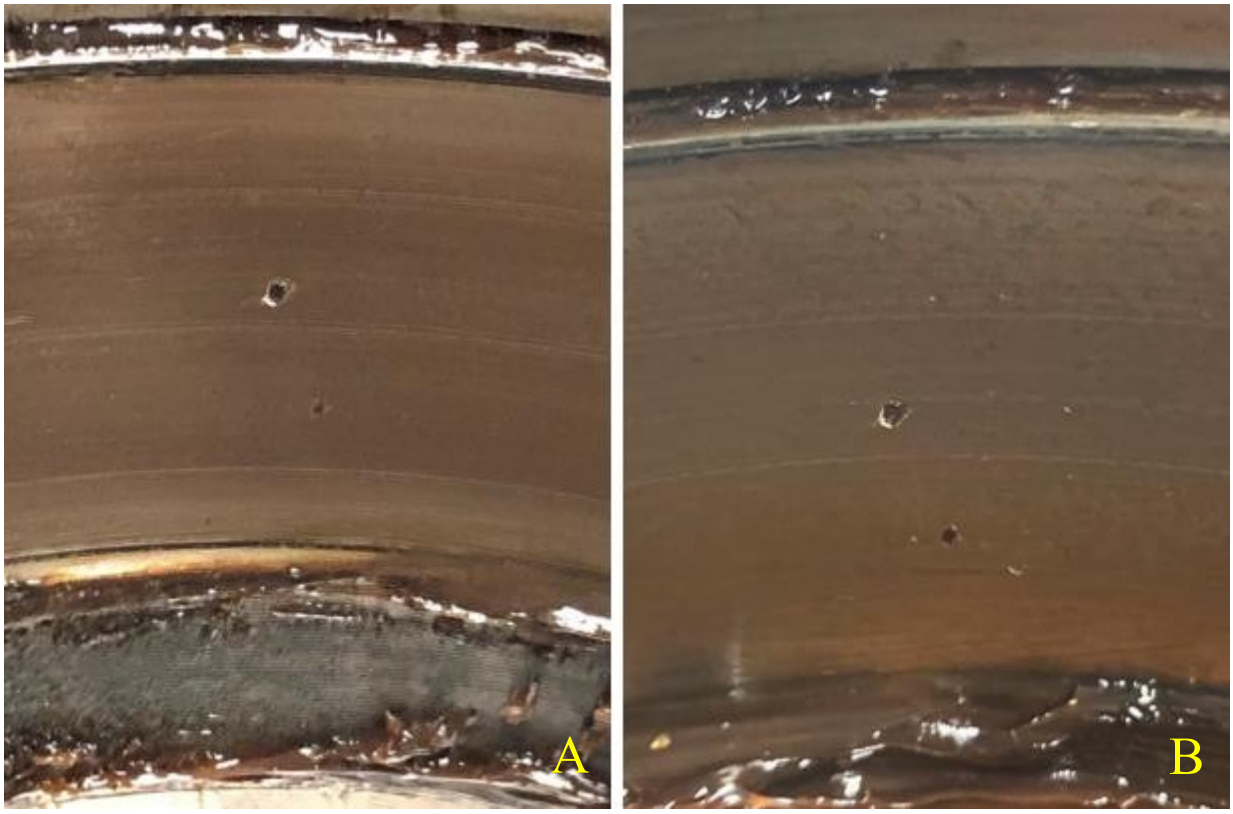

Figure 49. Test bearing B1 pit development: A) after 169,154 km (105,108 mi), and B) after 354,238 km (220,114 mi)

4.3 Broken Shaft Calculations

The shearing of the test axle that occurred in Experiment 227E and 229B raised concerns regarding the cause of this incident. All roller spacing measurements taken for the cone assemblies used to build the test bearings were within the tolerance specified by AAR standards, with the pocket of space between the roller and the cage being no greater than 0.152 cm (0.060 in). In fact, the cone assembly roller spacing measurements for all test bearings were well below the AAR threshold, with the highest measurement being 0.089 cm (0.035 in) for test bearings B2 and B4. Roller misalignment is usually triggered by imperfections or defects that develop on the raceways of cups and/or cones. The removal of material from the cup raceways during the reconditioning process creates such imperfections on the cup raceways that can potentially

trigger roller misalignment leading to abnormal operation of the bearing. To assess whether roller misalignment can potentially lead to shearing of the test axle, the following calculations were performed.

The stored kinetic energy (*KE*) of the axle will be calculated to determine if it is sufficient to justify shearing of the axle when met with an abrupt stop caused by roller misalignment. First, the moment of inertia (*I*) of the axle is found using Eq. (14), where the maximum radius (*R*) of the axle is 0.07863 m (3.09575 in). The mass (*m*) of the test axle with four bearings pressed on is estimated to be approximately 251.1 kg (553.6 lb).

$$I = \frac{mR^2}{2} \tag{14}$$

Then, (15) is used to estimate the stored kinetic energy (*KE*) of the axle using an angular velocity (ω) of 83.36 rad/s (which is equivalent to 796 rpm).

$$KE = \frac{1}{2} I\, \omega^2 \tag{15}$$

The resulting kinetic energy is then plugged in (16) with an assumed final kinetic energy of zero and an estimated angle of twist (ϑ) of 2°. This gives the average impact torque (*T*) which is then used in (18) to determine the maximum shear stress (τ_{max}). In (18), *R* is the maximum radius of the test axle and *J* is the polar moment of inertia calculated from (17).

$$T = \frac{\Delta KE}{\theta} = \frac{Change\ in\ kinetic\ energy}{angle\ traveled} \tag{16}$$

$$J = \frac{\pi}{2} R^4 \tag{17}$$

$$\tau_{max} = \frac{T * R}{J} \tag{18}$$

The maximum shear stress (τ_{max}) was calculated to be 101.2 MPa. The allowable shear stress (τ_{allow}) given by (19) utilizing a yield strength (σ_y) of 415 MPa (for the test axle material), was found to be about 239 MPa.

$$\tau_{allow} = 0.577 * \sigma_y \tag{19}$$

This gives a factor of safety (F.O.S.) of only 2.36 when using an angle of twist of 2°. Based on these calculations, the failure of the test axle may have been caused by roller misalignment occurring simultaneously in the two middle test bearings. The calculations demonstrate that the axle can reach the maximum yield stress when the kinetic energy of the axle is combined with transverse loading caused by roller misalignment and other forces generated by the moving components in the experimental setup.

CHAPTER V

CONCLUSIONS AND RECOMMENDATIONS

Railroad bearings may be removed from service for several reasons which include triggering a wayside detection system or as part of an entire wheel-axle replacement due to a wheel defect. Upon visual inspection, a portion of the railroad bearings that were removed from service may be sent to designated facilities to undergo a reconditioning process. Railroad bearing reconditioning is a common practice in the railroad industry that has been carried out for decades now. The efficacy and effectiveness of this process has not been carefully assessed or evaluated. This thesis presents the results of the collaborative work between UTRGV and TTCI aimed at exploring the performance of reconditioned bearings.

The results show that the proximity of the stress-relief holes to each other seems to be a factor in the initiation of spalls (defects). From the twelve test bearings in Batch 1, only five bearings experienced more steady temperatures and/or slightly lower operating temperatures after the reconditioning process as compared to before reconditioning. As for the vibration performance of the twelve test bearings, eight of these bearings experienced either a slight decrease in the vibration levels within the bearing or a noticeable improvement in the vibration levels within the bearing after the reconditioning process as compared to before reconditioning was performed.

The defects (spalls) that initiated on two of the twelve test bearings from Batch 1 would

not have been detected relying solely on the temperature histories of the test bearings since the operating temperatures of the test bearings ran well below the average operating temperature of defect-free bearings at the same load and speed. In fact, the defect was accurately detected by the vibration-based bearing condition monitoring algorithm developed by the UTCRS research team at UTRGV. The visual inspection verified that a spall had initiated on the cup raceway as predicted by the vibration-based algorithm.

All twelve test bearings from Batch 1 experienced an increase in the area of the stress-relief holes on the bearing raceways as a result of the bearings running on the test rigs. The areas of the stress-relief holes on the bearings became flatter as the bearings ran on the four-bearing tester which resulted in the areas increasing slightly.

Batch 2 bearings underwent a complete service life test in which the bearings were run for 400,000 km (~250,000 mi) or until the bearings developed a defect. To expedite the testing, the bearing cups were positioned such that the most severely reconditioned regions were under the maximum applied load, and the operating conditions were set to a simulated full railcar load (i.e., 153 kN or 34.4 kips per bearing) with the bearings running at a simulated train speed of 137 km/h (85 mph). Batch 2 bearings experienced multiple incidents including cone assemblies that spun on the test axles and sheared test axles. From the eight test bearings in Batch 2, six of these test bearings caused an incident during testing. Test bearings B1 and B2 had their cone assemblies spin on the test axle during Experiment 225 and sheared the test axle in Experiment 227E. Test bearings B5 and B6 caused the second test axle shearing incident in Experiment 229B in the B6 bearing location, and test bearing 5 (B5) had its cone assembly spin on the test axle in the next iteration of this experiment (i.e., Experiment 229C). Lastly, test bearings B7 and B8 had their cones (inner rings) spin on the test axle in Experiment 230D. It should be noted that all

axles were manufactured by the same manufacturer, without any prior issues. Moreover, every test axle was carefully inspected and measured prior to any experiment to ensure that it was within tolerance and met AAR standards and protocols. Test bearings B3 and B4 were the only test bearings from batch 2 that completed their service life testing without any incident.

The results from Batch 2 show that four of the eight bearings reached temperatures that would be flagged by Hot Box Detectors if the bearings were running in the field, and all eight test bearings surpassed the maximum thresholds for normal operation of a control bearing at one point. Like Batch 1, Batch 2 test bearings experienced slight increases in the areas (sizes) of the stress-relief holes on the bearing raceways from running on the test rigs. Of the eight test bearings from Batch 2, only test bearing 1 (B1) generated a small pit on the cup raceway which marginally increased in area (size) after it completed its service life test.

It is important to note that the reason of removal from service for Batch 1 bearings was not known to either TTCI engineers or UTRGV researchers. In contrast, Batch 2 bearings were removed from service for reasons not associated with the bearings themselves (i.e., AAR Why Made Code 11).

From the results of this study, the stress-relief holes that are made during the reconditioning process and their proximity may be the cause of spall initiation on the bearing cup raceway. Additionally, the reconditioning process which entails removal of material from the cup raceways can potentially alter the geometry of the cup raceways which can trigger severe roller misalignment at high operating speeds and result in axle failure. These findings are supported by the abnormal thermal performance exhibited by six of the eight bearings of Batch 2.

REFERENCES

[1] Vantuono, W C. *Wheel Failure Is Not an Option*. 1 Feb. 2018, www.railwayage.com/mechanical/freight-cars/wheel-failure-is-not-an-option/.

[2] Predikto.N.p.: Predikto, n.d. Predicting Hot Box Detector Failures. Predikto, 2015. Web.

[3] Karunakaran, S., and Snyder, T.W., 2007, "Bearing Temperature Performance in Freight Cars," *Proceedings Bearing Research Symposium, sponsored by the AAR Research Program in conjunction with the ASME RTD Fall Conference*, Chicago, IL, September 11-12.

[4] A. Mealer, C. Tarawneh, S. Crown, Radiative Heat Transfer Analysis of Railroad Bearings for Wayside Hot-box Detector Optimization. Proceedings of the 2017 Joint Rail Conference, Philadelphia, PA, April 4-7, 2017.

[5] J. Aranda, "Radiative Heat Transfer Analysis of Railroad Bearings for Wayside Thermal Detector Optimization," Master's Thesis, Department of Mechanical Engineering, The University of Texas Rio Grande Valley, December 2018.

[6] C. Tarawneh, J. Aranda*, V. Hernandez**, S. Crown, and J. Montalvo*. An investigation into wayside hot-box detector efficacy and optimization. International Journal of Rail Transportation, Vol. 8, No. 3, pp. 264-284, 2020. https://doi.org/10.1080/23248378.2019.1636721

[7] 3.10 – Accident Causes | Federal Railroad Administration, Office of Safety Analysis. Web. https://safetydata.fra.dot.gov/OfficeofSafety/publicsite/Query/inccaus.aspx

[8] Ose, Mixanikos. "Heat Detectors-box and Brake Disc (Hot Box & Hot Wheel Detection System)." *Heat Detectors-box and Brake Disc (Hot Box & Hot Wheel Detection System)*. N.p., 16 July 2015. Web.

[9] Anderson, Gerald B. "Acoustic detection of distressed freight car roller bearings." ASME/IEEE 2007 Joint Rail Conference and Internal Combustion Engine Division Spring Technical Conference. American Society of Mechanical Engineers Digital Collection, 2007.

[10] Transportation Technology Center, Inc. "TADS® Trackside Acoustic Detection System." https://aar.com/pdfs/TADSupdate_20160615.pdf.

[11] C. Tarawneh, J. A. Turner, B. M. Wilson, and L. Koester*. Service life testing of railroad bearings with known subsurface inclusions detected with advanced ultrasonic technology. Int. J. of Railway Technology, Vol. 2, No. 3, pp. 55-78, 2013.

[12] Zaretsky, E. and Branzai, E., 2005, "Effect of Rolling Bearing Refurbishment and Restoration on Bearing Life and Reliability," Tribology Transactions, 48(1), pp. 32–44.

[13] Price, P. (2002, May 16). High-quality railway bearing service at RBI. https://evolution.skf.com/us/high-quality-railway-bearing-service-at-rbi/

[14] Timken Engineering Manual – Metals Industry Edition, The Timken Company, North Canton, OH, 44720.

[15] Alexander, J. (2016). Using Bearing Repair To Extend Bearing Life: For Heavy Industries. Retrieved 2020, from https://www.timken.com/resources/bearing-repair-for-heavy-industries-technical-white-paper/

[16] Sullivan, R., Lonsdale, C., Oliver, J., & Iorio, J. (2018). 2003 AAR Car Repair Billing Wheel Removal Analysis. Retrieved 2020, from http://railcar-tech.org/wp-content/uploads/2018/10/2003-AAR-CAR-REPAIR-BILLING-WHEEL-REMOVAL-ANALYSIS-B.pdf

[17] Schaeffler Technologies "Repair and Reconditioning of Roller Bearings" (2020, May) https://www.schaeffler.com/remotemedien/media/_shared_media/08_media_library/01_publications/schaeffler_2/tpi/downloads_8/tpi_207_de_en.pdf.

[18] H-II. (2008, October). In 1062201241 809481722 Safety and Operations (Ed.), Manual of Standards and Recommended Practices (pp. H-II-i-H-II [S-756] 102). Washington, D.C.: Association of American Railroads.

[19] A. Gonzalez, "Development, Optimization, and Implementation of a Vibration Based Defect Detection Algorithm for Railroad Bearings," Master's Thesis, The University of Texas Rio Grande Valley, August 2015.

[20] R. Maldonado, "An Investigation into Temperature Trending in Railroad Tapered Roller Bearings Through Vibration Monitoring Techniques," Master's Thesis, The University of Texas Pan American, Edinburg, TX, 2011.

[21] I. L. Alvarado, "Defect Detection in Railroad Tapered-Roller Bearings using Vibration Analysis Techniques," University of Texas-Pan American, Edinburg, TX, 2012.

[22] Lima, J., "Residual Service Life Prognostic Models for Tapered Roller Bearings," Master's Thesis, The University of Texas Rio Grande Valley, May 2020.

APPENDIX A

APPENDIX A

MEASUREMENTS

Table 11: Cone Measurements for Batch 2 in English Units

Test bearing	Cage Shake [in]		Roller Spacing [in]		Cage Lift [in]		Lateral Spacing [in] Min/Max
	Inboard Min/Max	Outboard Min/Max	Inboard Min/Max	Outboard Min/Max	Inboard Min/Max	Outboard Min/Max	
B1	0.030 / 0.045	0.033 / 0.053	0.028 / 0.032	0.020 / 0.032	0.055 / 0.067	0.049 / 0.062	0.023 / 0.026
B2	0.042 / 0.053	0.035 / 0.050	0.032 / 0.035	0.019 / 0.032	0.076 / 0.096	0.062 / 0.095	0.021 / 0.026
B3	0.038 / 0.050	0.038 / 0.050	0.019 / 0.025	0.026 / 0.030	0.075 / 0.090	0.070 / 0.090	0.023 / 0.026
B4	0.054 / 0.067	0.045 / 0.055	0.023 / 0.035	0.028 / 0.030	0.055 / 0.085	0.075 / 0.095	0.023 / 0.024
B5	0.018 / 0.020	0.028 / 0.031	0.017 / 0.019	0.016 / 0.028	0.059 / 0.065	0.050 / 0.057	0.022 / 0.025
B6	0.010 / 0.012	0.012 / 0.016	0.011 / 0.015	0.008 / 0.013	0.061 / 0.066	0.059 / 0.068	0.027 / 0.028
B7	0.025 / 0.028	0.018 / 0.038	0.015 / 0.019	0.016 / 0.022	0.077 / 0.085	0.055 / 0.067	0.023 / 0.027
B8	0.019 / 0.023	0.020 / 0.025	0.014 / 0.018	0.015 / 0.019	0.060 / 0.067	0.062 / 0.083	0.024 / 0.026

Table 12: Cone Measurements for Batch 2 in SI Units

Test bearing	Cage Shake [cm]		Roller Spacing [cm]		Cage Lift [cm]		Lateral Spacing [cm] Min/Max
	Inboard Min/Max	Outboard Min/Max	Inboard Min/Max	Outboard Min/Max	Inboard Min/Max	Outboard Min/Max	
B1	0.076 / 0.114	0.084 / 0.135	0.071 / 0.081	0.051 / 0.081	0.140 / 0.170	0.124 / 0.157	0.058 / 0.066
B2	0.107 / 0.135	0.089 / 0.127	0.081 / 0.089	0.048 / 0.081	0.193 / 0.244	0.157 / 0.241	0.053 / 0.066
B3	0.097 / 0.127	0.097 / 0.127	0.048 / 0.064	0.066 / 0.076	0.191 / 0.229	0.178 / 0.229	0.058 / 0.066
B4	0.137 / 0.170	0.114 / 0.140	0.058 / 0.089	0.071 / 0.076	0.140 / 0.216	0.191 / 0.241	0.058 / 0.061
B5	0.046 / 0.051	0.071 / 0.079	0.043 / 0.048	0.041 / 0.071	0.150 / 0.165	0.127 / 0.145	0.056 / 0.064
B6	0.025 / 0.030	0.030 / 0.041	0.028 / 0.038	0.020 / 0.033	0.155 / 0.168	0.150 / 0.173	0.069 / 0.071
B7	0.064 / 0.071	0.046 / 0.097	0.038 / 0.048	0.041 / 0.056	0.196 / 0.216	0.140 / 0.170	0.058 / 0.069
B8	0.048 / 0.058	0.051 / 0.064	0.036 / 0.046	0.038 / 0.048	0.152 / 0.170	0.157 / 0.211	0.061 / 0.066

Table 13: Axle Measurements for Batch 2

Cone Location	Axles from Manufacturer			Axle from Exp. 230D		
	Avg. [cm / in]	Max. [cm / in]	Min. [cm / in]	Avg. [cm / in]	Max. [cm / in]	Min. [cm / in]
B1 - IB	15.7256 / 6.1912	15.7264 / 6.1915	15.7251 / 6.191	15.7241 / 6.1906	15.7246 / 6.1908	15.7239 / 6.1905
B1 - OB	15.7254 / 6.1911	15.7260 / 6.1913	15.7251 / 6.191	15.7244 / 6.1907	15.7246 / 6.1908	15.7241 / 6.1906
B2 - IB	15.7254 / 6.1911	15.7260 / 6.1913	15.7249 / 6.1909	15.7241 / 6.1906	15.7244 / 6.1907	15.7239 / 6.1905
B2 - OB	15.7251 / 6.1910	15.7260 / 6.1913	15.7249 / 6.1909	15.7239 / 6.1905	15.7241 / 6.1906	15.7239 / 6.1905
B3 - IB	15.7256 / 6.1912	15.7264 / 6.1915	15.7251 / 6.191	15.7244 / 6.1907	15.7249 / 6.1909	15.7241 / 6.1906
B3 - OB	15.7254 / 6.1911	15.7262 / 6.1914	15.7251 / 6.191	15.7241 / 6.1906	15.7244 / 6.1907	15.7239 / 6.1905
B4 - IB	15.7256 / 6.1912	15.7264 / 6.1915	15.7254 / 6.1911	15.7241 / 6.1906	15.7246 / 6.1908	15.7239 / 6.1905
B4 - OB	15.7254 / 6.1911	15.7264 / 6.1915	15.7249 / 6.1909	15.7246 / 6.1908	15.7251 / 6.1910	15.7241 / 6.1906

APPENDIX B

APPENDIX B

BATCH 1 AND BATCH 2 PLOTS

BATCH 1 PLOTS

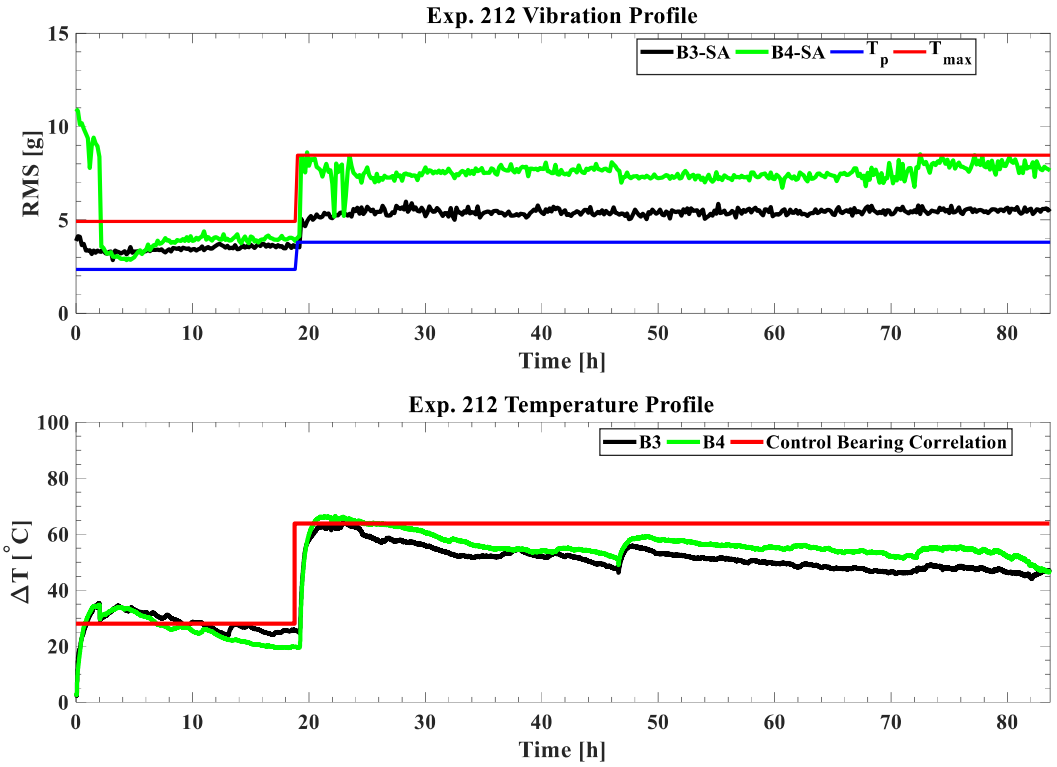

Figure 50: Vibration and temperature profiles for Experiment 212

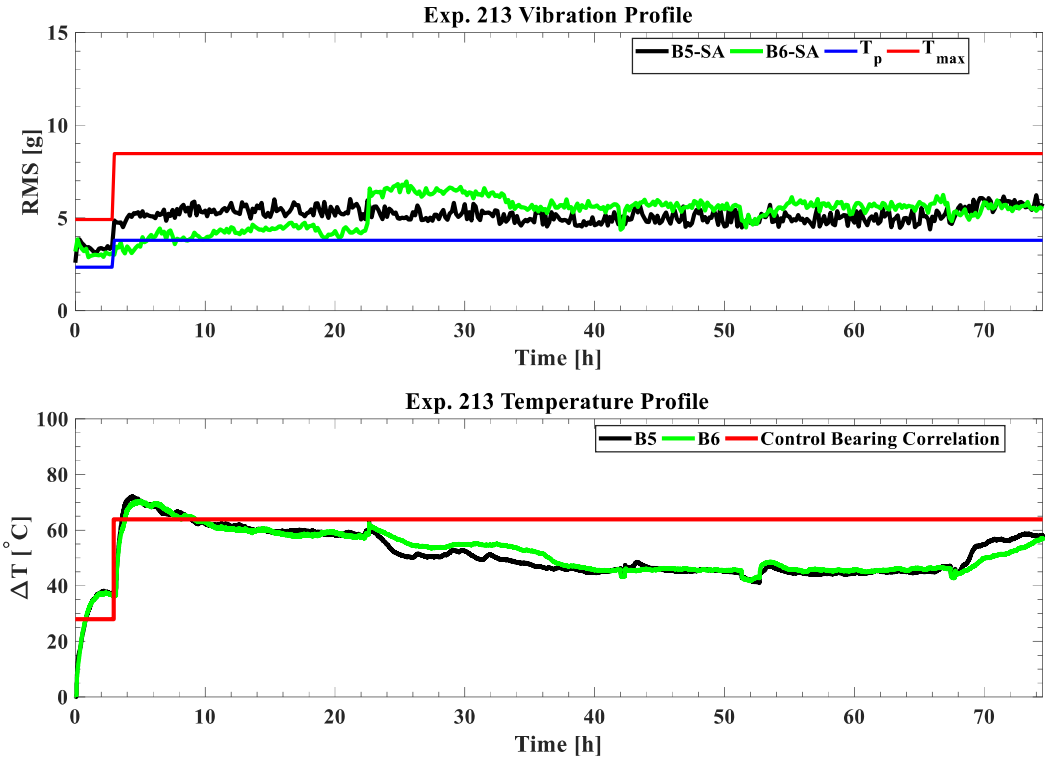

Figure 51: Vibration and temperature profiles for Experiment 213

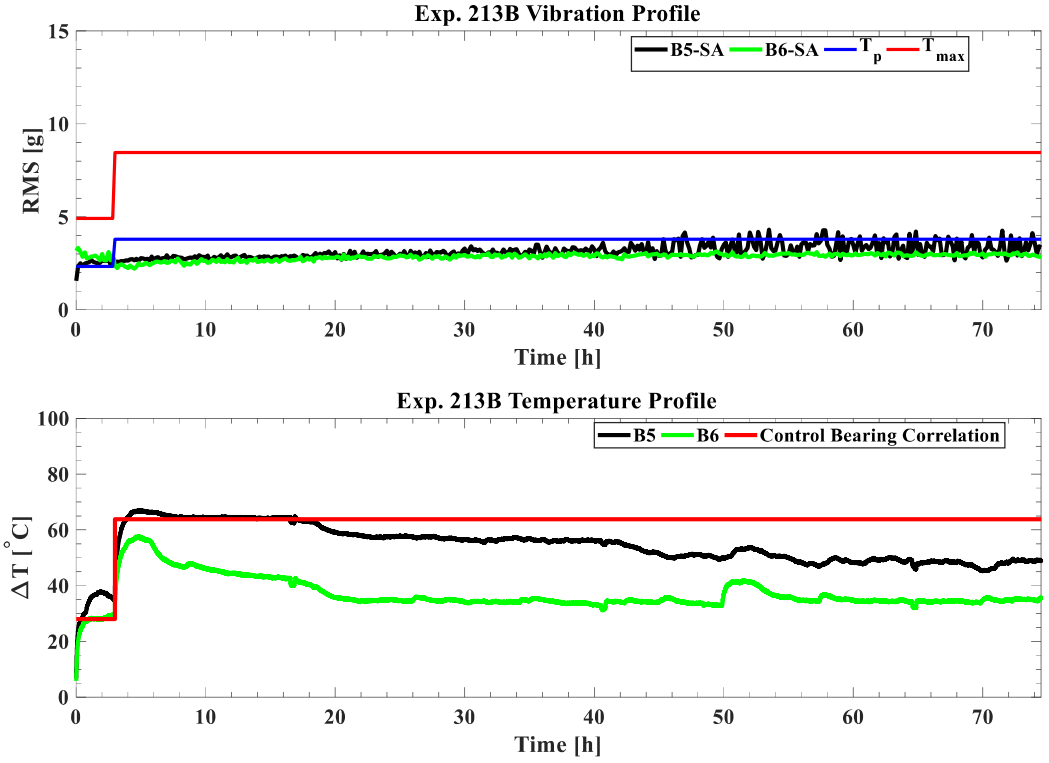

Figure 52: Vibration and temperature profiles for Experiment 213B

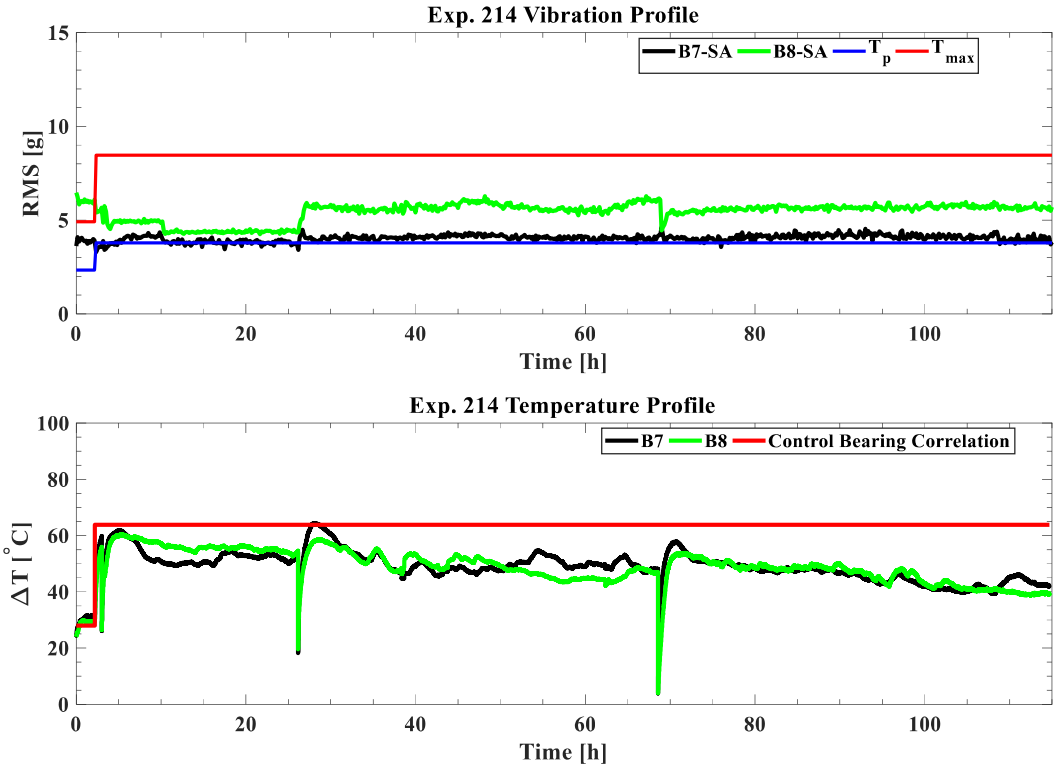

Figure 53: Vibration and temperature profiles for Experiment 214

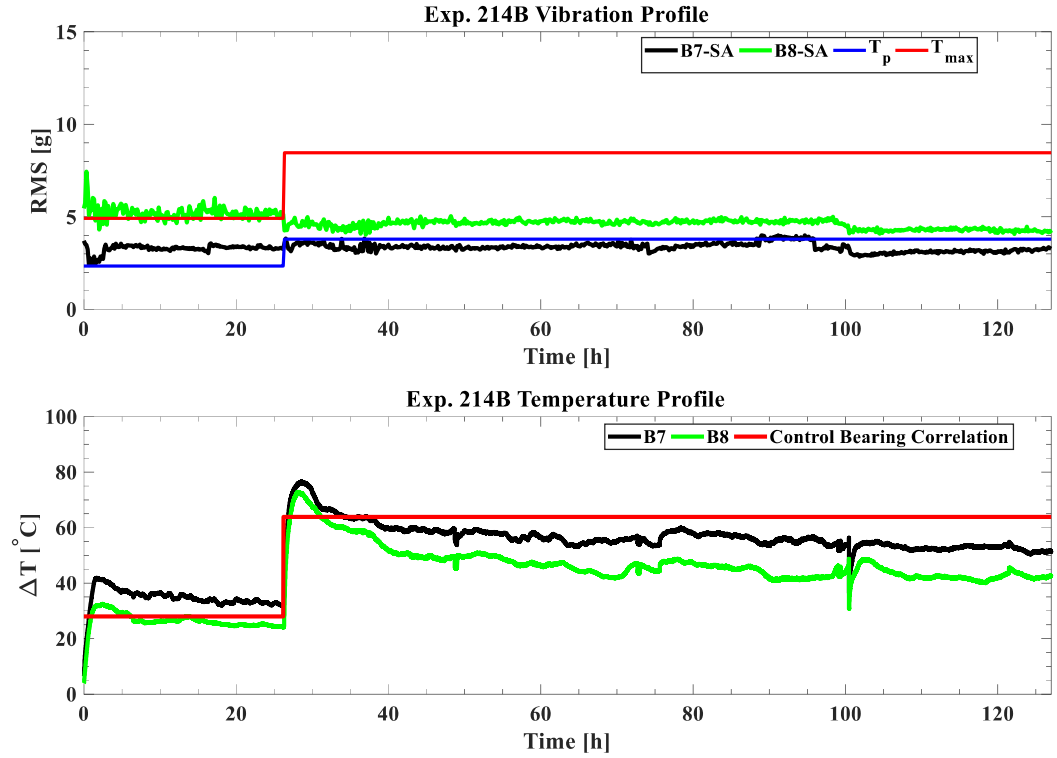

Figure 54: Vibration and temperature profiles for Experiment 214B

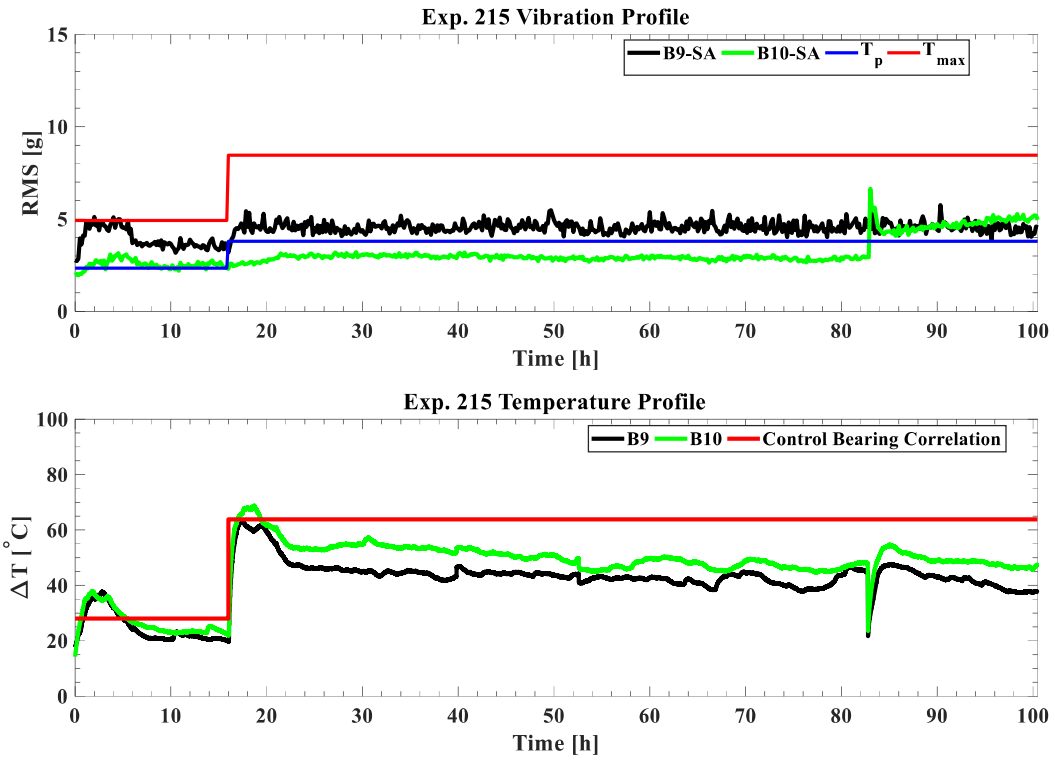

Figure 55: Vibration and temperature profiles for Experiment 215

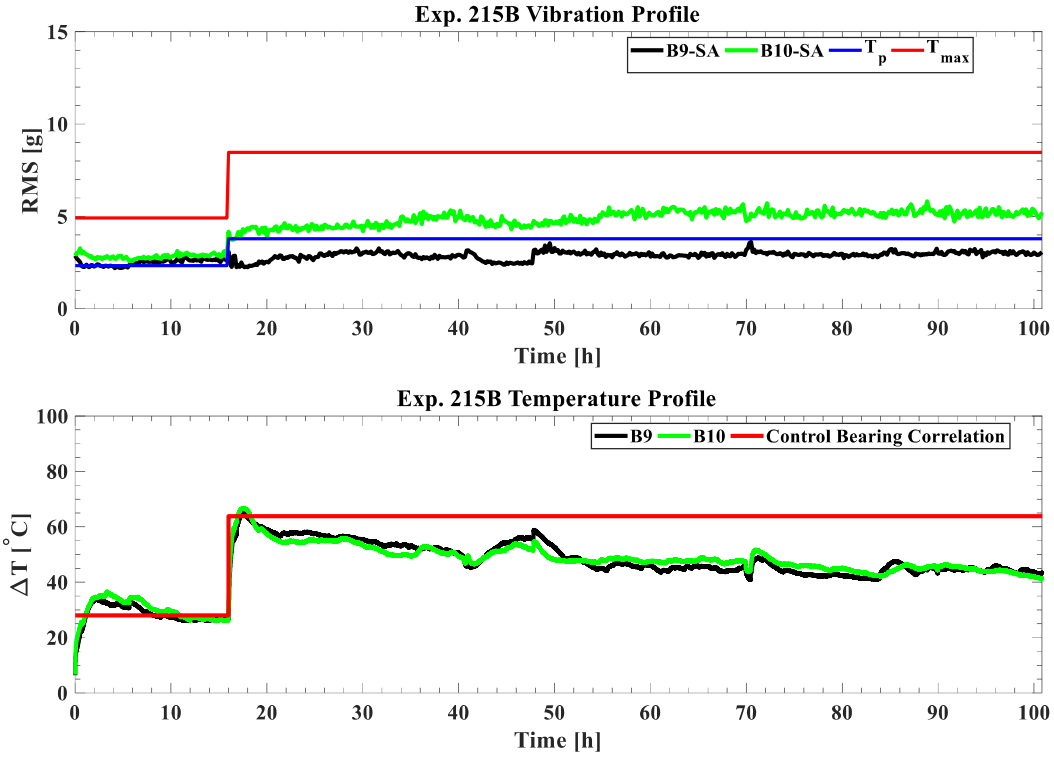

Figure 56: Vibration and temperature profiles for Experiment 215B

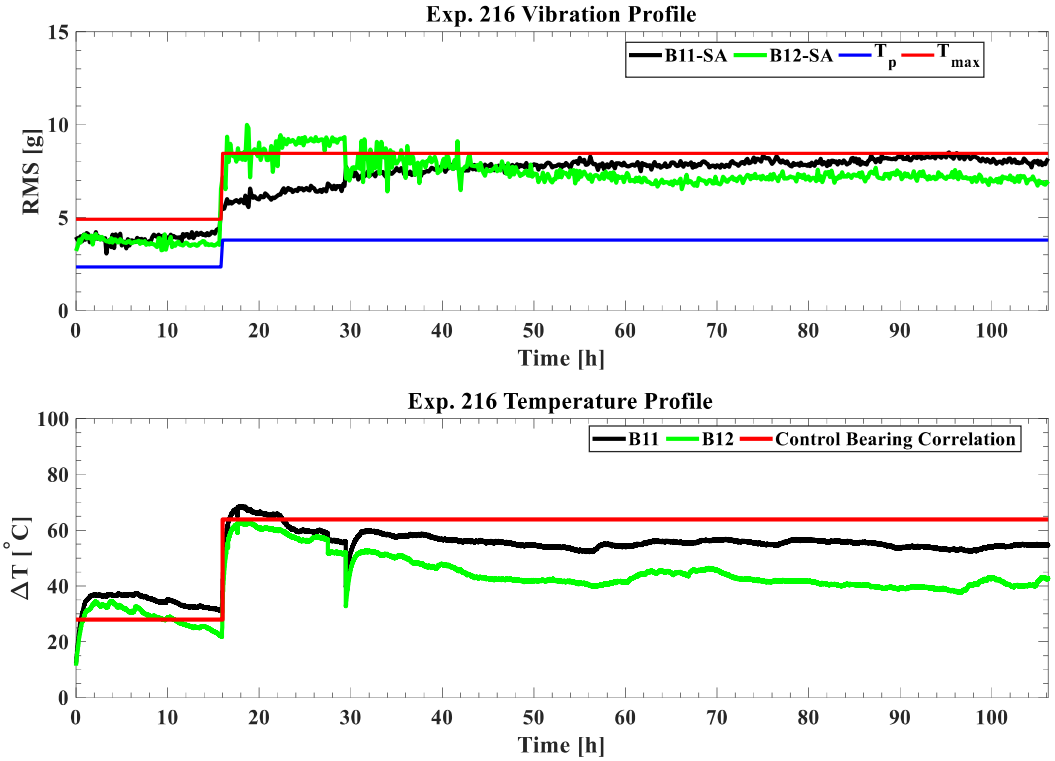

Figure 57: Vibration and temperature profiles for Experiment 216

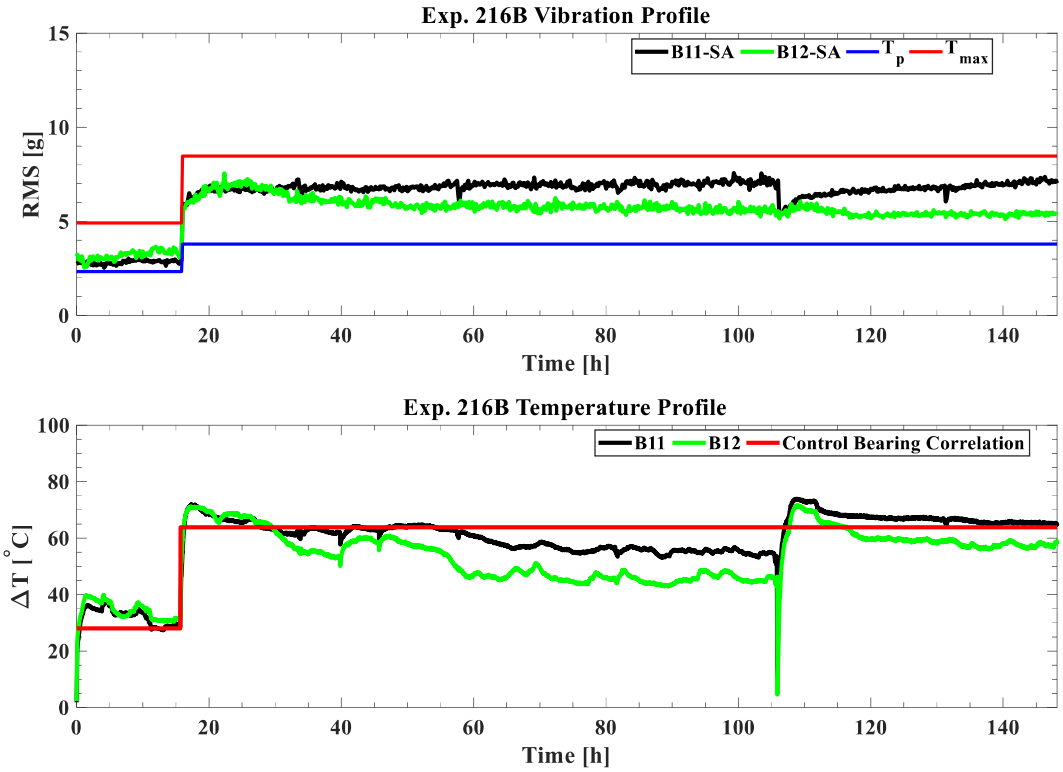

Figure 58: Vibration and temperature profiles for Experiment 216B

BATCH 2 PLOTS

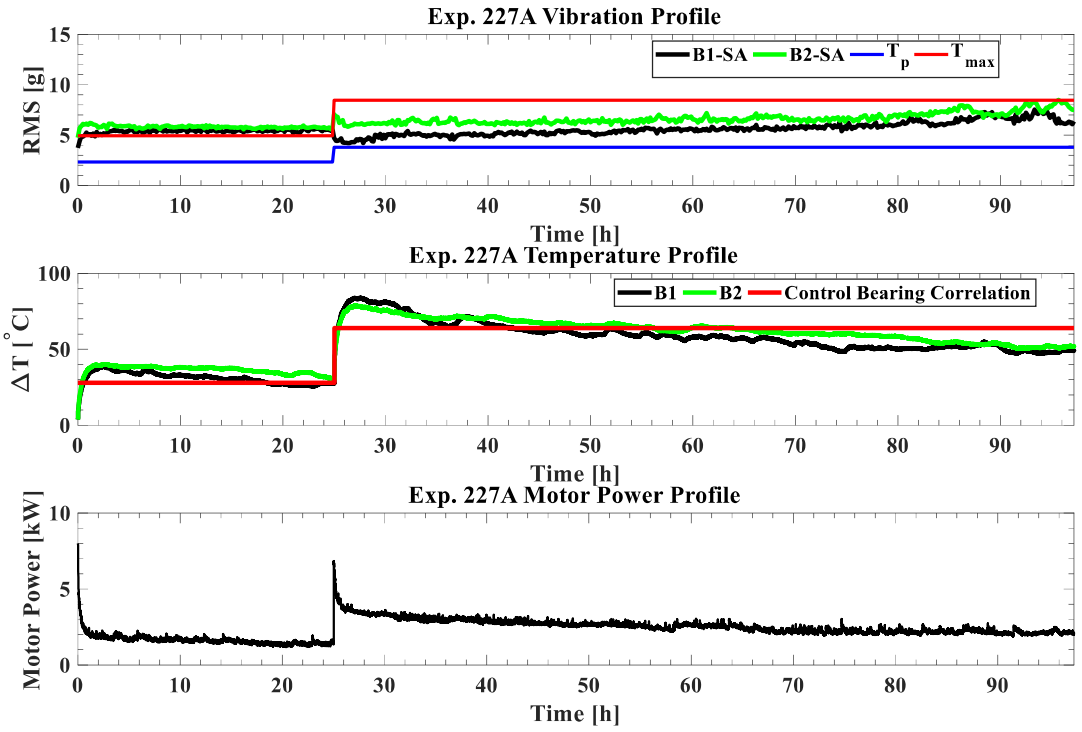

Figure 59: Vibration, temperature, and motor power profiles for Experiment 227A

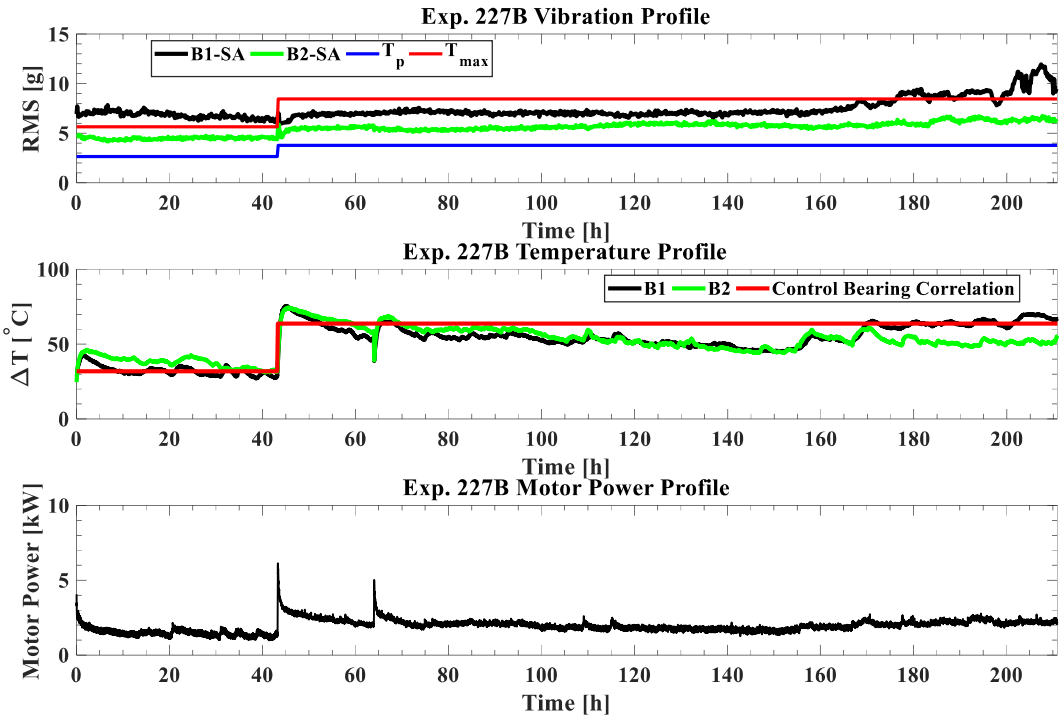

Figure 60: Vibration, temperature, and motor power profiles for Experiment 227B

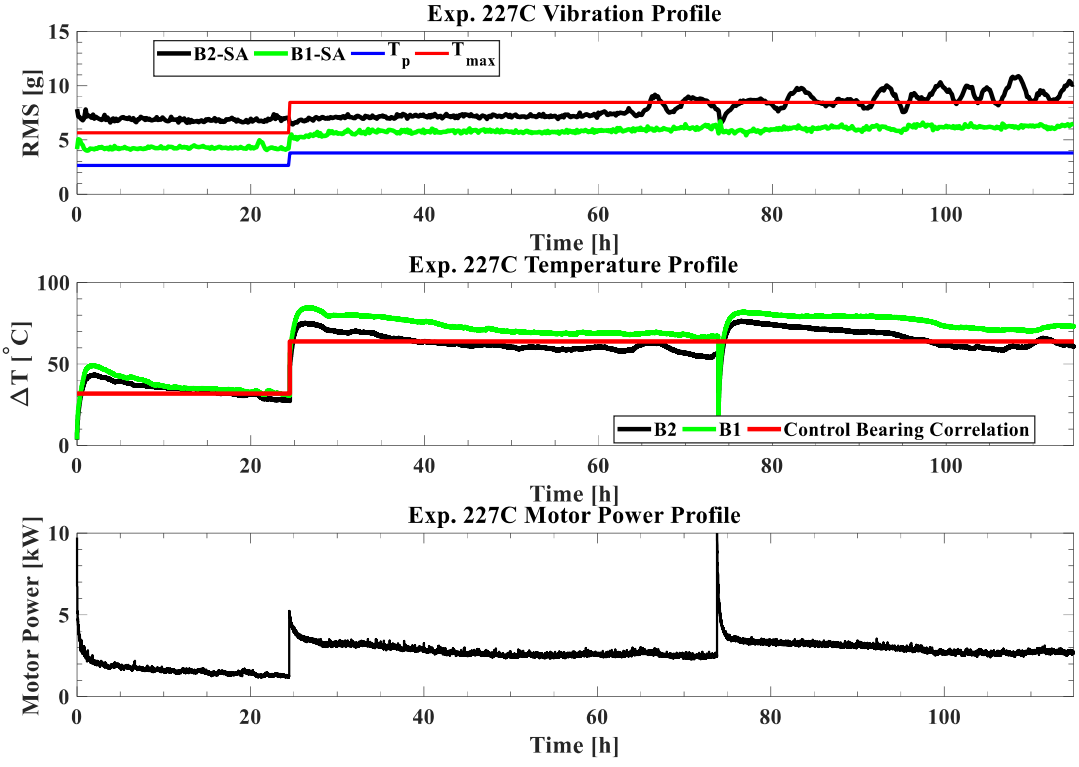

Figure 61: Vibration, temperature, and motor power profiles for Experiment 227C

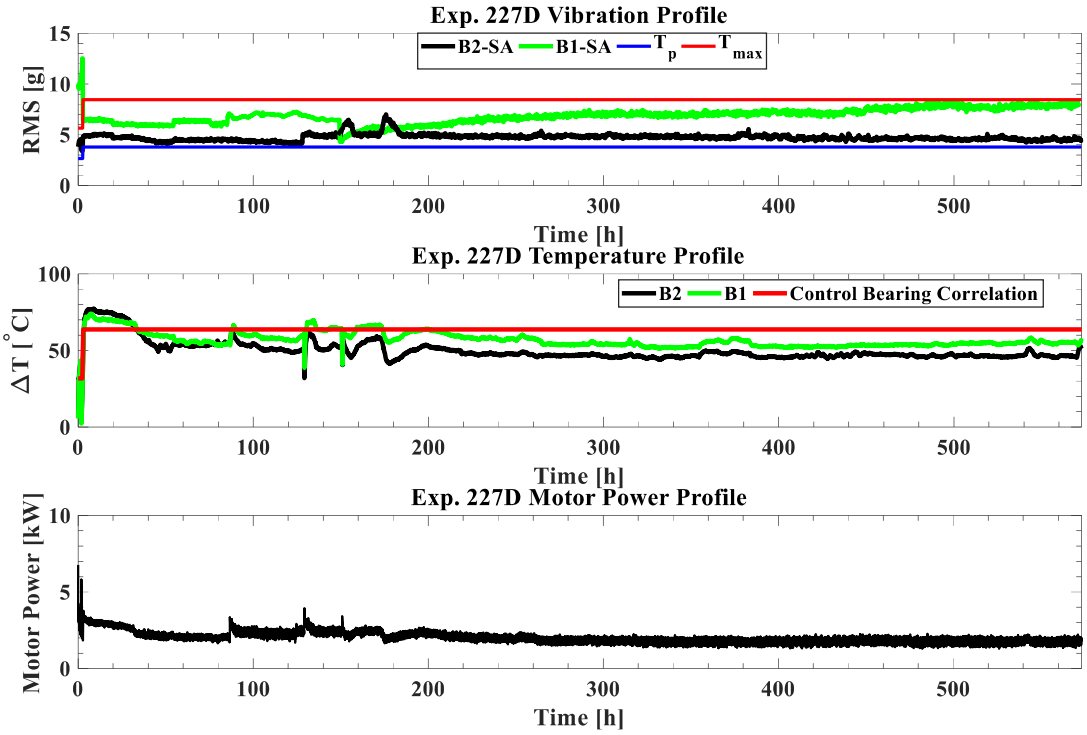

Figure 62: Vibration, temperature, and motor power profiles for Experiment 227D

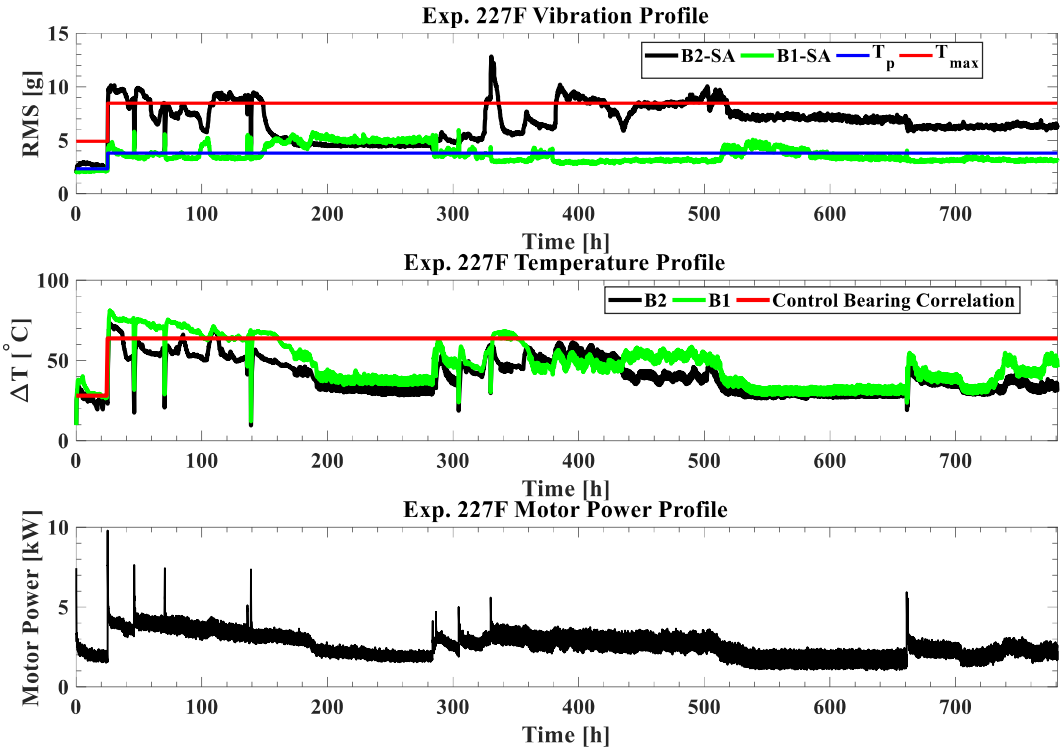

Figure 63: Vibration, temperature, and motor power profiles for Experiment 227F

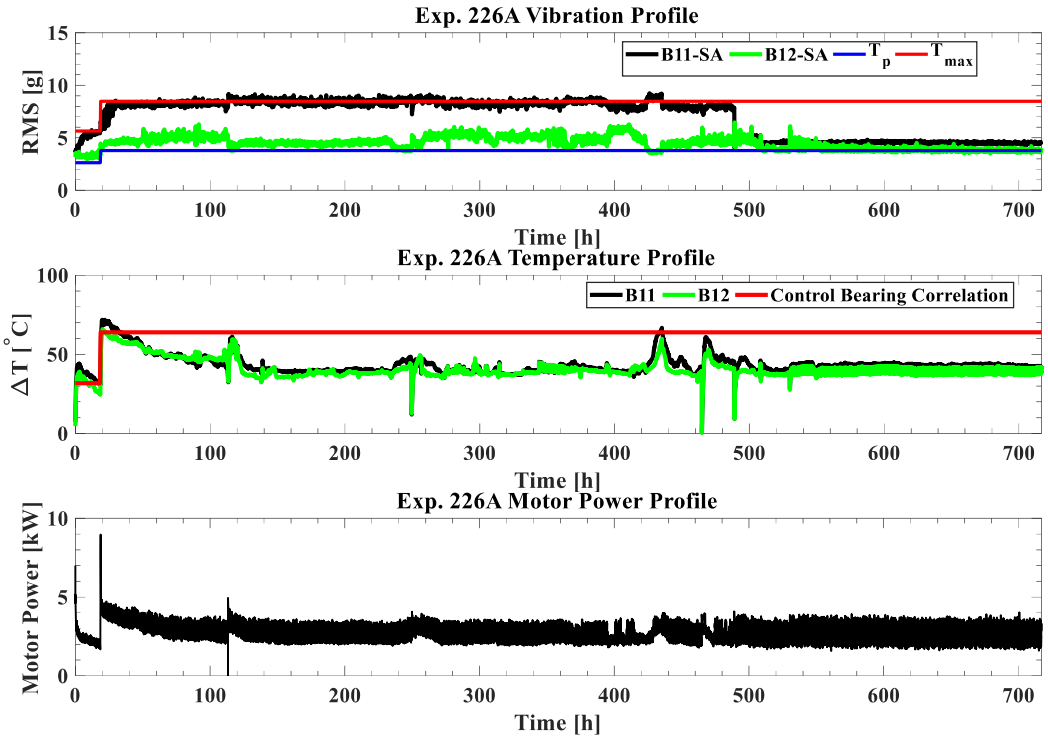

Figure 64: Vibration, temperature, and motor power profiles for Experiment 226A

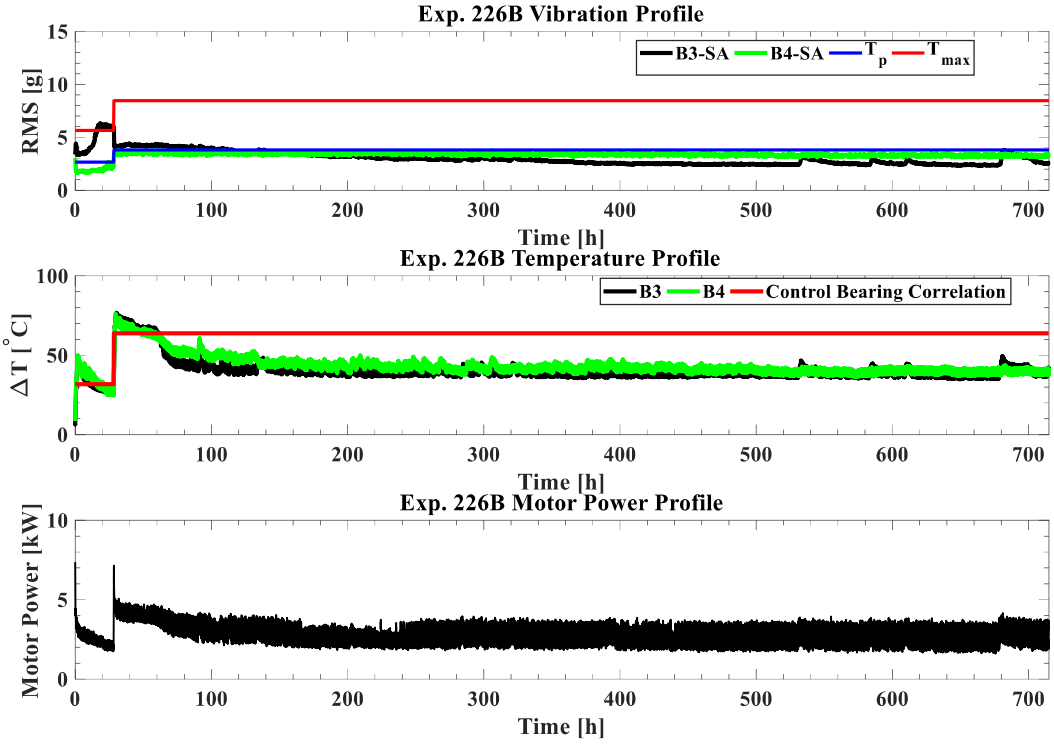

Figure 65: Vibration, temperature, and motor power profiles for Experiment 226B

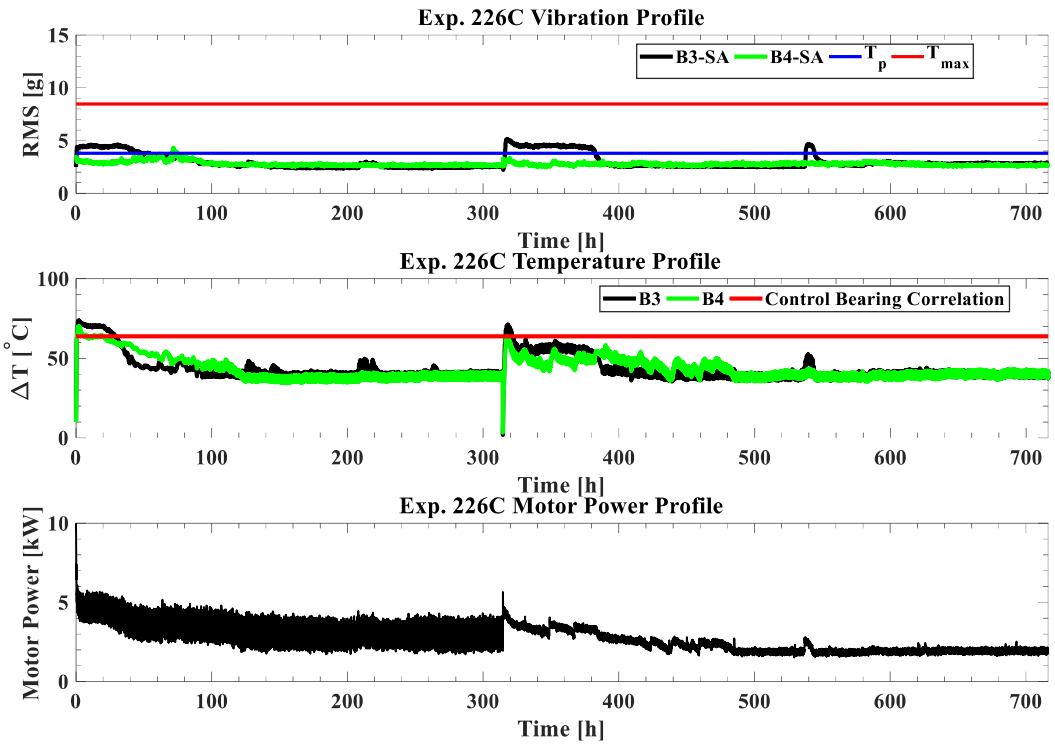

Figure 66: Vibration, temperature, and motor power profiles for Experiment 226C

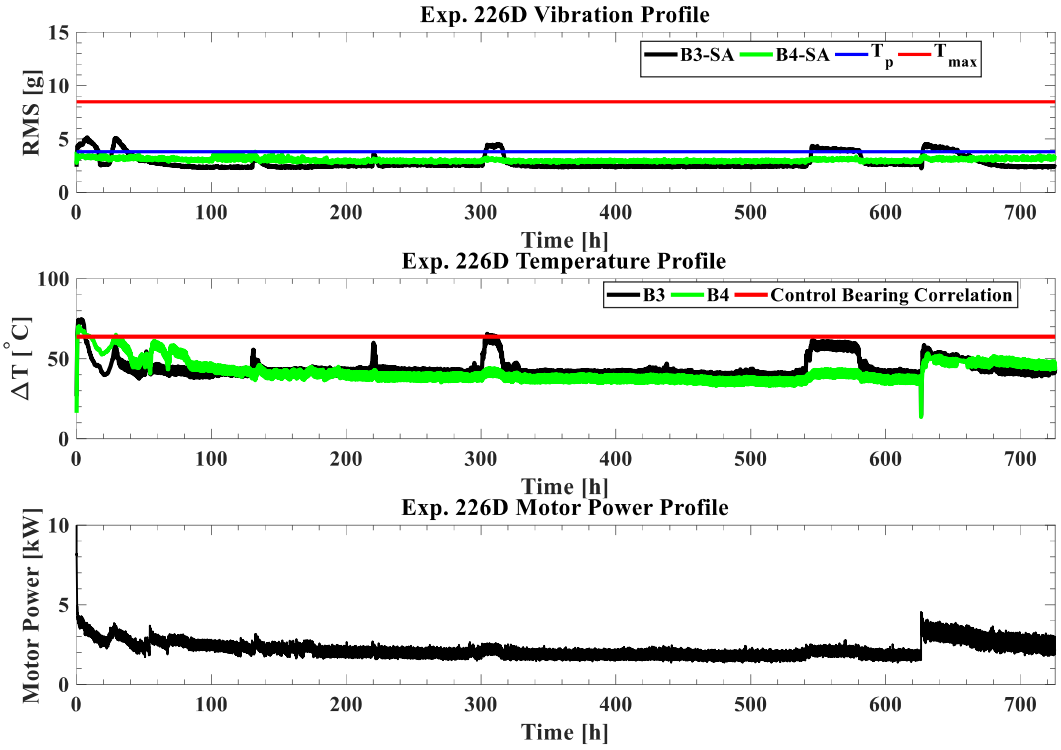

Figure 67: Vibration, temperature, and motor power profiles for Experiment 226D

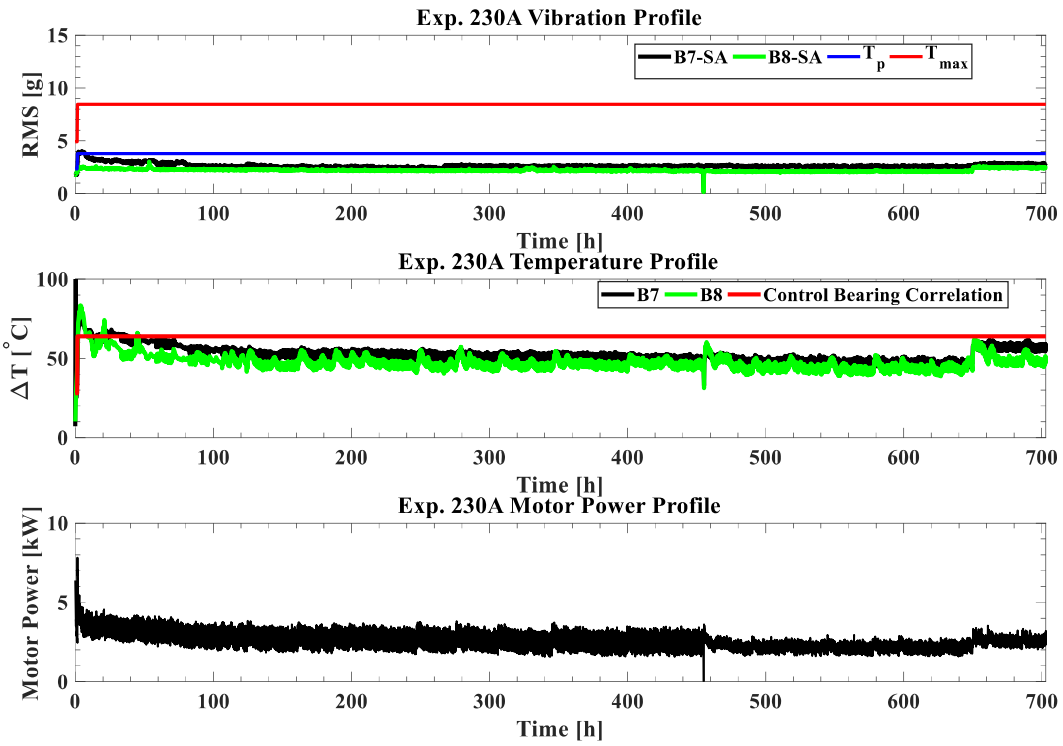

Figure 68: Vibration, temperature, and motor power profiles for Experiment 230A

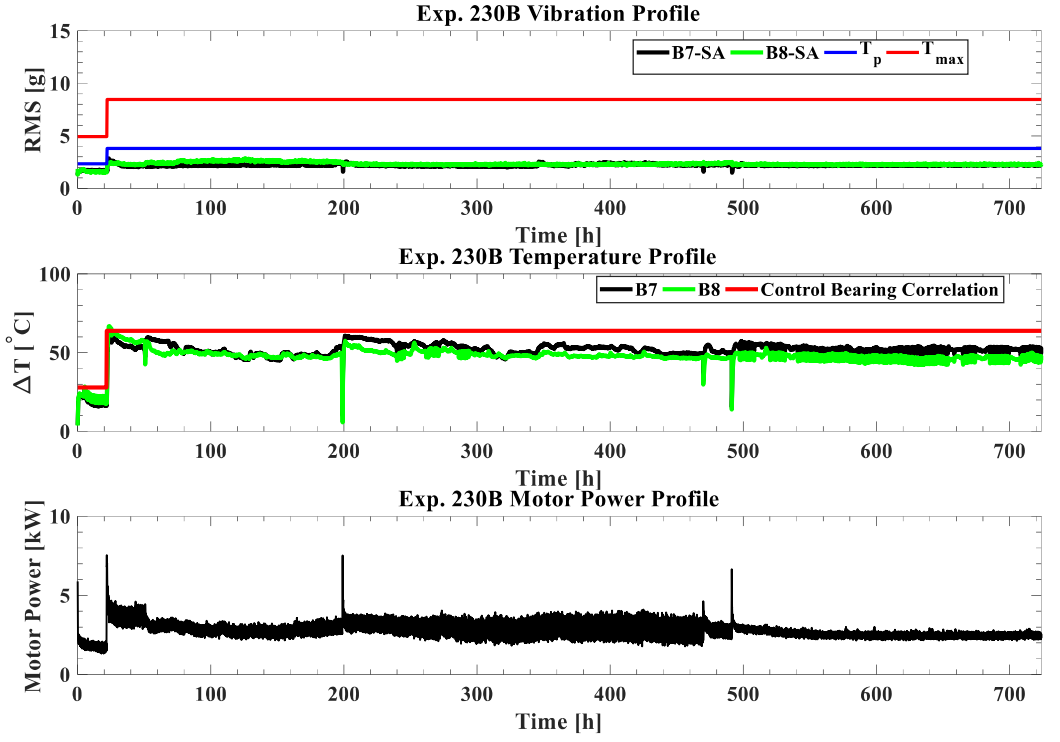

Figure 69: Vibration, temperature, and motor power profiles for Experiment 230B

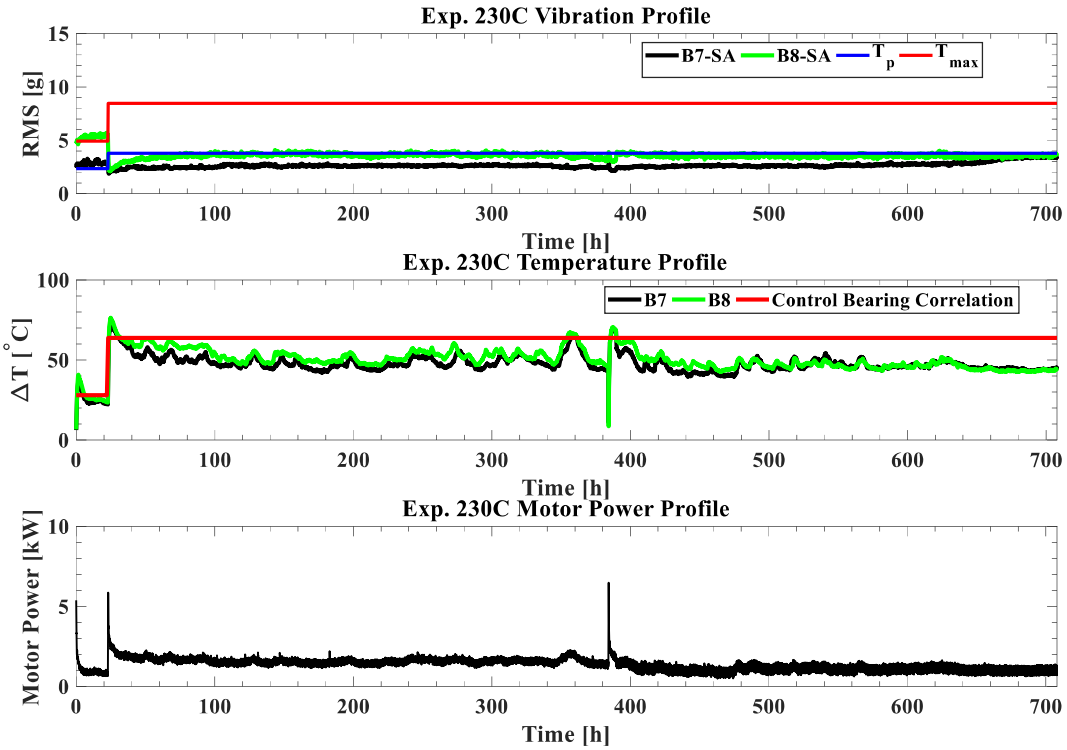

Figure 70: Vibration, temperature, and motor power profiles for Experiment 230C

BIOGRAPHICAL SKETCH

Veronica Valeria Hernandez was born in McAllen, Texas, US, on June 27, 1996. She attended Edinburg High School and Robert Vela High School where she graduated from in 2014. After, she attended the University of Texas Rio Grande Valley (previously known as the University of Texas Pan American), where she graduated Magna Cum Lade with a bachelor's degree in Mechanical Engineering in December 2018. Veronica received the only undergraduate scholarship at the 2018 ASME Joint Rail Conference. She continued her education and obtained her Master of Science degree in Mechanical Engineering in December 2020. During her second semester while pursuing her Masters, Veronica received the UTRGV Profiles in Excellence in December 2019. Veronica can be reached by e-mail at verovaleria96@gmail.com.